Multilink Suspension & Steering System for Cal Poly Formula Electric

Tristan French, E.I.T.
tristan.french@gmail.com

Alissa Roland, E.I.T.
alissaroland3@gmail.com

Subsystem Lead:
Maximilian Sluiter, E.I.T.
maximiliansluiter@gmail.com

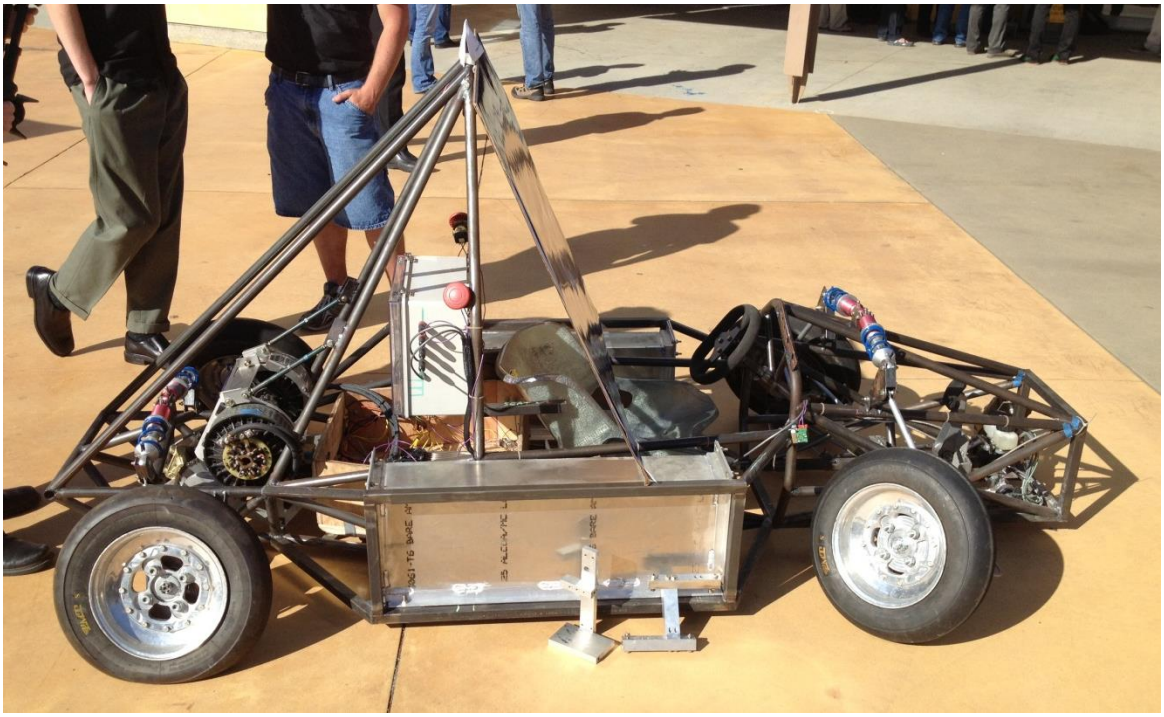

Mechanical Engineering Department

California Polytechnic State University

San Luis Obispo

2013

Statement of Disclaimer

Since this project is a result of a class assignment, it has been graded and accepted as fulfillment of the course requirements. Acceptance does not imply technical accuracy or reliability. Any use of information in this report is done at the risk of the user. These risks may include catastrophic failure of the device or infringement of patent or copyright laws. California Polytechnic State University at San Luis Obispo and its staff cannot be held liable for any use or misuse of the project.

Contents

List of Figures

Abstract

The purpose of this project was to design a suspension that would improve the performance of the Cal Poly SAE Formula Electric car around a racing track Performance would be quantified through skidpad, slalom, and straight-line acceleration tests as well as autocross lap times. The approach to meeting the objective was to increase the steady-state lateral acceleration and quicken the transient response while maintaining predictable handling so that the driver could extract maximum performance from the car.

The car uses round-section (motorcycle) tires at a large negative camber angle because the lateral force generated by a pair of negatively-cambered tires increases with lateral load transfer, which is opposite of the behavior of normal car tires. According to research, maximum lateral grip is achieved at a high-negative camber angle (-40 degrees) but best longitudinal acceleration is had with no camber.

The original design for the suspension was a passive, dynamic camber system which varied the camber in order to provide maximum grip in a straight line as well as in turns. The scale of this design was deemed to be too large for the time, resources, and manufacturing skill of the Formula Electric team this year. Therefore it was decided to produce a highly adjustable static camber suspension that could be tuned for best performance as well as adjusted to allow for testing of the dynamic camber concept.

The final design is a static camber system using the “five link” suspension configuration in both front and rear. The links have turnbuckle adjustment and are easy to manufacture so that many camber angles can be tried in order to find the optimal camber angle for a particular track. The uprights are of shell construction and the rear uprights can be used at any camber angle. The front requires a slightly different upright geometry for very large camber angles than for small camber angles. Tires are sized 100/85-R10 on all four corners and are meant for small racing motorcycles. They are lightweight and allow large camber angles to be used.

Component testing and validation consisted of Instron testing for link buckling, link thread pullout, link tensile strength, and rod end buckling. Testing on the suspension as a whole will involve skidpad tests to find the maximum steady state lateral acceleration from various camber configurations as well as acceleration tests to find the effect of camber on longitudinal acceleration. The goal will be to find the best static camber setup and determine if a dynamic camber system, active or passive, would actually provide a significant advantage if the manufacturing resources were available to build it.

Manufacturing on the primary camber setup is complete and production of the low camber setup is in progress. Testing of various camber setups and comparison with traditional racing car tires using the low camber setup will be continued by the Cal Poly Formula Electric team.

Background

The following is the final design report for the Cal Poly Formula Electric Suspension Senior Project Team. Important background concepts and research are introduced and the final designs are described, as well as analysis and testing procedures. The entire car has been assembled; however as of June 7, 2013 we are unable to run the car due to electrical issues. As a result, we have laid out a testing procedure, but have not been able to complete it.

The Cal Poly Formula Hybrid / Formula Electric car has used a "camber-car" configuration for the past 4 years. This design uses motorcycle tires tilted inward at the top to achieve high levels of lateral acceleration. It was first proposed in 1949 by William F. Milliken, though not actually tested until 1968, and was not widely publicized and is still a relatively unknown concept.

The Formula Electric car has carried-over suspension components since the team made their first camber car. What little tire performance data was recorded was not very useful, however, because too many variables (primarily tire compounds and track conditions) changed between each test. As a result, the team was looking for someone to design a new suspension for the 2013 car with the goal of being able to validate the camber concept and potentially run conventional car racing tires to confirm the benefit of using the lighter motorcycle tires over the heavier car racing slicks. The design had to follow the FSAE guidelines and pass technical inspection in order to be approved for competition. Maximilian Sluiter volunteered for this task and proposed the senior project during the summer. Alissa Roland and Tristan French then joined the team.

Max was responsible for designing the suspension in CAD and did extensive background research. Alissa and Tristan were responsible for sizing wheel bearings, analyzing the old suspension, and doing most of the load and stress analysis before the design freeze. They also spearheaded the manufacturing.

Fundamental Tire & Vehicle Dynamics

Tires generate the majority of the forces necessary for accelerating, decelerating, and turning a ground vehicle (aerodynamic devices which could provide additional maneuvering forces as well as downforce to increase tire grip will not be covered in this report). A vehicle's suspension system links the four tires to the "sprung mass", which is essentially the chassis and everything rigidly mounted to it. The term "unsprung mass" is applied to the tires, wheels, and some fraction of the inertia of each component of the suspension mechanism. Those fractions are based on the kinetic energy of the particular piece of the mechanism with respect to a single, simpler variable – usually the vertical displacement of the wheel. The unsprung mass on each corner of the car is separated from the ground by the compliant tire, modeled as a spring of between 100 and 350 kN/m stiffness[1] and sometimes a weak damper. It is separated from the sprung mass by the suspension spring(s), damper(s), and in some cases inerter(s).

[1] Cossalter, Vittore: Motorcycle Dynamics, 2nd ed., page 56

Suspension Basics

The purposes of a suspension system are as follows:

- Transfer forces from the tires to the sprung mass.
- Put the tire in the correct orientation to the road for maximum grip.
- Isolate the sprung mass from road irregularities.
- Manage the load on each tire to provide the best grip.

While meeting the requirements stated above, the suspension should also have as little inertia as possible. This not only reduces the total car mass but more importantly reduces the effective unsprung mass. Reducing the ratio of unsprung to sprung mass helps keep the load on each tire closer to optimal and improves the ride (isolates the sprung mass) from high frequency road inputs because the highly-underdamped wheel-tire system then has a higher natural frequency. This higher "wheel hop" frequency means that the unsprung mass is not excited as much by inputs from bumps in the road. Since the unsprung masses' motions are the forcing functions for the sprung mass, less unsprung mass excitation means less disruption of the sprung mass. The components with the largest effect on unsprung mass in most suspension systems are the uprights (which hold the wheel bearings and hubs), the wheels, the tires, and any brake components that may be mounted outboard. Lighter wheels and tires have the added benefit of reducing the inertia that the drivetrain must accelerate and reducing gyroscopic forces (which are usually not a significant factor in four-wheeled vehicle dynamics). For these reasons, lighter wheels are one of the best upgrades for any car.

Tire Basics

Tires generate forces through their interaction with the road surface. The normal load (weight) on a tire causes it to deform out of round and form a "contact patch" or "footprint" which grips the road via several mechanisms. These include mechanical interlocking, whereby the soft rubber is squeezed into small crevices in the road surface and acts like teeth in a rack and pinion gear mesh, and chemical bonding. Deformation of the contact patch is resisted by a distributed force arising where the rubber meets the road. This force pushing back on the tire is transferred through the suspension to the sprung mass in order to accelerate, turn, and brake the car as a whole. The objective of the suspension design in this report was to improve both steady-state lateral acceleration and transient response for better handling. Therefore, lateral force and the mechanisms to generate it will be the focus of the following discussion, with less explanation given for the source of tractive (acceleration and braking) forces since they also arise from a deformation of the contact patch, just in a different direction.

There are two main methods to deform the tire for the purpose of generating lateral force: slip angle and inclination angle. To understand what these terms mean, please refer to Figure 1. Slip angle results when a tire is steered about an axis normal to the road. Inclination angle is a tilting of the tire about an axis parallel to the plane of the road and orthogonal to both the slip angle axis and the axis about which the wheel rotates (the axis defined physically by the wheel bearings in the upright). In the figure, "direction of wheel travel" can be thought of as the direction the car is moving (in reality it takes into account both rotation and translation and so is a local velocity vector on the car) and "direction of wheel heading" is the direction the wheel is pointing or being steered towards. Slip angle is given the symbol of the Greek letter alpha (α)

and inclination angle gamma (γ). Inclination angle is shown measured from the vertical axis passing through the contact point (or the center of the contact patch) to the dotted line which is in the plane of the wheel and passes through both the contact point and the axis of rotation (rotation is called "spin" in the diagram).

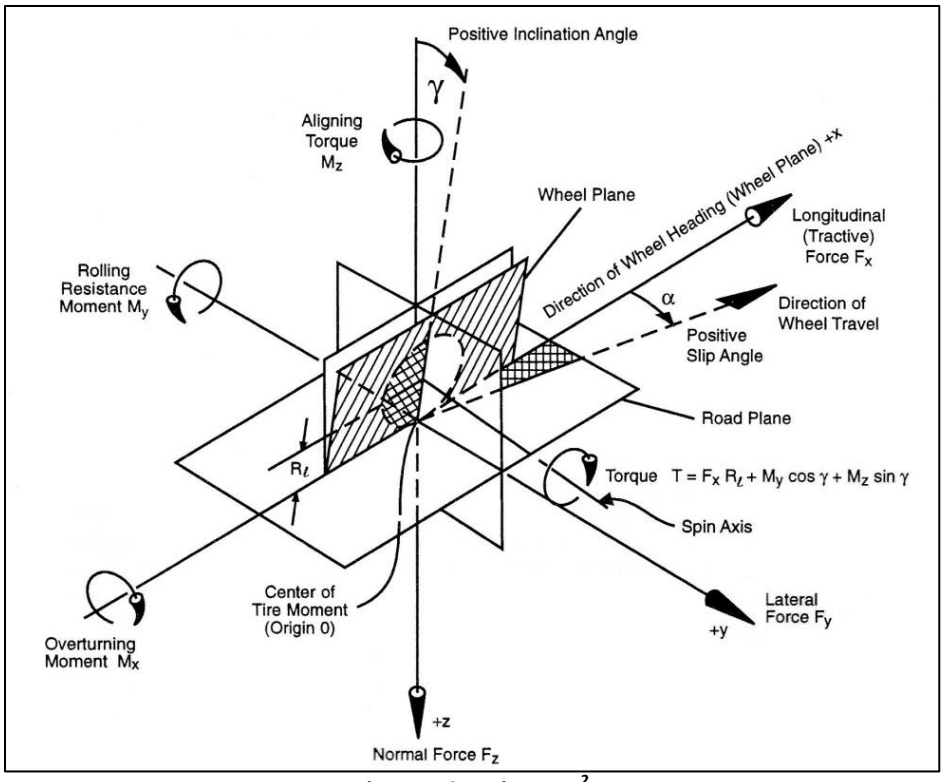

Figure 1: SAE Tire Axes[2]

Slip Angle

The manners in which slip angle and inclination angle deform the contact patch are different. With slip angle, the tire is twisted. As shown in the diagram of Figure 1, this comes about because the wheel is restrained to rotate about the axis defined by the wheel bearings, but the velocity of the upright in which the wheel bearings are mounted does not align with the plane of the wheel. Therefore, when a tread element (which can be infinitesimally small) makes contact with the road it adheres and stays in place while the wheel rolls over it and the next tread element enters the contact patch and sticks. The first tread element is now directly behind the second, with the tread elements aligned to the velocity vector of the upright (direction of wheel travel) rather than the tangential velocity on the bottom of the wheel (direction of wheel heading). This means that the tire must distort in the section of sidewall and carcass between the wheel rim and contact patch. The distortion of the tire combined with its stiffness causes both a lateral force and a restoring moment (which attempts to remove the twisting deformation and align the wheel heading to the direction of travel). The force and moment are reacted through the tire's grip on the road (which is the fixed reference frame) and the compliment of that force causes the car to accelerate laterally in response. A diagram of this deformation can be seen in

[2] Milliken, William F. & Douglas L.: Race Car Vehicle Dynamics, page 62

Figure 2, which is from a viewpoint of an observer below a transparent road surface and with the plane of the wheel along the x-axis. The curved line to the left of point A is the result of the lateral stiffness of the tire carcass (in the range of 100 to 200kN/m)[3] causing the deflection in the contact patch to propagate forward. The tread element makes contact at A, proceeds through B and H, and leaves the road at D.[4]

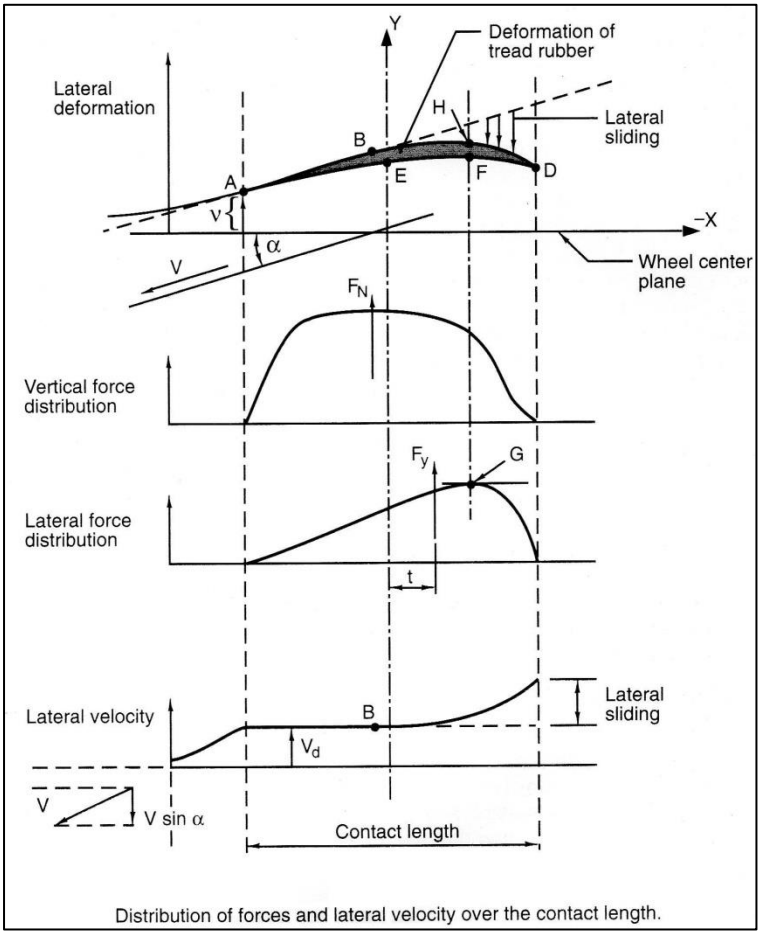

Figure 2: Tire Vertical Load, Lateral Force, and Contact Patch Deformation Distribution for Slip Angle[5]

The diagram also shows that, due to the roughly parabolic distribution of normal force within the contact patch and the linearly-increasing trend of deformation, the limit of static friction is reached before the end of the contact patch. Sliding occurs in the lightly-loaded aft portion of the patch and this region increases in area as slip angle increases until the whole footprint is sliding. A noteworthy point is that the maximum lateral force occurs behind the center of the contact length. The line labeled F_y is the resultant of the distributed lateral force and therefore passes through the centroid of the area under the lateral force curve. The length "t" denotes how far behind the center of the contact patch the lateral force resultant occurs and is called the pneumatic trail. Pneumatic trail causes a moment which attempts to reduce slip angle,

[3] Cossalter, Vittore: Motorcycle Dynamics, 2nd ed., page 56
[4] Milliken, William F. & Douglas L.: Race Car Vehicle Dynamics, page 22
[5] Milliken, William F. & Douglas L.: Race Car Vehicle Dynamics, page 23

aligning the tire with the direction of travel. As slip angle increases the sliding fraction of the contact patch grows from the rear forward and the force resultant moves forward because sliding friction is less than static friction. The lateral force resultant grows in magnitude but the pneumatic trail decreases, causing the restoring moment to peak, usually just before maximum lateral force, and fall off afterwards. The self-aligning moment is felt by the driver through the steering system and gives useful feedback about how close to the limit of performance the car is.[6]

For small values of α, lateral force is directly proportional to slip angle and the proportionality constant is called cornering stiffness. At larger slip angles the rate of change of lateral force with respect to slip angle decreases to zero at the peak lateral force and becomes negative past it, which means a polynomial curve fit is necessary for modeling the behavior of tires at higher slip angles. Cornering stiffness is actually a partial derivative because the lateral force produced by a tire also varies with the vertical load on it. It is possible, however, to normalize the lateral force to the vertical force and produce a graph of "lateral force coefficient". Plots of this quantity for three different loads are shown in Figure 3. The beginnings of the curves are linear, with a slope equal to the normalized cornering stiffness (to obtain cornering stiffness, multiply by the vertical load). At higher slip angles the curves roll off and reach a peak, past which the tire is mostly sliding.

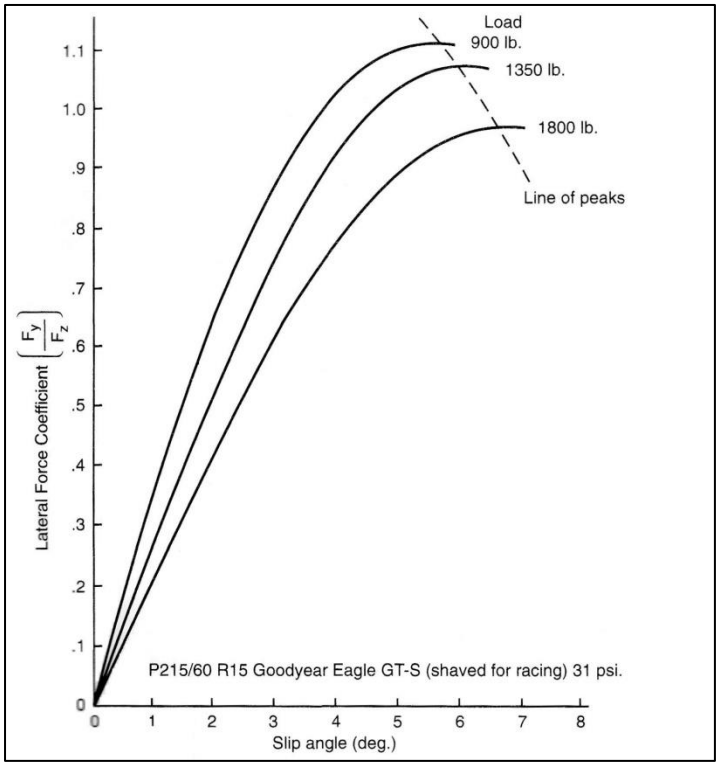

Figure 3: Typical Load Sensitivity Behavior[7]

[6] Milliken, William F. & Douglas L.: Race Car Vehicle Dynamics, page 404
[7] Milliken, William F. & Douglas L.: Race Car Vehicle Dynamics, page 27

It can be seen in Figure 3 that the peak lateral force coefficient decreases as vertical load increases. This is known as load sensitivity. If this trend were extrapolated to zero load, there would be maximum lateral force without the tire contacting the road so it is reasonable to speculate that the peak lateral force coefficient reaches a maximum at some light load, different for every type of tire, before again falling to zero with no load. Load sensitivity is a very important concept and dictates much of the design of racing cars. Conventional racing cars aim to have a low center of mass and a wide track (lateral spacing between the wheels). This reduces the lateral load transfer which results from the tire forces arising in the ground plane but being transferred to the mass center, which must be above the ground. This creates a roll moment that, in the absence of aerodynamic devices, must be reacted by a redistribution of the vertical load on the four tires. Less lateral weight transfer is desired for tires utilizing slip angle for lateral force because the peak lateral force coefficient decreases on the more heavily loaded, outside tire, meaning that combined lateral force capability is lost when weight is distributed unequally across an axle. In other words, more grip is lost from the inside tire than is gained from the outside.

Inclination

The deformation due to inclination is shown in Figure 4. Depicted are the shapes which the contact patch of a motorcycle tire and car tire would assume when placed on a frictionless surface, inclined, and under a vertical load. The round, motorcycle tire has more curvature (seen in the black line running through each patch) than the car tire and this results in more camber thrust (lateral force due to inclination). On a real road the curvature is suppressed by friction and this produces a lateral force. The greater curvature of the motorcycle tire gives one explanation for the greater camber stiffness of round-section tires compared to square-section car tires.[8] Camber stiffness is the partial derivative of lateral force with respect to camber angle and at a particular vertical load. Bias-ply tires with stiffer sidewalls generally have greater camber stiffness than radial tires, which let the contact patch deform too easily under the road load.[9] Camber is similar to inclination angle but its sign depends on which side of the vehicle the tire is on. Negative camber means that the tops of the tires lean in – towards the sprung mass, while positive camber means they lean outward. An excellent example of negative camber is the Milliken MX-1, which will be discussed later in this report and is shown in Figures 8 and 9.

[8] Pacejka, Hans B.: Tire and Vehicle Dynamics, 3rd ed., page 77
[9] Milliken, William F. and Douglas L.: Race Car Vehicle Dynamics, page 47

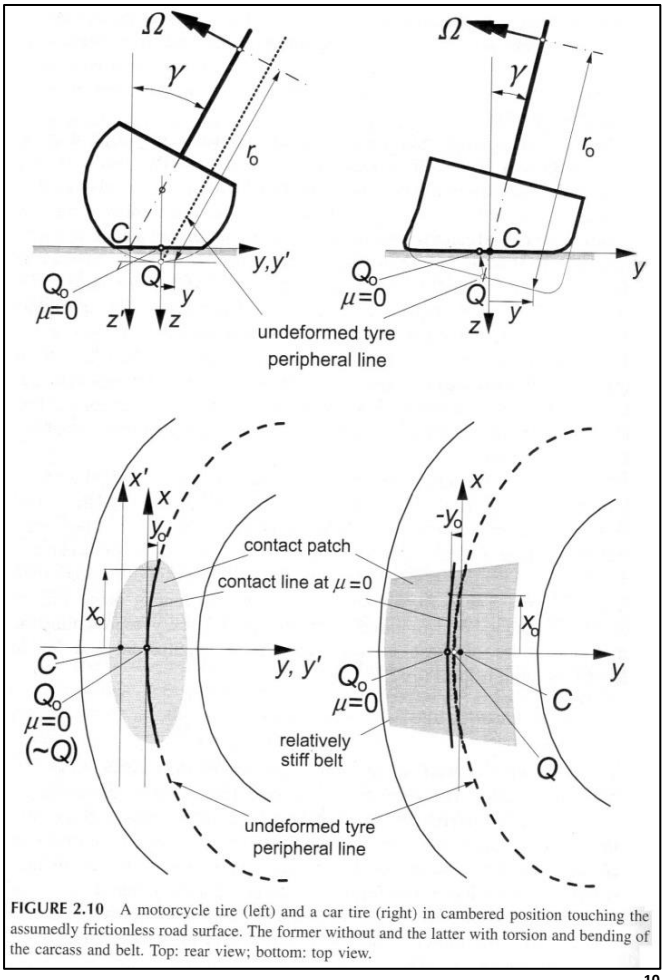

FIGURE 2.10 A motorcycle tire (left) and a car tire (right) in cambered position touching the assumedly frictionless road surface. The former without and the latter with torsion and bending of the carcass and belt. Top: rear view; bottom: top view.

Figure 4: Shape of Deformed Contact Patch for Frictionless Road[10]

Also apparent in Figure 4 is that the lateral deformation of the contact patch is symmetrical about the y-axis (positioned halfway back from the front of the contact area). This curvature more closely matches the distribution of normal load on the tire seen in Figure 2 and results in less sliding of the tire on the road.[11] The symmetry also results in much less (or even negative) self-aligning moment (pneumatic trail) than for slip angle.[12]

Figure 5 is a clearer look at how the contact patch shape changes for a motorcycle tire as inclination angle increases.

[10] Pacejka, Hans B.: Tire and Vehicle Dynamics, 3rd ed., page 76
[11] Milliken, William F. and Douglas L.: Race Car Vehicle Dynamics, page 47
[12] Milliken, William F. and Douglas L.: Race Car Vehicle Dynamics, page 47

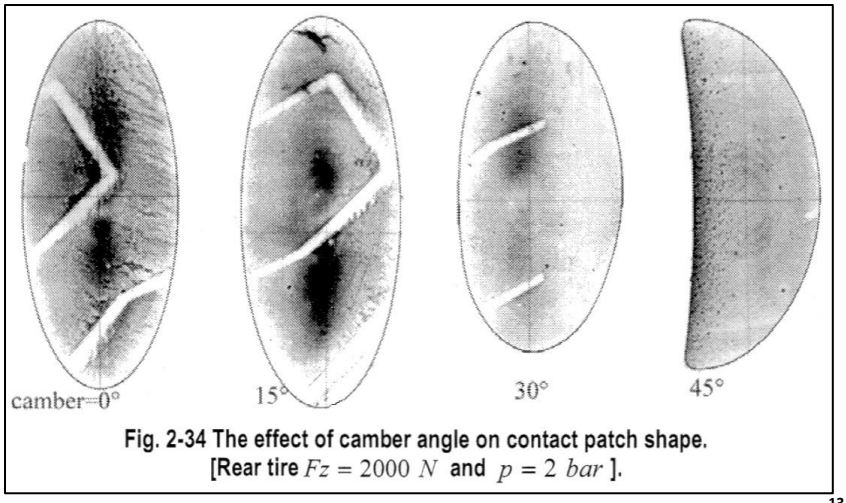

Fig. 2-34 The effect of camber angle on contact patch shape.
[Rear tire $Fz = 2000\ N$ and $p = 2\ bar$].

Figure 5: Changes in Contact Patch Area and Shape due to Camber and Tread Blocks[13]

Camber thrust behaves very differently than slip angle. It has an approximately linear relationship to both vertical load and inclination angle, even up to and beyond 45 degrees of inclination, as seen in Figure 6. The linear relationship to vertical load is evidenced by the normalized camber thrust data all falling on the same trend line even when the vertical load was increased five-fold, from 500N (112lb.) to 2500N (561lb.); thus the tire tested does not show camber thrust load sensitivity for the range of loads that would be seen on a lightweight racecar such as that of the Formula Electric team. From the two graphs it can be seen that this linearity is not only associated with the round section and construction of the particular motorcycle tested because the tire shows load sensitivity when subjected to slip angle deformation but not when inclined. The slip angle plots show curvature similar to that seen in the plots for car tires, although there is no peak to them because the range of slip angle tested is not as large as for car tires because motorcycles do not usually use large slip angles.

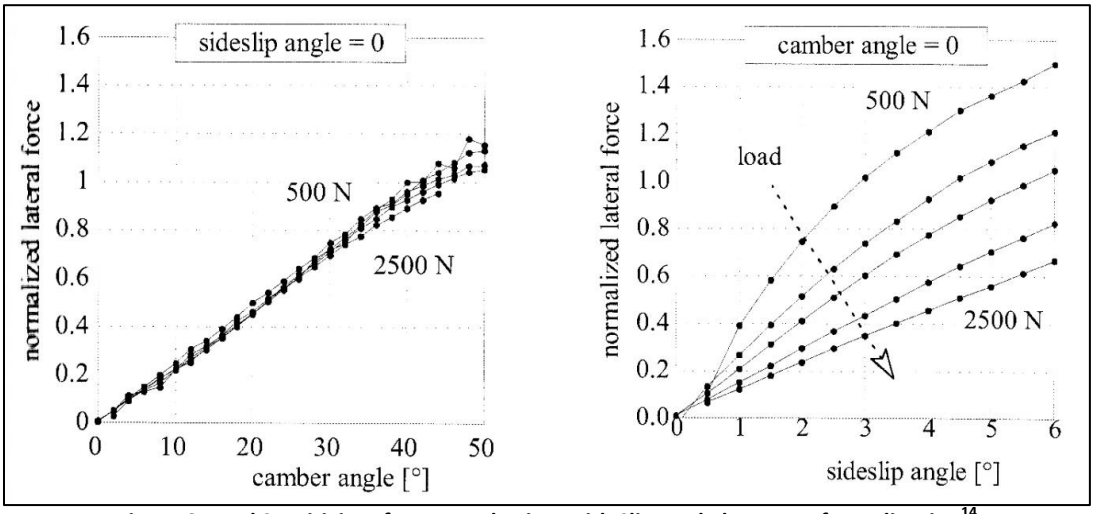

Figure 6: Load Sensitivity of Motorcycle Tires with Slip Angle but None for Inclination[14]

[13] Cossalter, Vittore: Motorcycle Dynamics, 2nd ed., page 67
[14] Cossalter, Vittore: Motorcycle Dynamics, 2nd ed., page 55

Combining Inclination & Slip Angle

The linearity of camber thrust holds true even when there is a small slip angle present, as is the case in Figure 7, where the right side plot shows it most clearly. The left side plot shows the saturation (leveling off of lateral force) of the tire at large inclination angles and small slip angles, with maximum lateral force occurring at lower slip angles when the inclination is increased. In the left-side plot of Figure 7 it is apparent that 40 degrees of inclination produces slightly more peak grip than 50 degrees, suggesting 40 degrees is possibly the optimum negative camber angle. The maximum lateral force at 40 degrees of inclination also occurs at a reasonable slip angle of about six degrees, similar to where most car tires (as opposed to round-section, motorcycle tires) produce maximum lateral force without inclination. The amount of slip angle required means that a car using 40 degrees of negative camber for maximum grip could still be controlled by the conventional method of steering via altering the toe angle of the front wheels (rotation about an axis normal to the road). If the maximum lateral force occurred at a nearly zero slip angle then a more complex steering system on both front and rear would be needed to eliminate slip angle and to control inclination in order to initiate the turn.

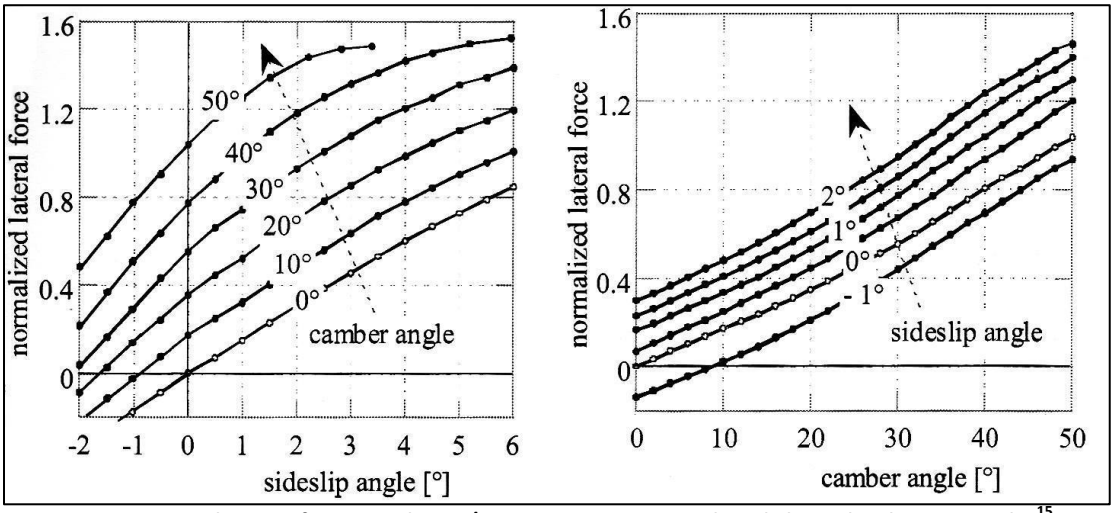

Figure 7: Lateral Force of Motorcycle 120/70-17 Front Tire at Combined Slip and Inclination Angles[15]

The plots of Figure 7 were made at a single vertical load. A more comprehensive test of combined inclination and slip angle was performed under the guidance of William F. Milliken while he was working on his MX-1 camber car and the vehicle dynamics behind it. This innovative test vehicle is shown in figures 8 and 9, showing its large negative camber angle and round-section tires, making it look like no other car on the road. With older, less high-performance tires it achieved greater than 1g lateral acceleration consistently, and with more modern Dunlop radials it achieved 1.3g[16], an impressive result for a machine with many compromises in order to have adjustability to run extensive vehicle dynamics tests. This was achieved with a negative camber angle of just more than 23 degrees, and a curb weight of 1,555 pounds distributed nearly equally between the front and rear axles. Results from tests of the original MX-1 bias-ply tires can be seen in figures 10 and 11.

[15] Cossalter, Vittore: Motorcycle Dynamics, 2nd ed., page 49
[16] Milliken, William F.: Equations of Motion, page 520

Figure 8: Milliken MX-1 Front View[17]

Figure 9: Milliken MX-1 Side View[18]

Figure 10 shows the lateral force generated by a motorcycle tire at a lighter load, while Figure 11 is at a 66% higher load. These plots show the increased lateral grip due to the addition of negative camber to slip angle at higher vertical loads. Camber values are reported as positive but represent the magnitude of the negative camber on the outside wheel. The dotted line represents the equilibrium state for a motorcycle without the rider hanging off to the inside of the bike and does not pertain to this discussion of four-wheeled vehicle dynamics.

[17] Photo from ultimatecarspage.com via Google Images
[18] Photo from joefenstermaker on flickr

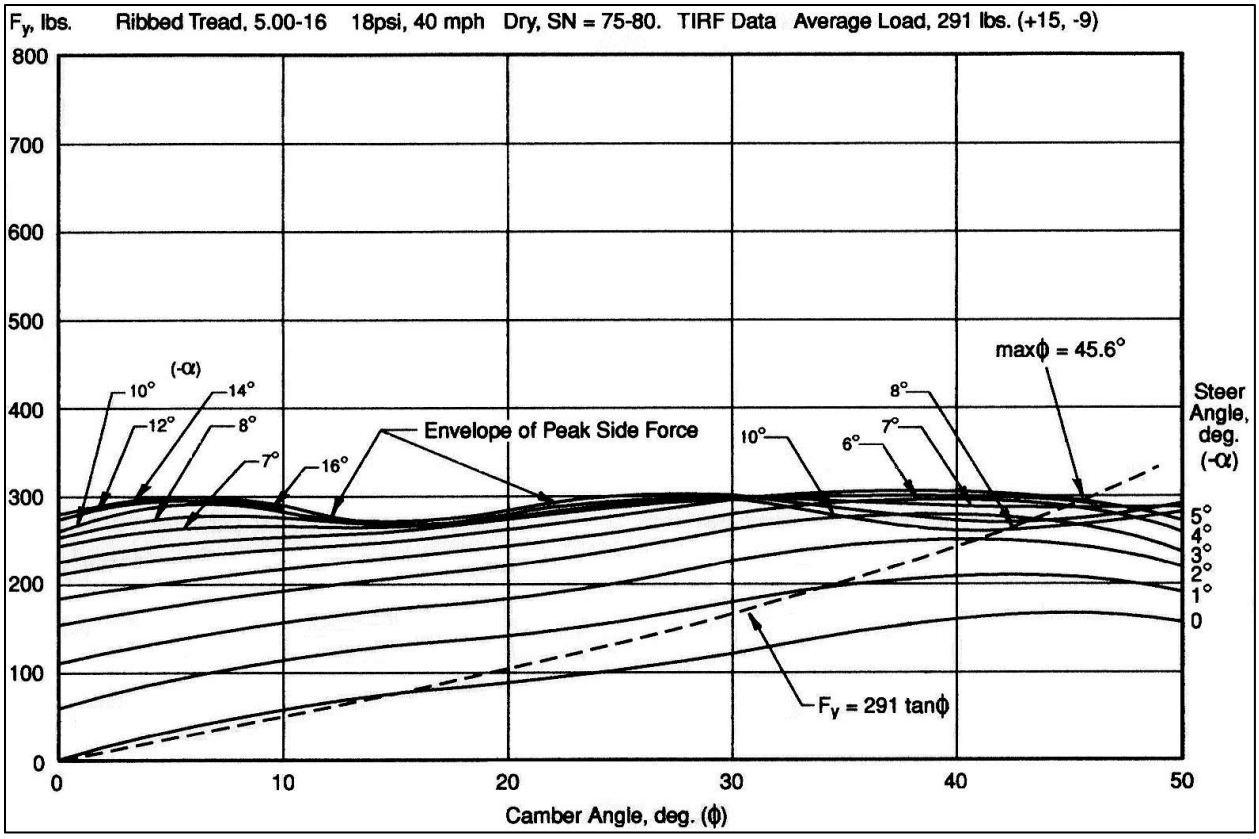

Figure 10: Lateral Force for Combined Camber and Slip Angles at Low Load (291 pounds) for 5.00-16 Bias-Ply, Ribbed-Tread Goodyear Eagle Motorcycle Tires[19]

The nonlinearity of the envelope of peak side force, particularly the decrease in grip between 5 and 25 degrees of inclination, is interesting. Based on the trend of lateral force against slip angle, one would expect a single peak, but the maximum lateral force increases again after 15 degrees of inclination and actually surpasses the first peak (near 5 degrees) at about 35 to 40 degrees of inclination. Since these tires had "ribbed tread" it may be due to the effects of tread blocks on the contact patch shape and area, as seen in Figure 5.

In Figure 11 there is only one peak but there is a distinct change in slope and curvature just after 25 degrees of camber. The peak grip still occurs at 40 degrees, similar to the highest peak in Figure 10. At 40 degrees of inclination the addition of slip angle increases maximum lateral force by more than 40%. The most significant point illustrated is that the addition of 40 degrees of inclination increases the maximum grip by 25% compared to a vertical tire.

[19] Milliken, William F.: Equations of Motion, page 521

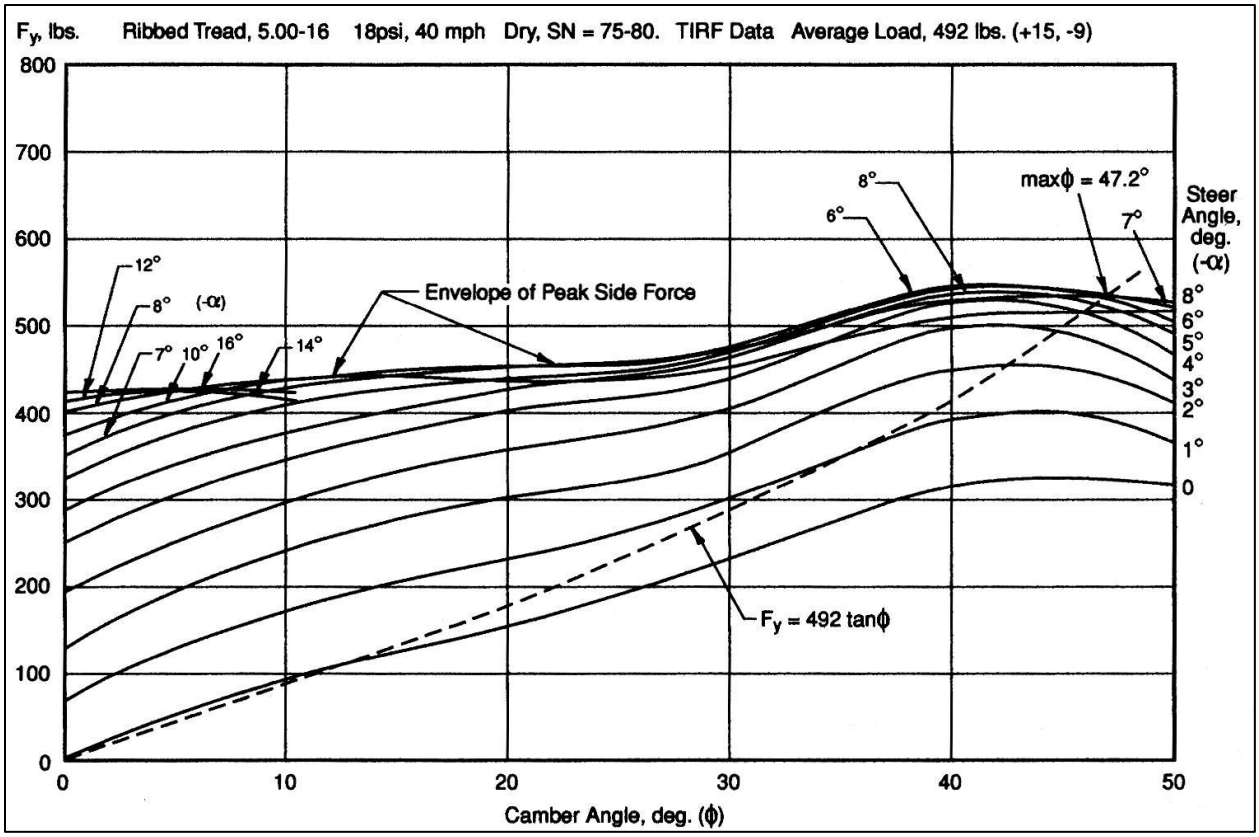

Figure 11: Lateral Force from 5.00-16 Bias-Ply, Ribbed-Tread Goodyear Eagle Motorcycle Tires at Combined Inclination and Slip Angles with Vertical Load of 492 pounds[20]

Based on figures 7, 10, and 11, the optimal inclination for the outside tire in a turn is about 40 degrees. Whether static camber of -40 degrees is optimal is not immediately clear because those figures do not show what the inside tire is doing. To determine the optimal camber, the behavior of tires under adverse inclination and light loads must be known.

If the trend of the maximum side force against camber angle in Figure 11 is extrapolated and assumed to be oddly symmetric about the intercept with the lateral force axis, then the inside tire looses as much lateral force coefficient (compared to zero camber) as the outside tire gains. Figure 10 shows, however, that at lower loads the effect of camber on maximum lateral grip is smaller. This behavior agrees with the way in which camber and slip angle distort the contact patch. Camber relies on vertical force to deform the tire out of round while the deformation due to slip angle is independent of load (though the amount of friction available to counteract that deformation does vary). Therefore, the inside tire gains lateral force coefficient when weight transfers off of it because the camber thrust is not fighting the slip angle force as much. Continuing the trend of peak side force seen in Figure 10 would mean that *the inside tire is not significantly hampered by adverse camber* and would likely not benefit enough from inclination into the turn to make a variable-camber system worth its weight and complexity. The load below which the leveling-off of maximum side force occurs is dependent on the particular model of tire but if it is true for the case of positive camber it would mean that a static camber configuration

[20] Milliken, William F.: Equations of Motion, page 522

would corner just as well as a tilting machine such as a motorcycle, even with less than 100% lateral weight transfer.

As found by William F. Milliken, lateral weight transfer increases the amount of lateral force which a pair of negatively-cambered tires can produce. This is the opposite behavior to traditional, vertical tires but is intuitive if one understands that the camber thrust of a tire is proportional to load. With a pair of negatively-cambered tires, even rolling straight-ahead, there will be a net lateral force if a disturbance causes one tire to be loaded more than the other since the camber thrust on one side increases and the thrust on the other side which opposes it will reduce. This net lateral force works to increase the lateral load transfer because of the mass center of the system being above ground level. As described above, however, the inside tire does not need to be completely unloaded to achieve maximum grip because at some point its lateral force becomes oriented into the turn. More load increases the force but less load increases the coefficient, so there should be an optimal, non-zero, load for the inside tire, unless the outside tire gains significant amounts of lateral force coefficient with more load, which is the opposite behavior of a normal car tire at small camber angles.

Interestingly, the maximum lateral force coefficient for a single tire at -40 degrees of camber increases by more than 5% (from 1.05 to 1.11) when vertical load is increased by 66% (from 291 pounds to 492 pounds). Those numbers are taking into account the tolerance on the load measurement and so may be higher or lower but still show positive load sensitivity. This means that the outside tire experiences a greater gain in potential lateral force than the increase in vertical load, the opposite of the conventional car tire behavior shown in Figure 3. Even if the increasing trend is weak, it is at least better than the decrease in lateral force coefficient with vertical tires. The vertical loads in Figure 3 are more than double those in Figure 11, however, so it is not conclusive whether normal tires would behave similarly to the cambered tires at lighter loads and if the camber tires would experience negative load sensitivity at much higher loads. The 900 pound load in Figure 3 would represent a small, road-legal sports car without aerodynamic downforce undergoing a high-lateral-acceleration turn which was causing nearly full lateral weight transfer.

It is clear from Milliken's work with the MX-1 and his subsequent analysis of the data that the gains in grip on the outside tire due to negative camber overwhelm the losses in grip on the inside tire due to its adverse camber, and if the loads are in the right range for the tires the inside tire likely gains grip. Fascinatingly, the beneficial effect of camber appears to be true even for the hypothetical case of zero load transfer. This conclusion is based on simulations which William F. Milliken and his associates performed after the extensive tests during the MX-1 program. The results of three simulations are shown in figures 12 and 13. The main point they convey is that a pair of negatively-cambered tires can produce more net lateral force with more lateral load transfer, while vertical wheels show the opposite trend (negative load sensitivity). Also apparent is that the normalized lateral force is higher at -40 degrees of camber than at -20 degrees, even at zero lateral load transfer (h/T=0).

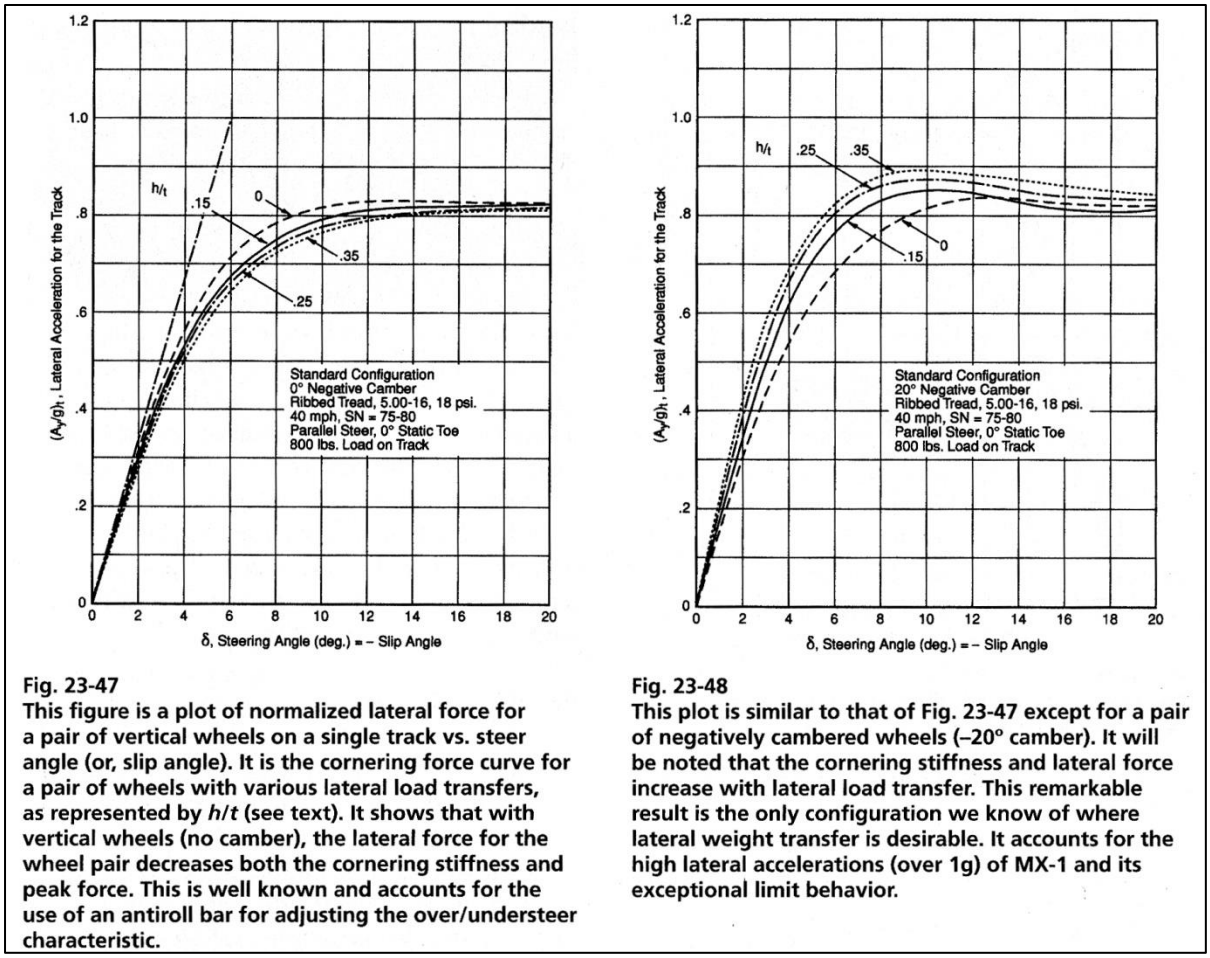

Fig. 23-47
This figure is a plot of normalized lateral force for a pair of vertical wheels on a single track vs. steer angle (or, slip angle). It is the cornering force curve for a pair of wheels with various lateral load transfers, as represented by *h*/*t* (see text). It shows that with vertical wheels (no camber), the lateral force for the wheel pair decreases both the cornering stiffness and peak force. This is well known and accounts for the use of an antiroll bar for adjusting the over/understeer characteristic.

Fig. 23-48
This plot is similar to that of Fig. 23-47 except for a pair of negatively cambered wheels (–20° camber). It will be noted that the cornering stiffness and lateral force increase with lateral load transfer. This remarkable result is the only configuration we know of where lateral weight transfer is desirable. It accounts for the high lateral accelerations (over 1g) of MX-1 and its exceptional limit behavior.

Figure 12: Simulation Comparing Effect of Lateral Weight Transfer on Total Lateral Force from A Pair of Tires With and Without Negative Camber

It can be seen by comparing the plots in Figure 12 and in Figure 13 that the lateral acceleration increases from about 0.825g to 0.925g when going from -20 degrees and -40 degrees, even without lateral load transfer. That is a difference of 12% and that difference increases to 15.5% at when lateral weight transfer is added, even though that transfer of load is only about 75% complete for the highest lateral acceleration in Figure 15, meaning there is still a decent safety margin against overturning. This supports the theory that -40 degrees of camber is best for lateral acceleration, despite Milliken using only -23 degrees on the MX-1, a value dictated largely by drivetrain restrictions (he used a Volkswagen transaxle and swing axles), a major issue for camber-car designers. Taller tires and a lower ride height can allow two constant-velocity joints to be used, sharing the angularity. More ground clearance both improves the car's ability to negotiate rough roads and increases the mass center height, increasing the lateral load transfer and therefore the lateral acceleration, so it is a delicate balance and is an area to concentrate on mechanical creativity to find a better solution.

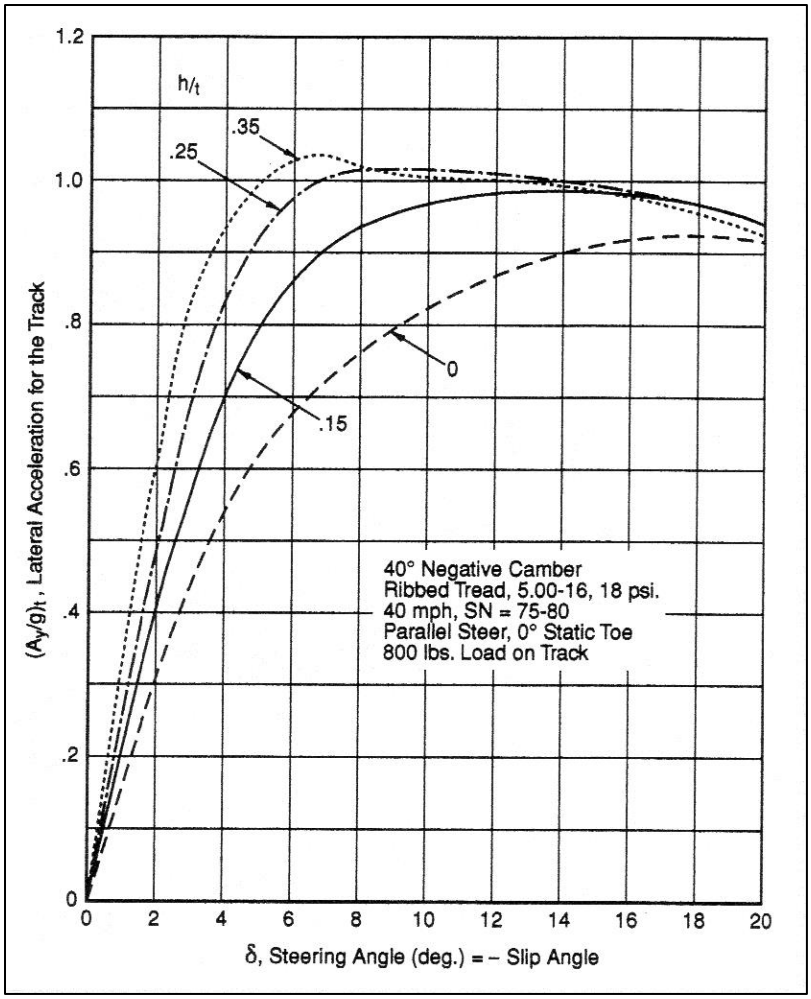

Figure 13: Simulation of Lateral Force for Pair of Tires at -40 Degrees of Camber Showing More Lateral Force than -20 Degrees

Round-Section Tires vs. Square-Shouldered Tires

The beneficial effect of camber appears to be associated most strongly with motorcycle (round-section) tires since large camber angles are necessary for significant gains and car tires with their rectangular section are not suited to camber angles much greater than 5 degrees. Figure 14 shows car tire data which show load sensitivity for small negative camber angles (5 degrees or less) and neutral load sensitivity for 10 degrees of negative camber. This data was taken at 7 degrees of slip angle, which produced nearly the peak lateral force at each camber angle. The tires in that test were 225/70R15 car tires, which are radial tires with relatively high aspect ratios (tall sidewalls which would be less stiff than short ones) and so would be more tolerant to large camber angles than wider, lower-profile tires. Extrapolating the trend, one would expect positive load sensitivity above -10 degrees of camber but car tires cannot use larger camber angles because the tire ends up riding on the stiffer shoulder, shrinking the contact patch and putting more pressure on it, which decreases grip. This is evidenced by the reduction in peak lateral force coefficient at -10 degrees of camber versus -5 degrees of camber, though -10 degrees produced more lateral force than 0 degrees at high loads and equal force at low load.

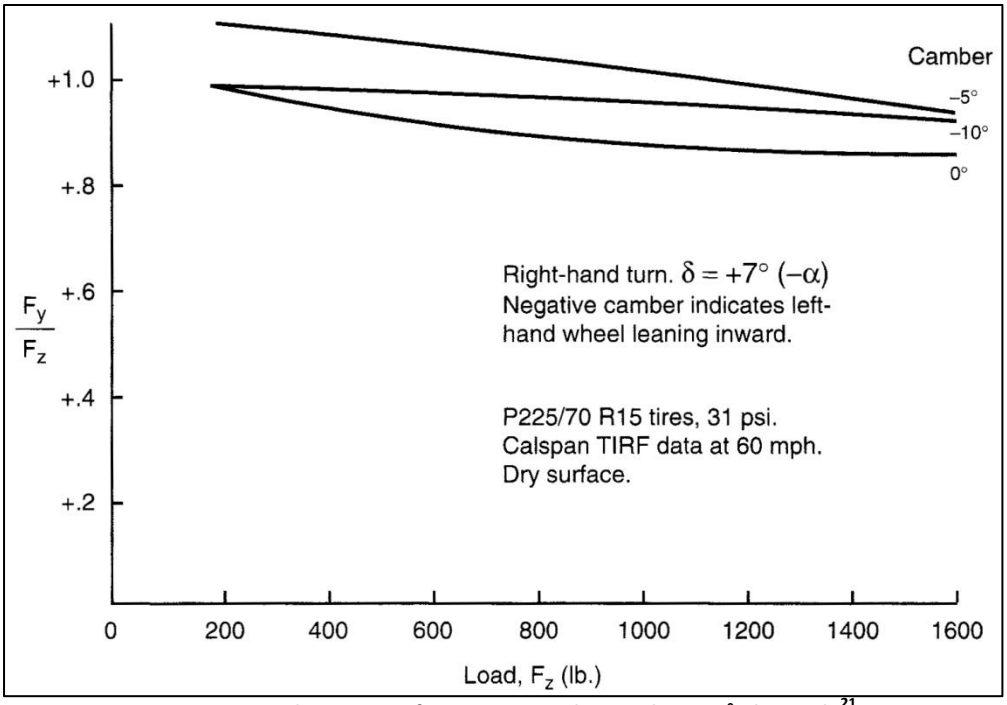

Figure 14: Load Sensitivity for Various Camber Angles at 7˚ Slip Angle[21]

Figure 15 is a plot of maximum lateral force versus camber angle at high load for three different round-section tires. This data was recorded by Albert G. Fonda, who made a sort of tilting go-kart where the rider leaned into the turn. William F. Milliken was impressed by its high lateral acceleration (1.2g) but wanted to avoid its shortcoming: what motorcyclists term "high-siding". If the kart was turning and encountered a lower-friction spot it would benignly "lay down" and slide with increased inclination, but when it encountered a high-friction surface again it tended to capsize to the outside of the turn and throw the rider out.[22] The tires Fonda tested for his 1956 paper "Tire Tests and Interpretation of Data" (published just after William F. Milliken patented his camber car idea) were not for the kart, however, being much too large for it but suitable for an automobile. These tires are not specified as motorcycle tires in the paper and it is mentioned in the conclusion that an expanded test could include motorcycle tires at 30 to 50 degrees of inclination, leading to the deduction that these are simply 1955 vintage automobile tires which were narrower and more rounded in section than today's "high performance" rubber. Once shaved of their tread (in order to remove the effects of tread pattern seen in Figure 5) these old tires (shown in Figure 16) appear to have a similar section to tires specifically made for motorcycles and the tires are also bias-plies, which are generally stiffer than radials in certain modes and so see more benefits from camber.[23] These car tires should therefore have behaved similarly to motorcycle tires, however the high load of more than 900 pounds at which the tires were tested is not representative of motorcycle loading.

[21] Milliken, William F. & Douglas L.: Race Car Vehicle Dynamics, page 54
[22] Milliken, William F.: Equations of Motion, pages 496,497
[23] Milliken, William F. & Douglas L.: Race Car Vehicle Dynamics, page 405

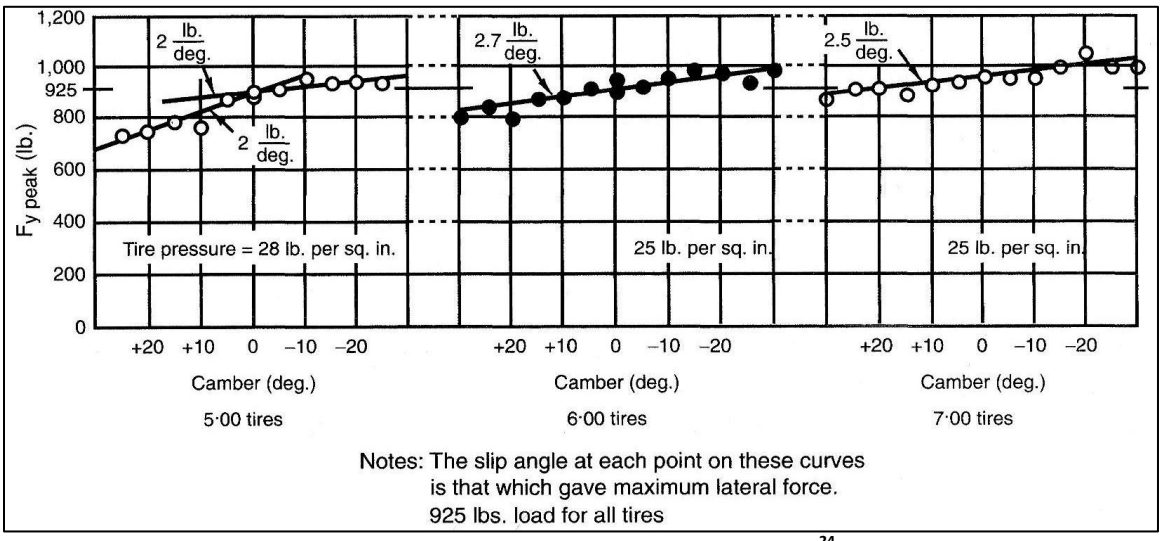

Figure 15: Peak Lateral Force vs. Inclination Angle[24]

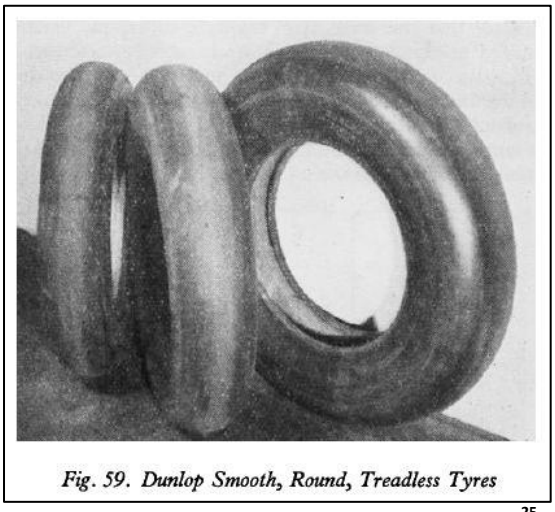

Figure 16: Tires Used to Generate Data for Figure 9[25]

The slip angle varies between data points in Figure 15 because the steering angle was adjusted for maximum lateral force at the specified camber angle. The plots show that the benefits of camber extend to tires not specifically for motorcycles, as extrapolating the trend lines to 40 degrees of camber produces a gain in lateral force coefficient of more than 10 percent. The plots also show that the trend of increasing lateral force with negative camber extends to the case of positive camber when the load is high enough. Lateral grip appears to be degraded by positive camber by about the same amount as negative camber improves it, though some tires may show a more nonlinear trend and have a steeper reduction in side force with positive camber, as seen in the leftmost plot of Figure 15.

[24] Graph as presented: Milliken, William F. & Douglas L.: Race Car Vehicle Dynamics, page 49
Original data and graph: Fonda, Albert G.: "Tire Tests and Interpretation of Data"

[25] Fonda, Albert G. "Tire Tests and Interpretation of Data"

Identically-sized 100/85-R10 PMT racing scooter rear tires are being used on all four corners of the 2013 Formula Electric car as have been used previously. Being round-section, they can support larger camber angles. The PMT's are about three pounds lighter than the smallest Hoosier square-section racing tires available and have less aerodynamic drag than the wider Hoosiers or taller, full-sized motorcycle tires.

The scooter tires are radials, which Milliken says shows less of the effects of camber than bias-plies[26] due to their greater lateral compliance, but being made for motorcycles should be stiffer than car radial tires, since the lateral stiffness and camber stiffness of the tires significantly affects the stability, safety, and performance of a motorcycle.

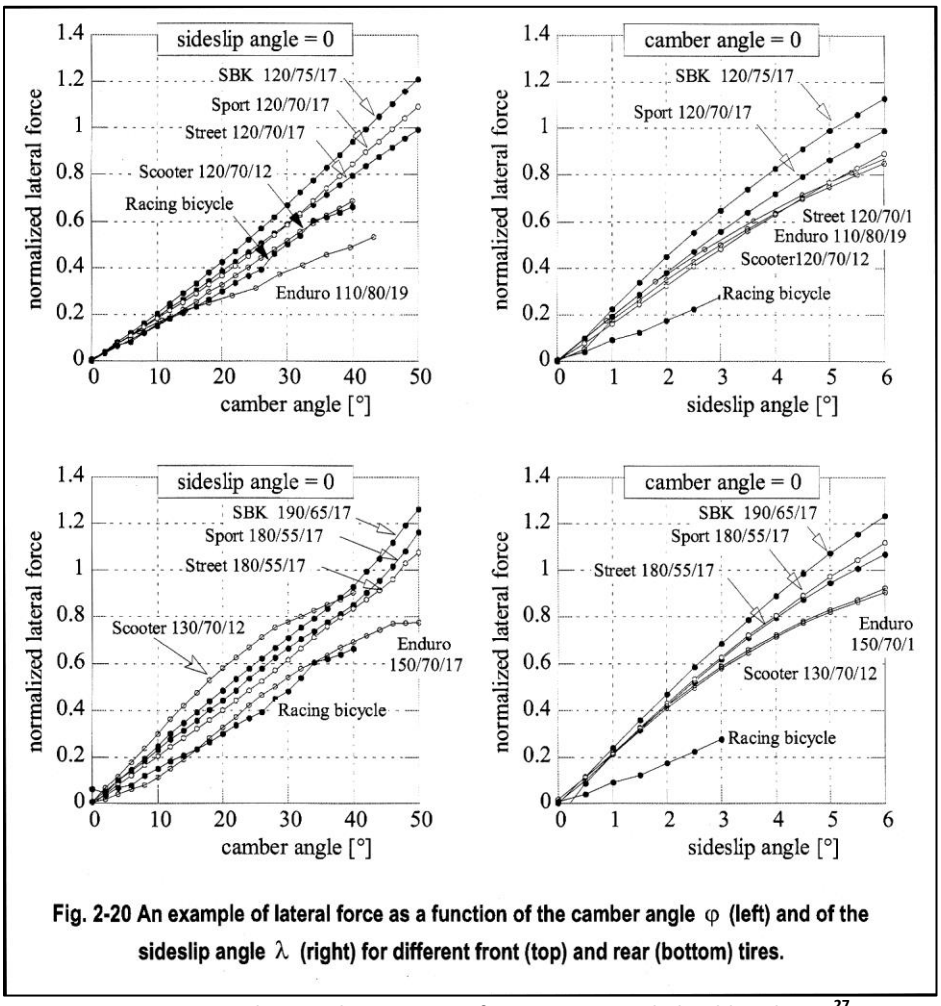

Fig. 2-20 An example of lateral force as a function of the camber angle φ (left) and of the sideslip angle λ (right) for different front (top) and rear (bottom) tires.

Figure 17: Lateral Force Characteristics for Various Round-Shouldered Tires[27]

The scooter tires can be expected to behave similarly to the other round-section tires which generated the data used to develop the camber tire model used here. Figure 17 shows that ordinary scooter tires generally have a linear relationship between camber thrust and slip angle

[26] Milliken, William F. & Douglas L.: Race Car Vehicle Dynamics, page 405
[27] Cossalter, Vittore: Motorcycle Dynamics, 2nd ed., page 54

similar to motorcycle tires. Due to the more intense use which racing scooters receive, they would logically be closer to the motorcycle or racing motorcycle (SBK) tires than the treaded scooter tires. The deviations of the enduro tires can be put down to their greater siping allowing tread blocks to squirm because of the change in number of tread blocks in contact with the road as camber increases, as seen in Figure 5. The rear tire data for the enduro, scooter, and racing bicycle are further from the motorcycles' than the front tire data for those vehicles are. This may be due to construction (ply orientation and composition) and rubber compound. The slip angle data does not extend far enough to show a peak and drop-off in lateral force because single-track vehicles do not typically corner at slip angles greater than those shown in the figure.

Square-shouldered, wide tires have an advantage in being able to have larger contact patches, which due to load sensitivity effects increases grip. When the tire is deformed under vertical load the contact patch is formed and the integral over the patch of the pressure on each differential piece of area must equal the normal load on the tire. Stiffer sections of the tire bear more pressure for an equal displacement. With wide, square-shouldered tires the contact patch ends up with the same area as a narrower tire with the same tire pressure and stiffness would have but the footprint is wide and short instead of circular or long and thin. The shorter patch means there is less deformation out-of-round and so less heating of the rubber. This, in turn, means that softer rubber can be used which increases grip even further. Lower pressures could also be run to return to the same level of deformation out-of-round but with a larger contact area.

Because round-shouldered tires can make more use of the benefits of camber, they are preferred for best lateral grip. Conventional, wide car tires are expected to be better for longitudinal grip.

Longitudinal Force

Longitudinal forces (for propulsion and braking) arise, like lateral forces, from the deformation of the contact patch. In this case the deformation is in line with the wheel heading and velocity vector. Because there is a limit to the amount of distortion in any direction the contact patch can support, there is a limit to the amount of force the tire can produce in any direction. This means that the magnitude of the ground-plane force vector from the tire is limited such that maximum lateral force and maximum longitudinal force cannot happen at the same time. This is visually represented by a "friction circle" or g-g diagram, which is usually more elliptical than circular. Such a diagram is shown in Figure 18, which is distorted by unequal scales on the two axes. Of note is that this data was recorded from the ace driver Ayrton Senna during practice for the Australian Grand Prix in 1987.

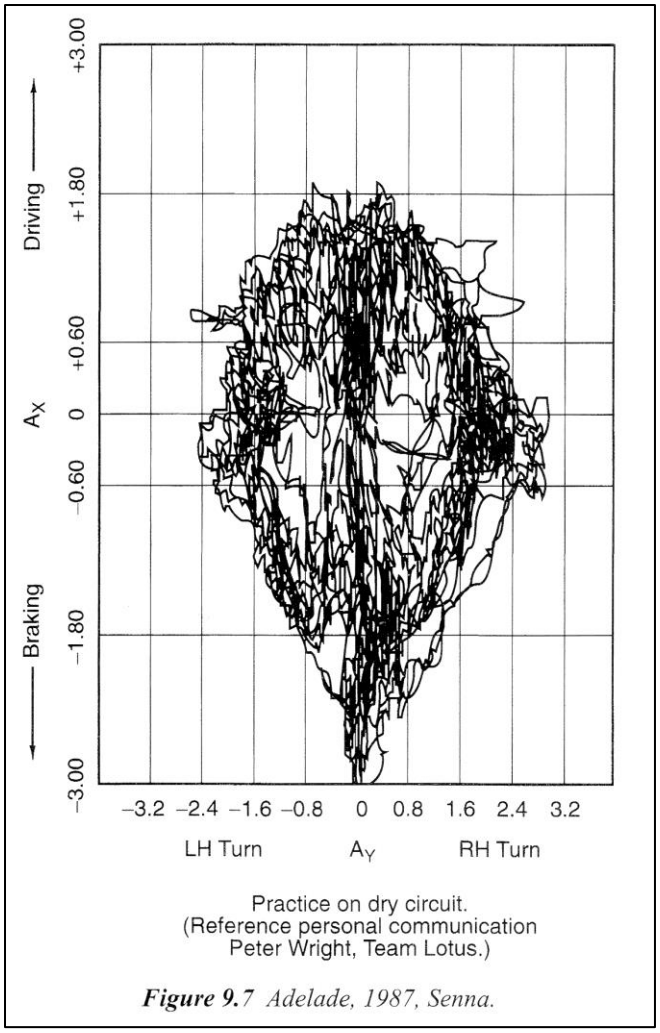

Figure 18: Friction "Circle" from Senna's Lotus at 1987 Australian GP[28]

In g-g diagrams, the longitudinal acceleration is graphed versus the lateral acceleration. The points are each simply the outputs from an accelerometer at the center of mass (or corrected to reflect the accelerations at the center of mass) at an instant in time. They give an idea for how much total performance a tire and vehicle can achieve. A tire or vehicle with a more rounded outer envelope to the graph should be easier to drive and more forgiving. The maximum lateral and longitudinal forces can have the theoretical advantage depending on the track, but generally the tire with the most area inside the "circle" will perform best over a lap of a race track.

Static camber reduces the maximum acceleration and braking which the car can achieve because lateral force is always being produced, even when there is no slip angle or lateral load transfer. The opposing lateral forces are using-up some of the grip of the tires and therefore leaving some potential performance unrealized. All-wheel-drive could be used to regain some

[28] Milliken, William F. & Douglas L.: Race Car Vehicle Dynamics, page 355

traction, but this is at the cost of extra weight and still the camber would be outperformed by an all-wheel drive car with vertical tires.

Induced Drag

Generating lateral force by means of slip angle has a drawback in the form of induced drag, which comes about because the lateral force produced is perpendicular to the wheel heading and not the direction of wheel travel. Therefore, a component (sine of the slip angle) of the lateral force is directed opposite the velocity vector, and only the remaining portion (cosine of the slip angle) is actually useful for lateral acceleration. The component opposing the velocity slows the car down or requires engine power to overcome, using more fuel and reducing lateral grip on the drive wheels through the friction circle effect. Induced drag is a significant problem, as seen by a sample calculation which appears in Race Car Vehicle Dynamics for the induced drag on an Indy car. This force turns out to be 225 pounds, which requires 132 horsepower to overcome at the 220 mph speed it is travelling.[29]

Camber thrust does not cause induced drag because the wheel heading aligns with the wheel velocity and, thus, all the lateral force is used for turning and less engine power is needed to maintain speed, which saves fuel and increases the grip on the driving wheels. All this could be offset if the rolling resistance of a tire increases with inclination, however. Fortunately, this does not appear to be the case.

The moment which opposes the rolling of a non-driven, non-braked wheel varies with the cosine of the inclination angle, meaning that rolling resistance actually decreases with camber angle. This is true for small inclination angles up to 10 degrees, where there is less than 2% difference compared to setting the value of the cosine function equal to unity. This is well within the scatter in tire data from test machines. Slip angle also causes similarly small changes in rolling resistance.[30] If the cosine trend continues to large camber angles, or even if the rolling resistance stays nearly the same, then the elimination of induced drag stands as a great benefit to using inclination to achieve high lateral force while reducing slip angle.

Effects of Camber on Vehicle & Suspension Design

In Figure 3 it can be seen that the slip angle at which peak lateral force occurs increases at higher loads. This is the reason reverse Ackermann steering systems exist. Geometrically, the inside front wheel in a turn is on a smaller radius than the outside and should be steered more. This condition is called Ackermann steering, diagrammed in Figure 19. Because of the lateral weight transfer and load sensitivity effects, however, reverse Ackermann produces more lateral acceleration for conventional cars than normal Ackermann but comes at the expense of high rolling resistance at low lateral accelerations due to scrubbing the inside tire across the road.[31]

[29] Milliken, William F. & Douglas L.: Race Car Vehicle Dynamics, pages 67-69
[30] Milliken, William F. & Douglas L.: Race Car Vehicle Dynamics, page 73
[31] Milliken, William F. & Douglas L.: Race Car Vehicle Dynamics, page 404

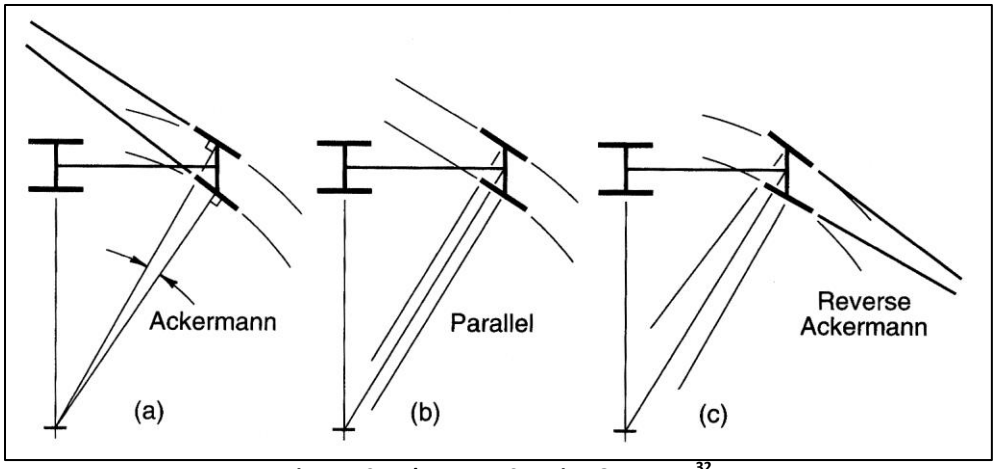

Figure 19: Ackermann Steering Geometry[32]

A camber car should use conventional Ackermann because the inside wheel needs more slip angle to counteract the adverse camber. Increased slip angle does result in more induced drag but the inside wheel generates less force than the outside due to the lateral weight transfer so the extra drag is insignificant. The need for more slip angle at low camber is seen in Figure 10, and the trend can reasonably be expected to continue to the case of inclination out of the turn.

The effect of scrub radius combined with caster angle causes a load transfer from one diagonal to another when steering is applied. Scrub radius and caster angle definitions are shown in Figure 20. Scrub radius is the distance from where a line projected along the steering axis intersects the ground and the centroid of the contact patch. It is the lever arm for longitudinal forces such as those from an impact with a bump in the road. A larger scrub radius decreases steering effort at slow speeds because the tire is able to roll around the steering axis rather than the contact patch twisting. Caster angle is the tilt of the steering axis in side view and is usually used to increase a quantity called the mechanical trail, which is the lever arm for lateral forces. Trail causes the steering weight to increase with lateral acceleration and increases the self-centering effect as speed increases. Caster also adds inclination to both the inside and outside wheel when steering is applied.

[32] Milliken, William F. & Douglas L.: Race Car Vehicle Dynamics, page 714

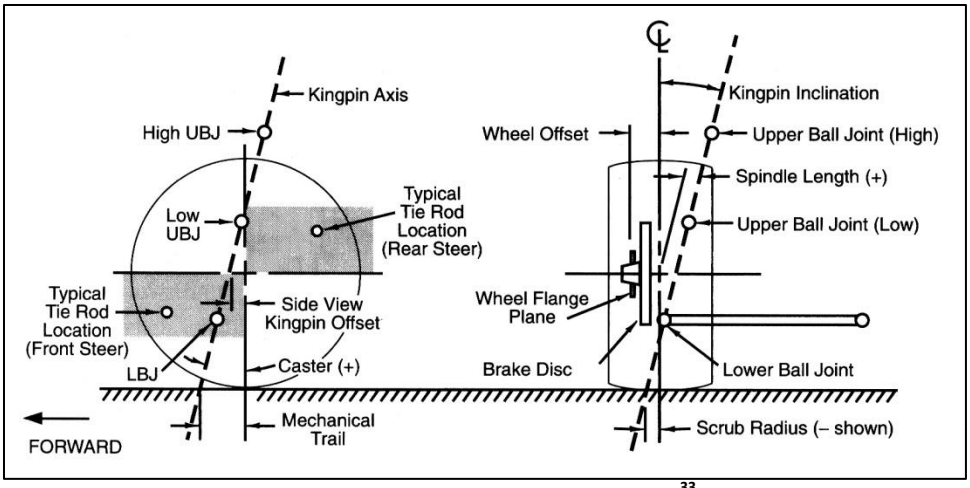

Figure 20: Steering Geometry Definitions[33]

Due to the effect of negative camber, the weight transfer caused by the caster and scrub radius creates either an understeer (positive scrub radius) or oversteer (negative scrub radius) yaw couple. Because this is a couple and not a simple moment due to increasing the lateral force of one end of the car, there is no significant benefit to caster jacking other than tuning turn entry behavior, and to a lesser degree steady-state, behavior to suit driver preferences. The magnitude of this yaw moment is limited by the arm strength of the driver unless a slow steering ratio or power steering is/are used. The sense of the yaw couple is also affected by how much the car relies on camber, since lateral weight transfer degrades the lateral force of vertical tires but increases the grip for camber tires.

Static negative camber on the front tires causes a lateral force and yawing moment that tend to counteract the yawing moment due to an impact with a bump in the road on one wheel. When the wheel hits the bump the increase in normal load on the tire increases the camber thrust on that corner and so produces a net lateral force at the front and a corresponding moment about the center of mass. The lateral force causes more lateral weight transfer, however, and this increases the lateral force such that the car tends to move away from the bump. The effect of negative camber on the rear tires is therefore stabilizing since the lateral force is in the same direction as in the front but the moment arm is reversed. Milliken notes that, from his experience with the MX-1, static toe-out of about 10% of the static camber angle tends to stabilize the wandering of a camber car.[34]

A camber car sees transient response benefits from faster lateral weight transfer. One way to do this is by sending forces through the suspension members themselves, rather than the springs, since the links are much stiffer than the spring on cars not using significant amounts of aerodynamic downforce. The kinematics of the suspension can be set to achieve this load path by placing the instant center of rotation in the correct place, which then puts the roll center at the right height above ground.

[33] Milliken, William F. & Douglas L.: Race Car Vehicle Dynamics, page 710
[34] Milliken, William F. & Douglas L.: Race Car Vehicle Dynamics, page 406

The instant center of rotation is the point about which a rigid body (the upright) is rotating at an instant in time. Perpendiculars to the velocity vectors on three or more points of the rigid body can be used to find the instant center, but the analysis is usually broken up into two planar representations of the suspension: front view and side view. An example of the instant center in front view is shown in Figure 21.

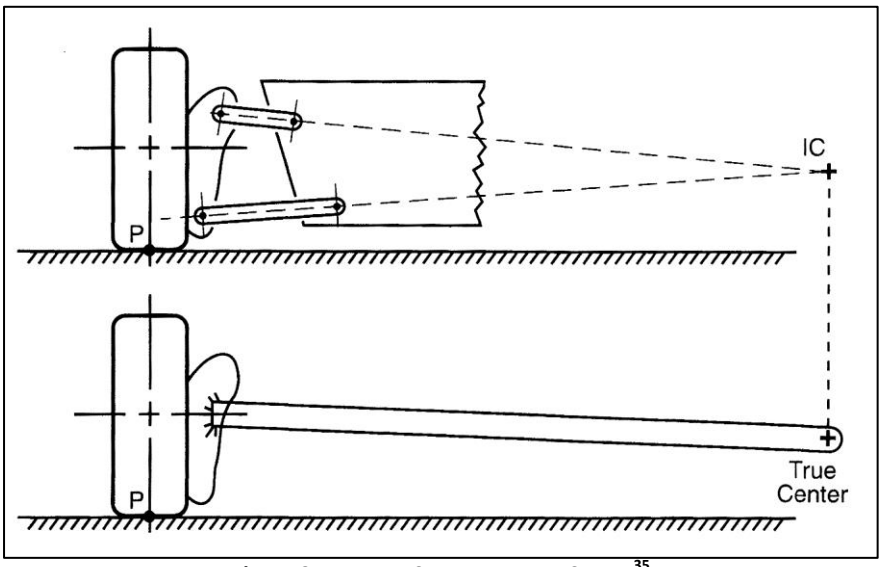

Figure 21: Instant Center vs. True Center[35]

The instant center will move as the wheel displaces on most suspensions. A swing-axle suspension, like that shown in the lower half of Figure 21 has an instant center that is also a true center and which does not move. There is only one suspension link in front view and the upright is rigidly attached to it so that it is constrained to rotate about one physical point. The advantage of a four-bar linkage like that in the upper half of Figure 21 is clear to see: it is much more compact while having the exact same kinematics for that instant in time. It can be much lighter and more rigid because there are no bending stresses and because the links are shorter, increasing buckling resistance. The construction of the instant center for suspensions with tension-compression members consists of drawing lines through those members and finding their intersection point. This is because the velocity of the upright where those members attach must be perpendicular to those (assumed rigid) links. The instant center affects the distribution of forces in the mechanism; in other words which links have more loading.

When the instant center is drawn for both sides of the car, another point can be drawn. This point is the roll center and represents the coupling point for the sprung and unsprung masses. In other words, a force applied at the roll center causes no roll of the chassis. A roll center is shown in Figure 22.

[35] Milliken, William F. & Douglas L.: Race Car Vehicle Dynamics, page 611

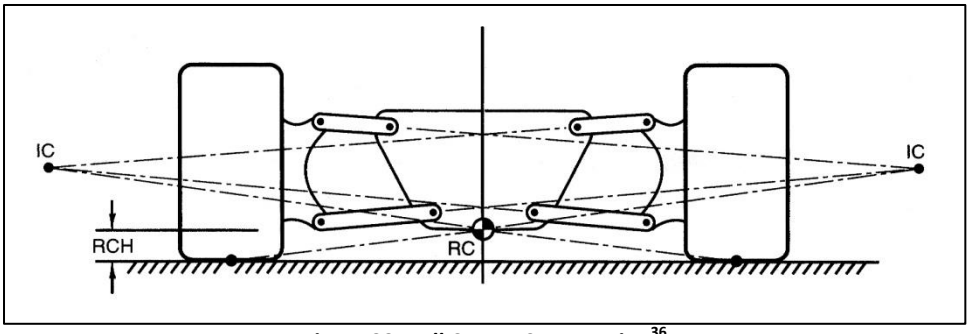

Figure 22: Roll Center Construction[36]

The roll center moves vertically and laterally with suspension displacement since the instant centers do as well. The roll center is found by drawing a line from the center of the contact patch to the instant center of that wheel. What this is mimicking is the true center of a swing axle suspension, where there is a force applied by the tire to a link with a pin connection at one end. Because of this end constraint it can transmit only forces and no moments to the chassis on which it is anchored. The true center is always above ground and since the contact patch is always on the ground the load path does not align with the load. In order to transmit the lateral load component through the slanted load path there must also be a vertical component, called a jacking force. This is shown in Figure 23.

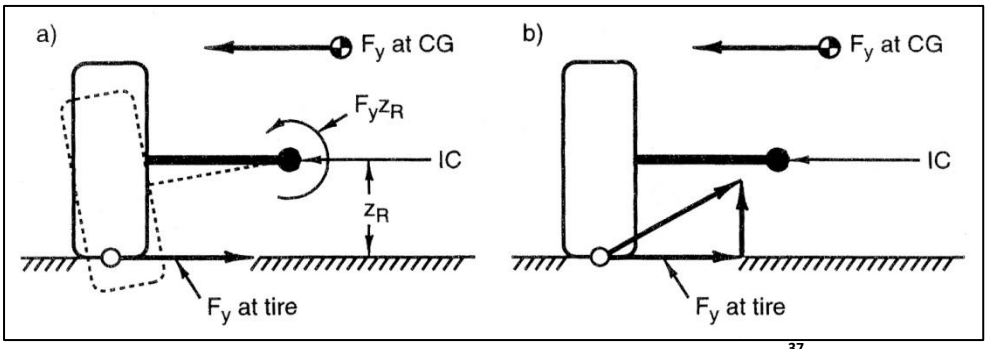

Figure 23: Vertical Jacking Force Due to Applied Lateral Force[37]

The instant center is shown above ground but can be below ground, as can the roll center. In that case the jacking force from the outside wheel is downwards. The jacking force on the inside and outside wheel would largely cancel if the two tires produced the same lateral force, but this is not the case due to lateral weight transfer, especially on a camber car. Because of this, the sprung mass sees a net vertical force with the direction of the jacking force of the outside wheel (usually). This net vertical force must be reacted by an equal displacement of the springs on both the inner and outer wheels. There can still be net compression on the outside and extension on the inside, but there is more extension and less compression than if the roll center was at ground level (meaning no jacking forces). Care must be taken to not let the sprung mass rise too much due to the jacking forces, lest the car overturn. This can be combated by using stiffer springs, which do not need to displace as much to absorb the jacking forces. These stiffer

[36] Milliken, William F. & Douglas L.: Race Car Vehicle Dynamics, page 614
[37] Milliken, William F. & Douglas L.: Race Car Vehicle Dynamics, page 615

springs further speed lateral weight transfer if they also contribute to roll stiffness and are not the "third spring" acting only in heave (both wheels moving equally).

For the case of the roll center above ground the sprung mass moves up. The jacking force also has a complimentary reaction at the tire which adds load and therefore counters lateral weight transfer (when the roll center is above ground). This reduces the amount of load transfer the springs must support, thereby reducing body roll. Because of this effect the roll center can be used as the pivot point of an inverted pendulum consisting of the sprung mass of the car at the end of a massless rod which is equal in length to the distance between the mass center height and roll center height. The centrifugal inertia force is applied to the mass center and the tire forces are applied to the roll center, causing a roll couple. If the roll center and mass center coincide there is no roll, if the mass center is higher than the roll center the sprung mass rolls to the outside of the turn, and if the mass center is lower than the roll center the sprung mass leans into the turn.

Since jacking forces are transferred through the suspension links they react faster than elastic weight transfer (through the springs). Geometric weight transfer (through the links) therefore, can be used to speed transient response on a camber car which reacts favorably to lateral weight transfer. The jacking effect of a roll center above ground can also be used to raise the mass center for more total lateral weight transfer in steady-state cornering, but this rise must be kept in check so that the car does not capsize.

William F. Milliken did not like high roll centers on the MX-1 because they caused so much jacking that the camber was severely reduced, compromising the handling. This can be countered by stiffer springs, however. The other reason he did not like the high roll center was because a high roll center usually comes with a very short front-view-virtual swing arm length. This means that the instant centers are nearer to their respective wheels and the shorter radius means more camber change when the wheel is displaced vertically. If the front-view swing arm length is equal to half the track width, then there is no change in inclination relative to the road on either tire when there is pure body roll (inside and outside wheels displaced equally and opposite). If the front view swing arm length is shorter, then there is inclination gain on both inside and outside wheels- in other words the inside wheel loses negative camber and the outside wheel gains it. This sounds good but contributes to poor rough road handling and increases gyroscopic kickback through the steering wheel. A swing arm longer than half the track width loses inclination but is better over bumps. Milliken did not like large camber gain when he performed a turn reversal maneuver[38], which means starting out turning in one direction and then turning immediately in the other direction. Presumably this was because of gyroscopic effects as the car rolled, but this was tamed with a steering damper and a droop-limiting device which caused Milliken to be surprised at how well the car handled rough roads despite the short swing arm. Optimal roll center height is still a compromise between faster lateral load transfer and rough road handling (steering) effects, along with how stiff the springs can be made to control jacking without being unduly harsh over bumps.

[38] Milliken, William F.: Equations of Motion, page 517

Transient Response

When a step steering input is applied to a tire there is a delay before the steady-state lateral force is reached. This first-order delay is called relaxation length and represents how far the tire must roll to achieve full lateral force. According to Cossalter the relaxation length to slip angle for motorcycle tires is generally between 0.12m at 20kph and 0.45m at 250kph, increasing slightly with load.[39] He then states that the relaxation length for camber thrust is much less, and has been shown in some tests to be almost negligible.[40] Pacejka, however writes that the relaxation length for camber is about equal to the one used for slip angle and on the order of magnitude of the wheel radius,[41] but this appears from context to be referring to conventional car tires with squared-off shoulders.

If the response time to camber for round-section tires is negligible, then the incomplete block diagram shown in Appendix A gives a starting point to model the transient response of a static-camber car or a conventional car. Tire properties, vehicle mass properties, and suspension settings must be determined before it could be used to provide transient response estimates. The model assumes symmetrical camber gain on bump and rebound. For an operational model, it is strongly suggested to break the car into four tires rather than front and rear axles, so that all the nonlinear effects of load and camber can be taken into account.

The camber car responds faster because it has more paths which increase lateral force. Elastic weight transfer, if the car is stiff enough, can help reduce the time to steady-state by using the lateral force generated by the front tires to aid the rears. The distance from the front tires to the mass center will be greater than the mass center height, however, so the yaw acceleration will be greater than the roll acceleration and the yaw displacement should therefore increase quicker than roll angle. Therefore the rear slip angle may develop quickly enough that the benefits of camber would not be significant.

Roll damping, producing velocity-dependent forces, begin sooner than the elastic weight transfer and potentially sooner than the yaw displacement. Once a net lateral force is present the geometric weight transfer produces a positive feedback in a camber car configuration, speeding the lateral force response time on both axles.

Because camber cars begin making lateral force on the rear axle sooner than a conventional car they reach yaw equilibrium sooner and should feel "tighter" on turn entry (less oversteer) than a conventional car. A similar affect can be obtained on a car with vertical tires by steering all four wheels. In this case the rears would need to turn in the same sense as the fronts. Many premium automakers today employ small amounts of active rear-wheel steering. These systems usually vary the phase of the rear wheel steering as speed changes. For slow speeds the rear wheels turn opposite the front to enable a tighter turning radius for parking lot maneuvers. As speed rises, the rear wheels turn less relative to the fronts until they begin to turn in the same direction at high speeds. This speeds the lateral force response from the rear axle, but by

[39] Cossalter, Vittore: Motorcycle Dynamics, 2nd ed., page 56
[40] Cossalter, Vittore: Motorcycle Dynamics, 2nd ed., pages 58
[41] Pacejka, Hans B.: Tire and Vehicle Dynamics, 3rd ed., page 22

applying the input earlier rather than reducing relaxation length. This type of in-phase rear-wheel-steering also creates an understeering moment to make the car feel more stable to most drivers. Passive rear-wheel-steering, as is often done on multilink rear suspensions via body roll, do not speed transient response as much as active systems do because it takes time for the sprung mass to roll. The passive rear-wheel-steer delay has the same drawback as a passive dynamic camber system.

Milliken writes that the MX-1 had a time to 90% steady state of 0.182 seconds and that response time near maximum lateral acceleration was short and desirable.[42] Corrections for rear-end breakaway were necessary to reach maximum lateral acceleration but this was possible for sustained periods so the car was still stable enough despite fast response times. The response time quoted for the MX-1 on antiquated, treaded tires is only 75% longer than that for a 1993 Grand Prix car, if the example calculations in Race Car Vehicle Dynamics are based on reasonably accurate tire properties.[43] The MX-1 was therefore closer to a modern racing car in terms of response than it was to contemporary road cars. Camber cars are therefore at least as good in transient response as conventional cars, if not better.

Conclusions Regarding Vehicle and Suspension Design

For maximum steady-state lateral acceleration and fastest transient response, a car using round-section tires at a camber angle of -40 degrees is best.

Track width should be as narrow as practical while still achieving benign roll center behavior and the desired amount of suspension travel. Benefits of a narrow track include improved rough-road handling due to smaller yaw moment arms for impact forces[44] and less steering input needed to negotiate slaloms (the track effectively becomes wider). The mass center should be placed low enough that the car does not capsize except in extreme situations but high enough to increase lateral load transfer. Track width adjustments can be substituted for mass center height in order to reduce the total mass of the vehicle, which can be increased if extra chassis members are required to raise the mass center. Wheelbase should be kept short (but greater than the minimum 60 inches) for an FSAE car or any car which will be negotiating lower-speed, tight turns and need the maneuverability but the wheelbase should be long enough to achieve the desired front-to-rear weight distribution. A longer wheelbase increases directional stability and reduces longitudinal weight transfer, aiding braking but hampering acceleration.

A good ratio of mass center height to track width to design with initially is 0.25, which is where diminishing returns in maximum lateral grip appear in the Milliken simulations of Figure 13. This ratio results in a maximum (limited by inside wheel lift) lateral acceleration of 2g, found using the formula $a_{y,\max} = \left(\frac{2h_{cg}}{T} \right)^{-1}$, where $a_{y,max}$ is the maximum lateral acceleration in g, h_{cg} is the height of the mass center, and T is track width (the same units of length must be used to measure both the mass center height and track width). This formula is derived from a front-view

[42] Milliken, William F.: Equations of Motion, page 520
[43] Milliken, William F. & Douglas L.: Race Car Vehicle Dynamics, page 257 & 258
[44] Milliken, William F. & Douglas L.: Race Car Vehicle Dynamics, page 408

free body diagram of the car as a rigid body and summing moments about the outside tire. The moment arm for the inertial force is the mass center height and that for the weight is half the track width. For a Formula SAE racecar without aerodynamic aids, 2g is more than the tires can support and so gives a margin of safety against tipping over. In order to pass the 60 degree tilt test during tech inspection, corresponding to a lateral acceleration of 1.7g, the h/T ratio must be less than or equal to 0.285. A benefit to being able to use a higher mass center is that the ground clearance can be increased in order to clear bumpier or steeper roads as might be found on a rally stage on a mountain road.

Theoretically, more than 2g of lateral acceleration can be achieved with an h/T ratio of 0.25 if aerodynamic devices producing downforce are used. These could be either conventional wings or a wing split along the centerline of the car and using actuators with a control system to keep the load on the inside tire near zero while also preventing the car from overturning. This active system should never create lift as this reduces the total normal force on the tires and so also the lateral force capability. At low speeds, corresponding to tight turns, aerodynamic devices are ineffective but in this case control-moment gyroscopes could in theory be used to maintain weight transfer or even eliminate it for a conventional car, but this comes at a severe weight penalty and does not increase vertical load the way that aerodynamic downforce does. A better method for achieving very high lateral accelerations at slow speeds would be to use a fan and side skirts to evacuate air from under the car in the manner of the Chaparral 2J.

Weight distribution for conventional cars should be equal left-to-right to ensure equal cornering performance in each direction and between 50% rear for best lateral acceleration with identical tires on each corner[45] and more rearward for best braking and acceleration[46]. A mass center forward of mid-wheelbase speeds transient response[47], but the camber achieves the same effect due to the much shorter relaxation length compared to slip angle without causing limit plow with equal-sized tires, as would be the case for a conventional car but which is not proven for a camber car. Equal front-to-rear weight distribution is best for lateral acceleration because a car must have the moments created by the lateral force on both the front and rear axles about the mass center balanced. If mass center height, roll couple distribution, and all other parameters are held constant and the only change to the car is a redistribution of mass towards the rear, then both the inside and outside tires will see the same increase (on the rear wheels) or decrease (front wheels) in load at all times. The lateral load transfer will be the same at each end, therefore making the car oversteer. Roll couple distribution should follow the static front-to-rear weight distribution, with small deviations to tune the over/understeer to suit the driver.

With a rearward mass center, the lateral force moment arms are not equal so the front must produce less lateral force and the rear more. If there were no load sensitivity, then the necessary adjustment in lateral forces would occur through the redistribution in vertical forces. With negative load sensitivity (as seen with slip angle), the rear does not gain enough lateral force to balance the front. In the case of positive load sensitivity (camber), the front does not gain enough. Either way, one end must give up some of its lateral grip to aid the other, usually

[45] Milliken, William F. & Douglas L.: Race Car Vehicle Dynamics, page 394,401
[46] Milliken, William F. & Douglas L.: Race Car Vehicle Dynamics, page 391
[47] Milliken, William F. & Douglas L.: Race Car Vehicle Dynamics, page 401

accomplished by use of an anti-roll bar to adjust front-to-rear roll couple distribution. If load sensitivity (rate of change of normalized lateral force with vertical load) is linear (no matter the slope) then roll couple distribution adjustments can achieve in the same lateral acceleration as the equal front-to-rear weight distribution and roll couple distribution. If the load sensitivity is nonlinear there are more cases to examine. If decreasing and either concave up or concave down then less lateral acceleration is possible even after tuning the car for neutral steer. Similarly, if the trend is increasing and concave down then less lateral acceleration is possible after changing roll couple distribution. Only if load sensitivity is increasing and concave up is more lateral acceleration possible than with the mass center at mid-wheelbase, and only after redistributing roll couple to achieve neutral steer. Therefore, it is important to find out whether the tires have either a direct or an increasing, concave up relationship of maximum lateral grip under combined inclination and slip angles with regard to vertical load. If either of these is true, the optimal weight distribution should be more rearward than mid-wheelbase for best acceleration on a rear-wheel-drive platform and for more even loading under braking which increases the maximum braking force due to load sensitivity effects[48].

Using a very limited data set, consisting of the two graphs in Figures 6 and 7 of the MX-1 tires at two different loads, maximum lateral force coefficient at -40 degrees of camber increases by more than 5% (from 1.05 to 1.11) when vertical load increases by 66% from 291 pounds to 492 pounds, meaning there cambered tires show positive load sensitivity. More than two points of data from the same tires are required to determine if the load sensitivity is nonlinear, however it is promising that mass center can be moved rearward to improve the longitudinal acceleration capability (which is compromised by camber) without incurring a lateral acceleration penalty.

Round-section tires and a narrow track provide aerodynamic benefits and weight reduction compared to wide, square-shouldered tires. According to William F. Milliken, a camber car could have about 60% of the frontal area of a conventional car while the narrow tires would open up more plan-view area for efficient under-car aerodynamics such as diffusers. The slanted sides also would make the car much more stable in yaw, which is something that modern sports-prototypes have trouble with (lifting off the ground and flipping once getting a little sideways). Tire pressures should be set at 30psi hot initially but testing should be used to find the pressures which result in the best handling. 30psi is the best value according to the research by Fonda[49] and is also close to the value which the Millikens found as optimal for the MX-1[50]. Cossalter shows camber and cornering stiffness dropping off with increasing pressure[51], however, so lower than 30psi may be better but should be very much dependent on the particular model of tire.

Bump steer should be minimized on any suspension system so that the wheels point in the direction the driver wants, but on a camber car there is a tendency to use large amounts of camber gain in bump, which can cause a different kind of bump steer: gyroscopic kickback through the steering system. On a smooth road the consequences of this can be kept to a

[48] Milliken, William F. & Douglas L.: Race Car Vehicle Dynamics, page 391
[49] Fonda, Albert G.: "Tire Tests and Interpretation of Data",
[50] Milliken, William F.: Equations of Motion, page 520
[51] Cossalter, Vittore: Motorcycle Dynamics, 2nd ed., page 55

minimum and by using a swing arm length (virtual or otherwise) of approximately half-track the camber angle changes less relative to the road during roll than with more or less camber gain. If the wheel maintains its attitude relative to the road there is less gyroscopic kickback because the spin axis of the wheel is not precessing in inertial space, which is, rather than orientation relative to the car, what matters for gyroscopic kickback. William F. Milliken writes after testing the MX-1 that a swing arm length approximately corresponding to swing axles (meaning a length of about half the track width) was "a very good configuration. In every respect, seems a desirable configuration."[52] Conventional Ackermann should be used due to the adverse camber of the inside wheel. Static toe-out of about 10% of the camber angle can be used to stabilize the car if the driver complains of wandering. Mechanical trail is not effective in this situation[53].

Suspension stiffness will be as stiff as possible while still being manageable over rough roads. The roll center should be above ground at all times, no matter the combination of wheel displacements. A higher roll center speeds transient response but requires stiffer springs to manage jacking and the loss of camber as a result. Front-view virtual swing arm length should be approximately half-track.

When attempting to maximize the benefits from camber the drivetrain tends to become a limiting factor. The issue of transmitting drive torque to the wheels at large camber angles can be overcome with wheel hub motors or clever use of chain drives and gearboxes to circumvent constant-velocity joint angularity restrictions. An example would be two, counter-rotating motors (cancelling gyroscopic forces) with their axes parallel to the longitudinal axis of the car. These motors would drive sprockets on the uprights via chains (located so as to minimize the amount of tensioning adjustment required) and those sprockets would connect to a right angle gearbox which then drives the wheel hub riding in the wheel bearings. The chains would accommodate the small static toe angle necessary in the rear suspension. The right-angle gearbox would incorporate a speed reduction so that the outboard sprocket could be reduced in diameter, allowing more camber angle before contacting the ground. This would make the drivetrain able to handle any camber angle while being mounted higher for more ground clearance and better rough-road handling. It would also add anti-squat (if done properly), which could aid traction if kept at a reasonable magnitude. A yaw moment would be generated if this system was applied to a variable camber system but this could be used to advantage. Due to the high percentage of lateral weight transfer, a limited-slip differential is necessary to make best use of the limited longitudinal grip available by beginning acceleration as soon as possible after the apex of a turn. This could be either a torque-biasing type, clutch & ramp type, or spool. A high-ratio torque-biasing differential would be the best option for a car with a reasonable mass center height to track width ratio of about 0.25 because of the greater longevity of the gear mesh compared to the clutch type, because more torque is sent to the outside wheel, and because differential wheel speed is allowed, unlike the spool. The spool would be best for cars with higher mass centers and little aerodynamic downforce, which would have the inside rear wheel almost completely unloaded in a turn. In such a case even a 3:1 torque bias to the outside wheel may be insufficient if the inside wheel has almost no traction.

[52] Milliken, William F.: Equations of Motion, page 517
[53] Milliken, William F.: Equations of Motion, page 517

The drawback to an extremely high negative camber configuration is poor braking and acceleration performance due to the inability to eliminate lateral force and so reach the peak longitudinal force point on the friction circle for the tires. Race tracks are combinations of tight turns, open sweepers, and straights. Aerodynamic downforce and camber can increase the speed at which both tight and open turns can be taken, but on the straights the camber is detrimental.

The static camber car responds more quickly to steering inputs than a passive dynamic camber car and can achieve the same steady-state lateral acceleration (assuming identical mass properties), but the dynamic camber car would have advantages on certain circuits where quick transitions are not necessary or do not make up a significant portion of the lap and where acceleration and braking dominate. An active dynamic camber system could improve transient response but would be difficult to control properly in all situations. To determine either the best compromise for static camber angle or the benefits to a dynamic camber system the affect of camber on longitudinal force must be known, but this data is scarce to non-existent. Friction circle diagrams are about all that exists, but this is usually based on conventional cars without significant camber. Keeping the load on the rear tires low with a long wheelbase and equal front-to-rear weight distribution would reduce the camber thrust and mean that the tires could operate closer to their peak longitudinal grip coefficient even with camber, but the lighter load reduces the total longitudinal force which would result. Without four-wheel drive there would still be a loss in longitudinal acceleration potential, perhaps even greater than with a rearward mass center. Braking would be improved with a rearward mass center because it would produce a more even dynamic weight distribution and the typical four-wheel brake system can make use of this.

Ideally, the camber would change from highly negative for best cornering to zero for best acceleration on turn exit and braking before the next turn.[54] Alternatively, the static camber angle can be reduced to strike a compromise for a particular track. Both of these methods were considered when designing the 2013 Formula Electric suspension.

Dynamic Camber

Active vs. Passive

An active suspension which can change the camber angle to the optimal setting for cornering and for acceleration or braking would have fast transient response, high steady-state lateral acceleration, and high longitudinal acceleration. The challenge is in the control system. If simply based on steering angle, pilot-induced-oscillation can result from any correction of an oversteer disturbance. Reducing steering angle will reduce camber, decreasing grip at both ends and causing the car to drift wide instead of causing the yaw correction desired with normal front-wheel steering. A combination of steering angle, brake position, lateral acceleration, and throttle position may be the best. If the steering angle is reduced and throttle dropped, no action is taken. The control system would be looking for a reduction in lateral acceleration below a certain amount, throttle or brake application, and steering angle reduction all at once. The difficulty is still in discerning corrective inputs for a slide or spin versus accelerating out of a corner. GPS

[54] Milliken, William F. & Douglas L.: Race Car Vehicle Dynamics, page 405

correlation of track position and turn proximity may be the ultimate answer, but this is not as versatile as a passive system.

As seen in Appendix A, passive dynamic camber has the drawback of slow response time because it requires time for the sprung mass to displace in roll but it offers benign handling below a certain input frequency without being as hard to setup as the active system. Depending on how much of the track is made up of fast, wide-open sweepers, the passive setup may be fine, as long as there are not many quick turn reversals required.

Both the active and passive dynamic camber systems will be heavier than simple static camber setups and this must be taken into account when the gains in longitudinal grip from camber reduction are found through testing. This weight gain is due to the increased complexity for both (including drivetrain complexity) and actuators for the active system.

A system under manual control and separate from the steering would theoretically accomplish the desired effect but would put too much work load on the driver if the "camber switch" was anything other than a bi-polar one: vertical or full negative camber and only to be activated before or after a corner, not entering or exiting a turn.

Polynx

The initial suspension concept was a passive dynamic camber system which has the tires vertical when not turning but which generates a large negative camber angle on the outside tire and a small positive camber angle on the inside tire when turning. The difference in camber angles is in recognition of the fact that the lightly-loaded inside tire does not benefit from camber as much as the heavily-loaded outside one. A single spring and damper unit is installed on each corner and an additional spring and damper connects the inside and outside wheels on each axle in order to provide additional spring rate in ride and pitch. This minimizes the pitch angle and therefore keeps the wheels more vertical during acceleration and braking so as to maximize longitudinal force.

The desired camber change happens in response to the opposing displacements of the wheels when the sprung mass rolles, similar to the effect of a front-view swing arm length of less than half the track width. The issue with using a conventional suspension (such as dual A-arms) with a short swing arm length is that it usually comes with a high roll center, which reduces the roll couple and so the roll angle which the suspension relies on (though a higher roll center would increase the natural frequency in roll and so reduce the response time). The other issue with a conventional suspension design was that it was impossible to achieve the highly-unequal camber change between bump and rebound travel. As a result, a novel new suspension mechanism was devised.

This is a system incorporating a four-bar linkage with an extended coupler link forming a rocker arm controlling the path of the lower ball joint of the upright. Connecting to the upper ball joint is a link that connects to a floating node, which is a pivot on the end of a link that has its "ground" pivot point on the chassis. A third link connects to this floating node, but this third link has its other pivot point floating as well. This floating pivot point is shared with the lower four-bar linkage and is also the floating fulcrum for the rocker arm controlling the lower ball joint.

This suspension falls into the category of VXI suspensions because it uses two floating pivot points and a "camber link" connecting to the upper ball joint. Figure 24 shows a basic sketch of the general concept but with equal inclination on the inside and outside tires rather than the approximately vertical inside tire that was deemed superior because it reduced the amount of plunge necessary in the driveshafts.

Mechanism Design

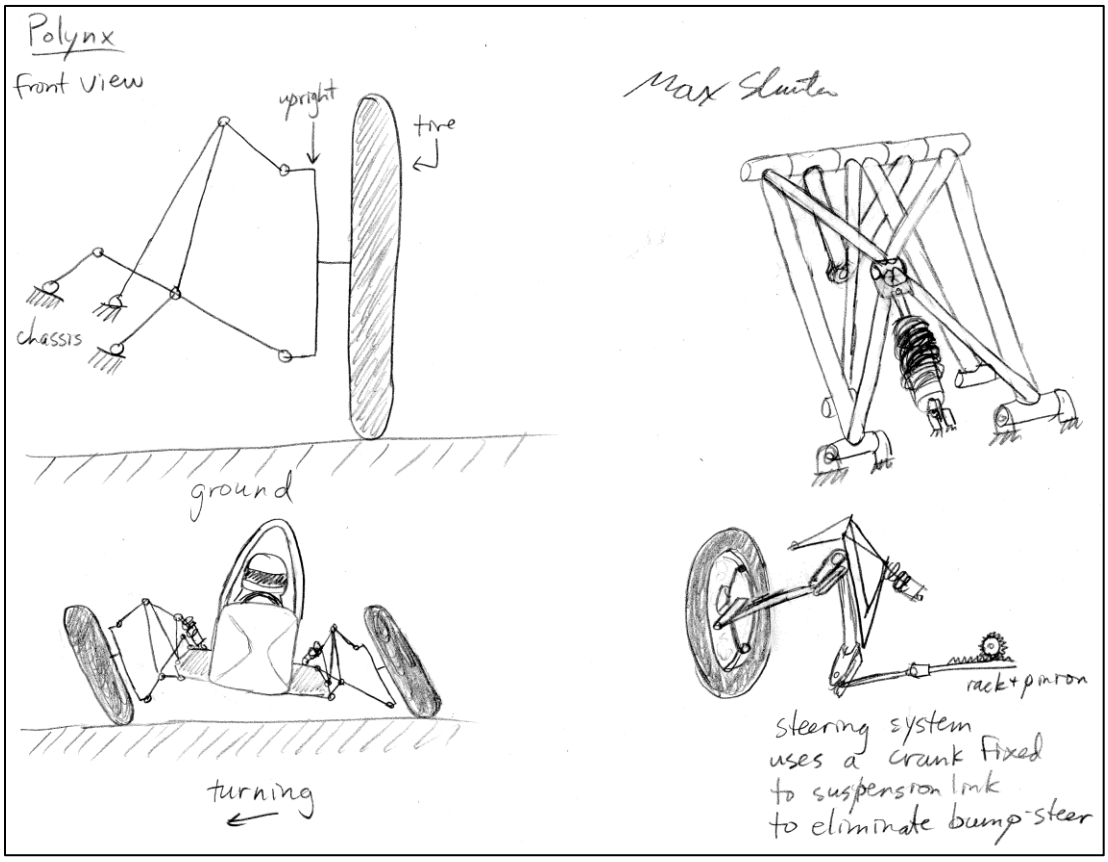

Figure 24: General Polynx Design

In order to minimize bump steer, an intermediate crank is used so that the steering linkages follow the suspension links' centers of rotation as camber changes. This crank is anchored to one of the suspension links which connect to the chassis. There is an inner tie-rod connecting one of the crank arms to either a steering rack or a lever at the end of the steering column (like a go-kart). Another tie-rod connects the other crank arm to the steering arm on the upright. This system eliminates bump steer in a straight line but not when the wheels are steered.

This suspension design was given the name Polynx as a reference to both Cal Poly and the number of links in the system. Polynx is a planar (in front view) mechanism with three pivot points on the chassis, but for certain kinematic profiles two of those pivots can be in the same spot, resulting in two rocker arms in the suspension, reducing the number of joints and increasing the rigidity. The three-pivot version allows more complicated wheel paths such as short-travel, high camber change ones, but can also be used to achieve a high-travel suspension with little camber change. The two-pivot design provides a convenient position for a direct-acting coil-over

shock absorber (coil spring concentric over a linear damper). Figure 25 shows a CAD rendering of the steering system on a 2-pivot Polynx system but without the spring-damper unit installed.

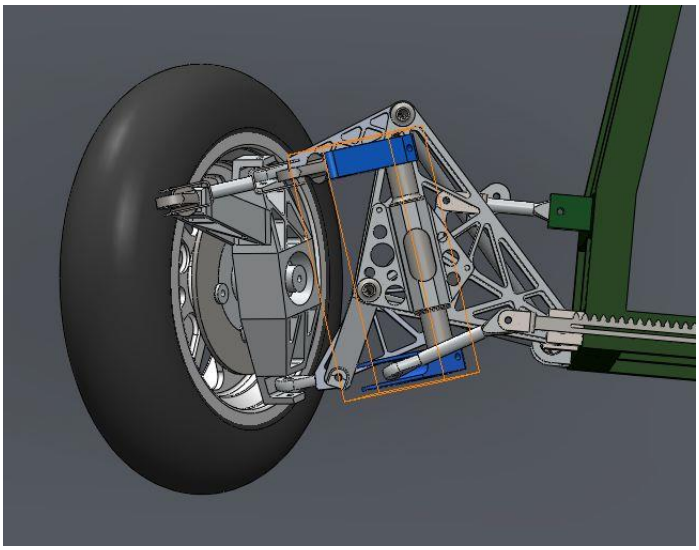

Figure 25: Steering Mechanism Shown on a Simplified (2 Pivot) Polynx Suspension

The roll center of the Polynx configuration chosen for the FSAE camber car is fixed relative to the chassis and is at ground level at static ride height in order to increase the steady-state roll angle without causing jacking of the sprung mass or lateral tire scrub.

With the extreme camber change and low roll center the driveshafts must change length significantly. One solution would be wheel-hub mounted electric or hydraulic motors. What was settled upon, primarily due to familiarity, was a system using conventional, Rzeppa-type constant velocity joints and a shaft that can change length by means of ball-bearing splines.

Driveshafts were also to be used in the front for inboard brakes because the current Formula Electric wheels are too small to fit the brakes inside them and larger wheels would be heavier and require heavier, larger tires. Mounting the brakes on the inside of the uprights, as was already done on the previous Formula Electric cars, would interfere with linkages. These driveshafts will add weight and so cancel the weight advantage of the small motorcycle tires, but the inboard brakes relieve the suspension links of the need to react brake torque and so they can be made lighter. Full-size motorcycle tires would be large enough in diameter to fit brakes in and would allow the camber angle to be shared better between the inner and outer constant-velocity joints, therefore permitting more camber. Running inboard brakes does show that a four-wheel-drive Polynx version is possible. The main drawback of the inboard brakes is a smaller maximum steering angle, but this should only affect very tight parking maneuvers which are not important for track performance. This version of Polynx would be better suited to vehicles larger than FSAE cars, where the weight penalty of tires large enough to fit outboard brakes in the front would not be such an issue. Inboard brakes are a logical choice in the rear because the drivetrain is already there for propulsion.

Design Direction Change

As the time to manufacture the Polynx suspension drew near, it was decided that the Formula Electric team did not have the resources to manufacture the Polynx suspension for the 2013 competition. Additionally, the team did not wish to redesign the electronic stability control system to account for the inherent torque-vectoring that the dynamic camber system included due to the change in rolling radius when the tires lean. Along with the complex drivetrain (plunging shafts and high-angle constant-velocity joints) necessary for Polynx, the necessary changes to the electronic yaw & traction control system and the manufacturing difficulty prompted the decision by the team to abandon the Polynx suspension system and adopt an approach of optimizing the much simpler static camber setup.

The suspension team still desired to know more about camber and the specific characteristics of the small motorcycle racing tires being used (due to their light weight). Therefore, the design goals became to design a suspension system that could accommodate any camber angle between approximately -30° and +6°. This would enable testing of many different camber configurations so that the optimal static camber angles on the front and rear could be determined for the competition. The second main goal of the adjustability was to simulate the Polynx suspension's steady-state cornering grip by performing skidpad tests with asymmetric camber of -24° on the outer wheels and +2° on the inside wheels.

Final Design: Static Camber

Kinematics

The front-view swing-arm length was set at approximately half the track width, in accordance with Milliken's recommendations. The roll center static height in the front was set at about 2 inches above the ground. This was largely determined by the minimum clearance between the inner suspension pivot point and the ground, as well as the necessity for the suspension links to clear the brake rotor. The rear roll center height is about 0.25 inches higher than the front to speed transient response by having more geometric weight transfer in the rear than the front. The front-view suspension pivot points are shown in Figure 26 for the front suspension and in Figure 27 for the rear suspension. Dimensions are in inches and the solid, horizontal, black line is the ground level. The dotted, vertical line is the centerline of the chassis. The shorter, dotted lines represent the springs and connect to triangles which show the rocker pivot geometry. The four lower points are the inner pivot points for the two pseudo-A-arms.

The steering link (going to the steering rack) is positioned 0.012 inches lower and 0.114 inches further outboard than the inner pseudo-A-arm pivot points. This was the best position for minimum bump steer as determined by SolidWorks after the upright geometry had been set, including the steering arm location. This location was set so that the steering link would clear the brake rotor, to provide correct Ackermann, and to simplify the manufacturing of the clevis parts of the uprights. Therefore, the inner pivot point was allowed to be out-of-line with the pseudo-A-arm points in front view.

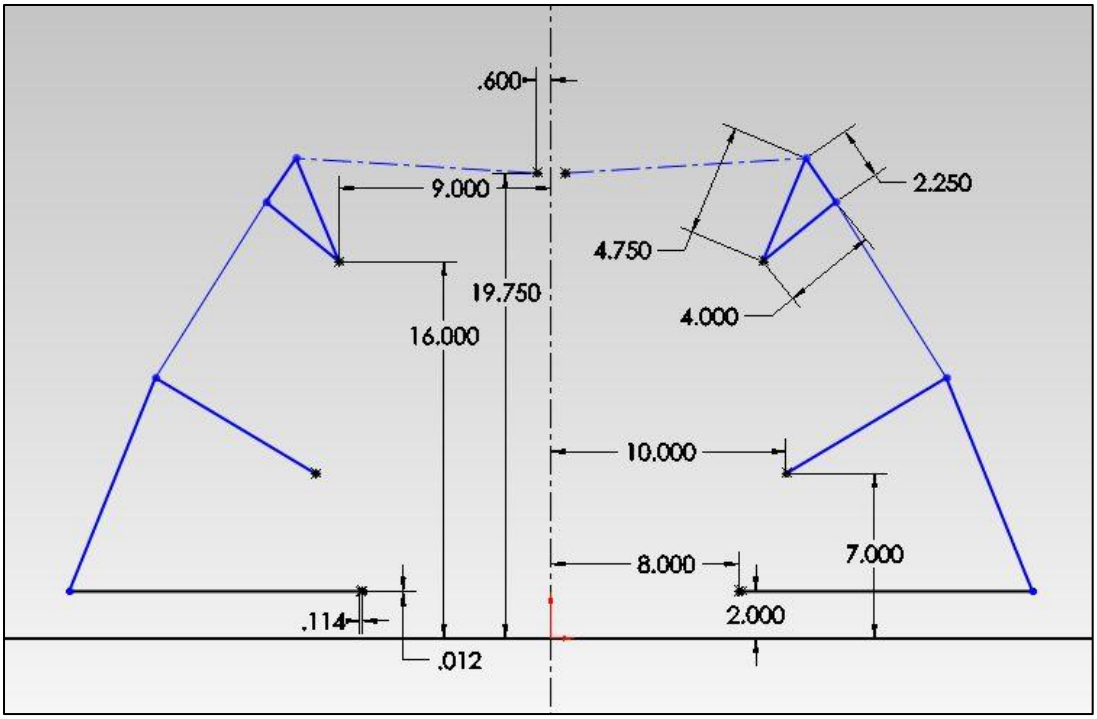

Figure 26: Front Suspension Pivot Point Front View Geometry

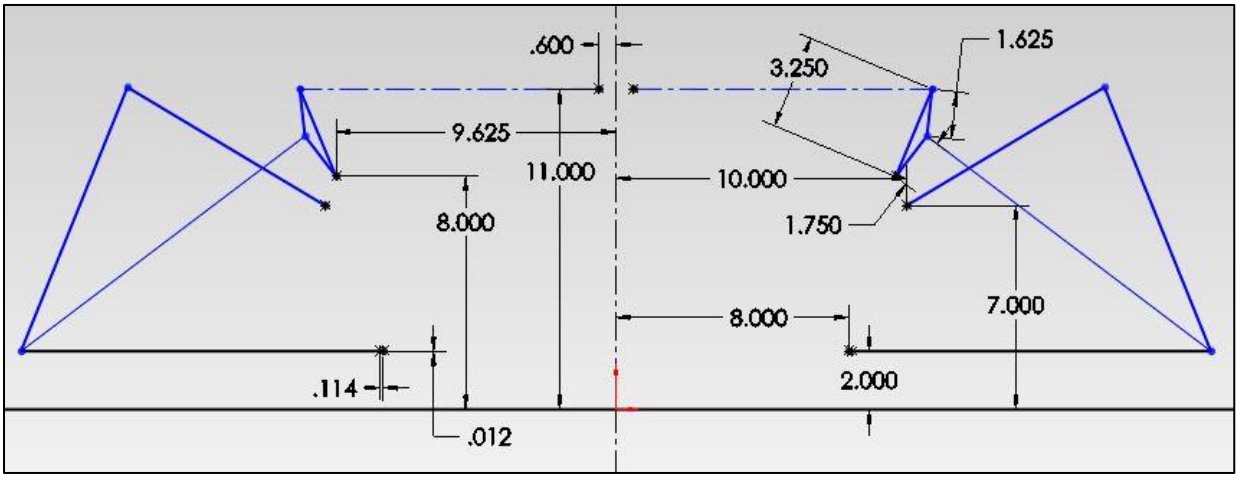

Figure 27: Rear Suspension Pivot Point Front View Geometry

Both the front and rear suspensions have only one spring per corner (no heave springs) and there are no anti-roll bars because they would add weight and complexity and their purpose can theoretically be fulfilled by changing spring rates.

The static camber angle is -22 degrees on all four wheels because it is near the limit of the constant velocity joints being used. Joints that would allow higher angularity would be heavier, and more complicated drivetrain layouts were rejected by the drivetrain team as too much work.

There is no anti-dive or anti-squat built into the suspension because the undamped oscillations caused by the coupling of longitudinal and jacking forces through the suspension members tends to reduce the braking or acceleration capabilities.

The side view geometry of the front suspension is very important because it sets the steering geometry. The pseudo-A-arms define upper and lower virtual ball joints at the intersection points of lines projected along the suspension links in those pseudo-A-arms. In the rear the side view geometry is set in order to reduce the maximum forces in the links between braking/driving and turning. This is accomplished by adjusting the splay angle of the links. Side view geometry is shown in Figure 28 for the front suspension and Figure 29 for the rear.

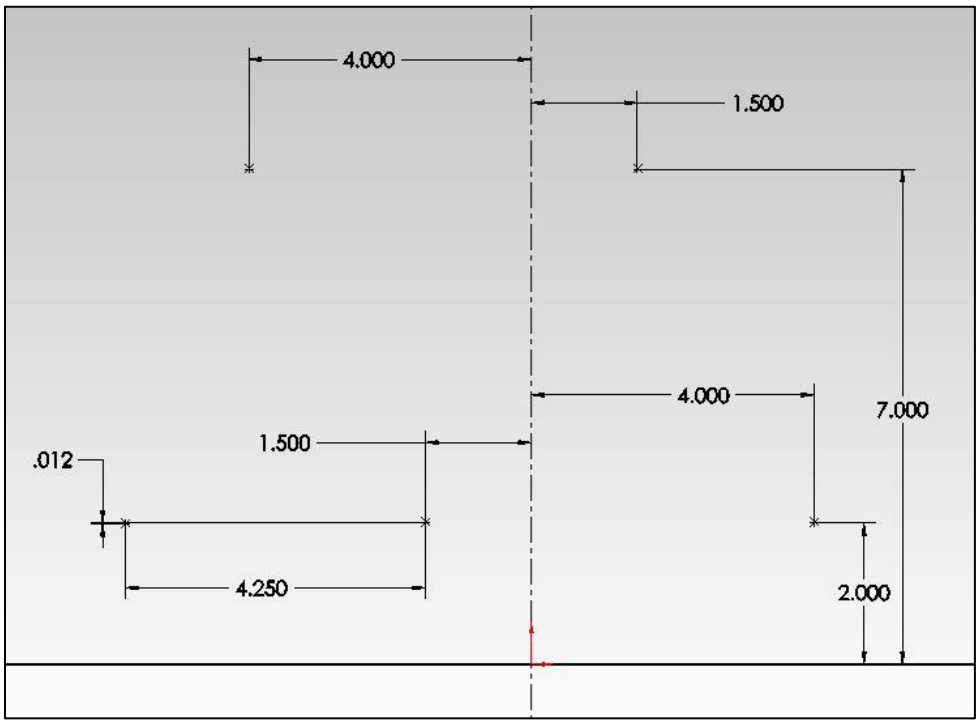

Figure 28: Side View of Front Suspension Points

The vertical centerline is the center plane of the rocker arm and coil-over spring mount. The solid, horizontal line is represents the ground level. The front pushrod is in the plane of the rocker arm when the wheels are pointed straight-ahead but the rear pushrod is slanted because the rocker arm had to be moved rearward to clear drivetrain components.

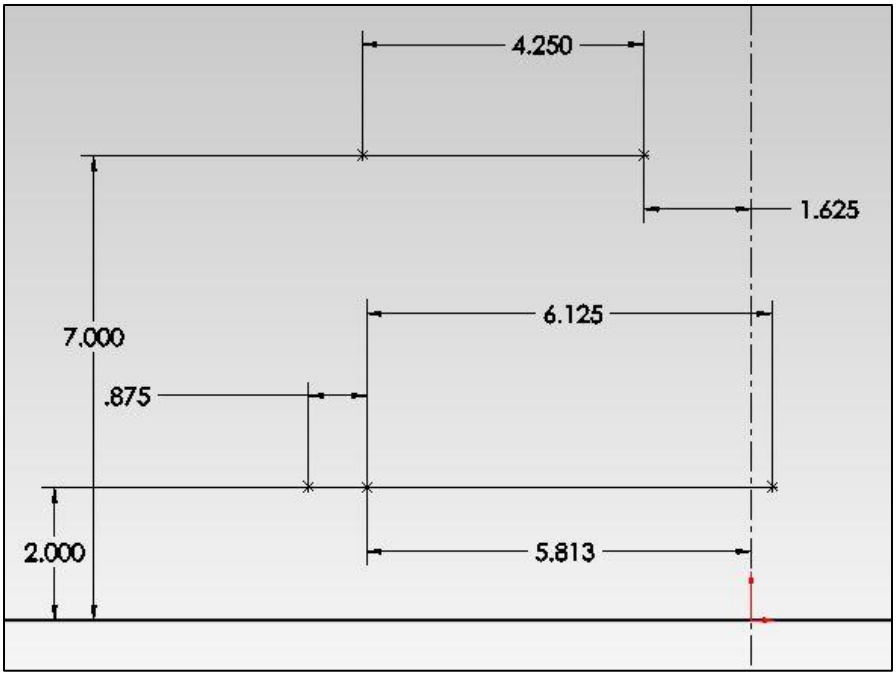

Figure 29: Side View of Rear Suspension Points

Upright geometry is more complex, especially on the front where the clevises are angled. The front view geometry of the front upright is shown in Figure 30 and the front view of the rear upright is in Figure 31.

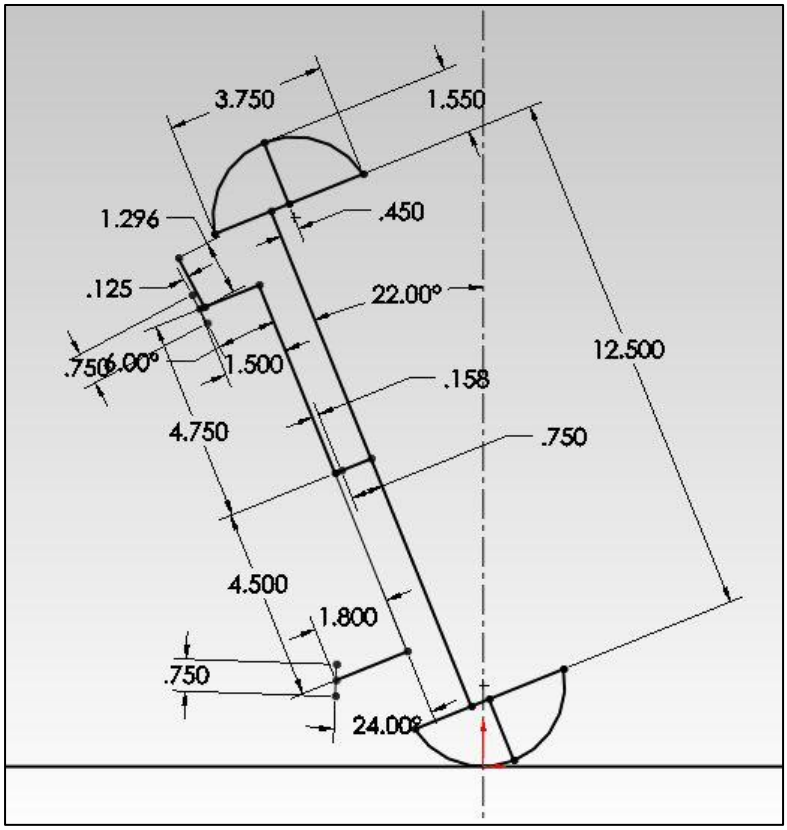

Figure 30: Front View of Front Upright Geometry

In the front view sketches of the uprights and tires the wheel offset of +0.45 inches can be seen, as well as the 0.75 inch thickness of the hub and the 0.158 inch or 0.177 inch protrusion of the inner bearing race from the outer face of the upright. In Figure 30 the angle of each clevis block is shown (24 degrees for the bottom and 6 degrees for the top), as well as where the pushrod clevis spherical bearing is located (the 1.296 inch line at the top of the upright). The solid horizontal line is the ground level in both drawings.

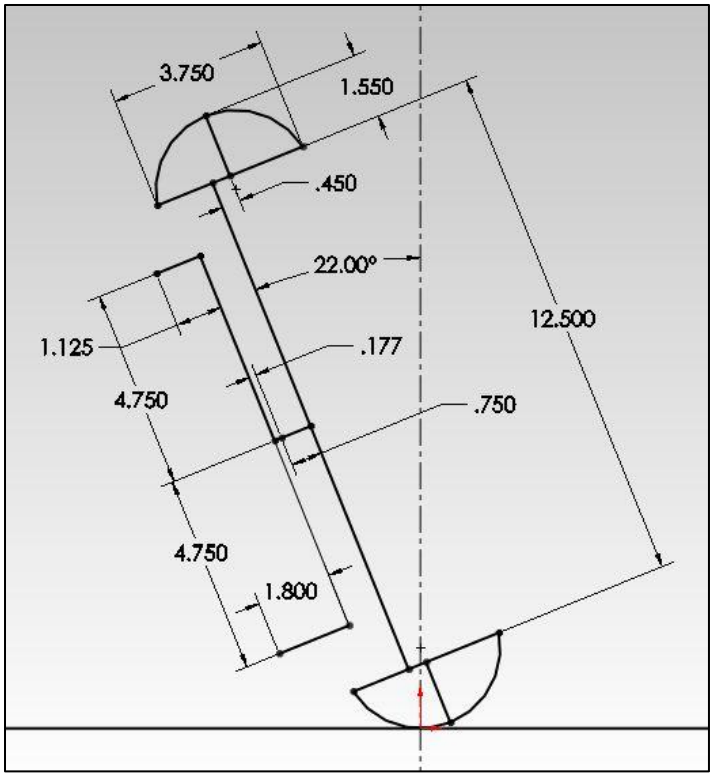

Figure 31: Front View of Rear Upright Geometry

The side view of the uprights is harder to show because of the three-dimensionality of the parts. The lower pivot point shown in Figure 30 is only for the pseudo-A-arms. The steering arm is mounted in the same clevis but is not in line with the lower pivot points. This geometry is seen in Figure 32, and the construction of the upright will be discussed in a following section.

Figure 32 is a top view of the left front upright's lower clevis block, but the part is the same on the right side, just flipped over so as to be mirrored. The part is also the same for the high and low camber parts. The offset of the bolt hole for the steering rod end (0.906 inches) is necessary for the correct Ackermann with a front-mounted rack. The front-mounted rack is necessary to allow a one-piece steering column, or at least one without multiple universal joints or right-angle gearboxes.

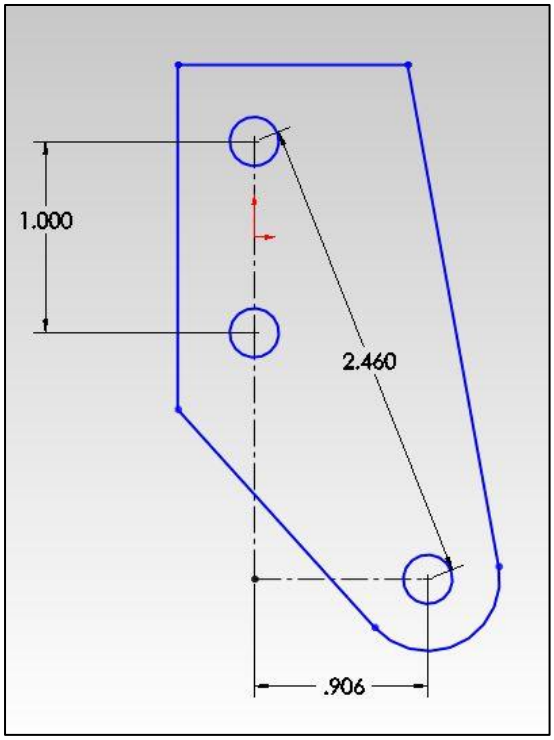

Figure 32: Top View of Left Front Upright Lower Clevis Plate

Figure 33 shows the top clevis block for the high camber front uprights. The upper and lower plates of the top clevis are different from each other and are different for the high and low camber configurations because the length of the plate must be adjusted to meet and weld to the outer face of the upright when the angle of the top clevis changes for high or low camber.

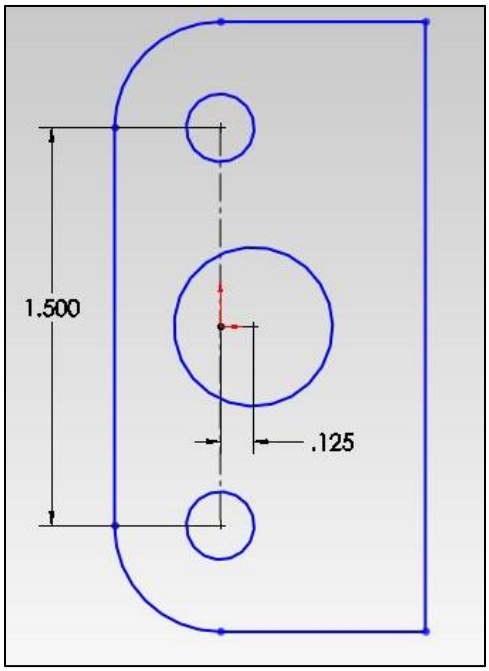

Figure 33: Top View of Left Front, High Camber Upright

The 1.5 inch spacing between the pseudo-A-arms, as well as the relative location of the hole for the rotating clevis bushing tube (the large hole in the middle) do not change between high and low camber parts.

The four spherical bearing center points are symmetrical about a plane perpendicular to the clevis plates and containing the wheel spin axis. This plane is also perpendicular to the road when the wheels are pointed straight-ahead, meaning the upright is not leaned forward or backwards in side view. Caster is achieved entirely by the top-view angles of the suspension links.

The side view geometry of the rear upright is easier to show, but the rear hub and constant velocity joint are not normal to the plane containing the suspension points. As a result, the vertical spacing shown in Figure 34 is not exactly to scale. The fore and aft location of the spherical bearing center points relative to the vertical centerline is correct, though. This centerline passes through the axis of wheel rotation. The view is once again from the left looking right, with the front of the car being out of the picture frame to the left of the page. The toe link connects to the forward-most point and the pushrod to the rear-most. The other points are for the pseudo-A-arms.

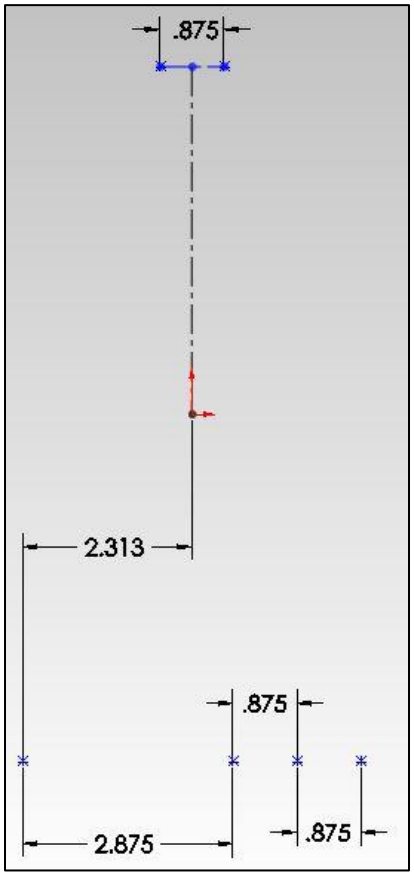

Figure 34: Side View of Rear Upright Geometry

The motion ratios for the front and rear spring systems are slightly less than 1:1, meaning that the spring and damper compress slightly less than 1 inch per inch of upward wheel travel.

This ratio was chosen to provide the most leverage for the spring without exceeding the limits of the damper stroke. The leverage is important to provide a stiffer suspension so that it does not bottom out. This could also be achieved with stiffer springs but it was desired to save money by using springs already in inventory. The spring rates are equal front and rear at 200 pounds per inch because the weight is distributed approximately equally between the front and rear axle. A slightly higher rear natural frequency helps provide a level ride and increases driver comfort. An anti-roll bar could be used on one end to tune the understeer/oversteer balance through changing the roll couple distribution without affecting the ride. If the weight distribution was slightly rear-biased this would not be necessary because the stiffer springs which provide a higher rear natural frequency also increase the rear roll stiffness and balance the handling. Geometric anti-roll must also be taken into account when choosing spring rates.

Ride height is 1.25 inches to the bolt heads for the front lower suspension points which are the lowest point on the car. Rake angle is zero. The low ride height is necessitated to reduce the angle of the outer constant-velocity joints. A higher ride height was desired in order to increase the mass center height (and so the lateral load transfer which camber relies on) along with improving performance over rough roads by preventing the chassis from scraping the ground over bumps.

The desired weight distribution for the car was 55% rear to provide a good compromise between lateral grip and longitudinal grip but the actual weight distribution turned out to be slightly less than 50% rear when the driver was in the car. The wheelbase of the car shrank from 66 inches to 62 inches because the chassis was longer than necessary in the midsection and it was not desired to move the front wheels forward along with the rear because it was believed that would result in too rearward of a weight distribution while increasing the turning radius. In hindsight, extending the wheelbase via moving the front wheels forward would have been better because it would have improved driver compartment ergonomics as well as returning the weight distribution to the desired value. The track width was set at 48 inches based on a projected mass center height of 12 inches which turned out to be much higher than the actual value, which was about 8 inches.

The tires being used are PMT rear tires for small racing motorcycles. The size is 100/85-10 on all four corners. These are what have been used previously on the Formula Electric car and what the current wheels fit. They are lightweight and grip well.

Component Design & Analysis

The final design for the suspension is based on the traditional multilink (or 5-link) concept. Six individual links constrain the upright in all six degrees of linear and rotational freedom. In such a system four of the links replace the pair of A-arms in a conventional system. A fifth link controls the toe angle of the wheel (and would be called a steering tie-rod on the front suspension). The sixth link is either the spring itself or the pushrod (or pullrod) which connects to the spring through a rocker arm. In the design chosen there are pushrods for both the front and rear suspensions because the spring-damper units are too bulky to attach directly from the chassis to the upright without interfering with other components. Each of the six links per corner are simple, aluminum-alloy rods with right-hand female threads on one end and left-hand female threads on the other so that two heim joint rod ends can be threaded into each end and the

center-to-center length of each link can be adjusted by loosening jam nuts and rotating the rod in one direction or the other without removing the heim joints from their clevises. For large changes in camber (which would exceed the limitations of the threaded lengths of the rod-ends), new aluminum rods can be made much more quickly and easily than welded steel A-arms, which was what the previous suspension used. Figure 35 is a CAD rendering of the full suspension in isolation. The left side wheels have been removed to show the uprights and hubs better.

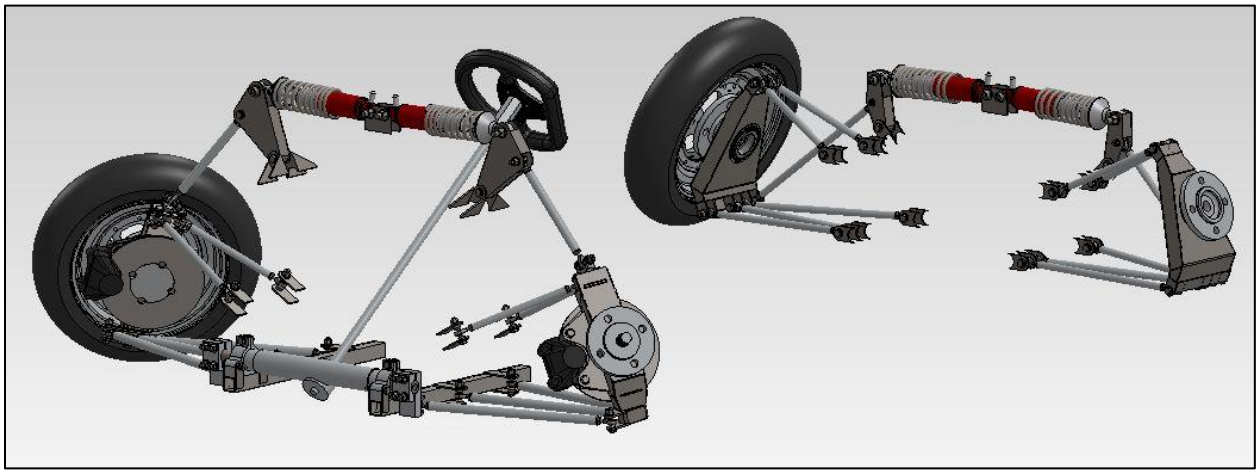

Figure 35: Final Suspension Design

In the rear, the heim joints are oriented with their axes of full rotation oriented longitudinally so that the camber can be adjusted throughout an extremely large range without requiring changes to the upright or chassis. The rear links are splayed, forming a "V" in plan view, similar to an A-arm, in order to better react braking and drive forces. The consequence of this is that the heim joints are very near their maximum misalignment angle but this is acceptable because only a few degrees of static toe-in or toe-out are necessary for tuning the stability and response and both ride motion and camber adjustment are accommodated by the heim joint's axis of infinite rotation (about the bolt axis). The right rear upright and suspension links are depicted as-manufactured and unpainted in Figure 36.

Figure 36: Right Rear Suspension Corner

The pushrod from the rear spring and rocker is attached to the bottom of the rear upright because it allows the pushrod to be more in line with the resultant force vector from the lateral tire force and the weight than if it attached to the top of the upright. It also allows a lower spring

and damper placement which means that the rocker arm mounts can share a chassis tube with the suspension points and therefore reduce the complexity and weight of the chassis. Locating the pushrod on the bottom of the upright also means it does not need to change length significantly with large camber changes, as would be the case with the pushrod mounted on the top of the upright. What this means in practice is that fewer rear pushrods need to be made since the turnbuckle adjustment can cover a large range of camber. By having the pushrod acting on the upright through its own clevis, rather than acting on an A-arm as on the previous suspension, all the suspension links are two-force members in theory, and can therefore be lighter and/or have a higher factor of safety.

Both front and rear coil-spring-over-damper pairs are horizontally-opposed, as seen in Figure 35, so that forces due to brake dive, acceleration squat, and heave (all four wheels moving up or down equally) are canceled within the spring-damper unit mount and putting less stress on the chassis. These mounts consist of two metal tabs in front and two similar tabs in the rear which form clevises for the spherical bearing in each spring-damper unit. There are two holes in each tab, one for the left side spring-damper unit's bolt and one for the right side unit. The net forces resulting on the chassis at that point are lower than with separate mounts or with spring-damper units that are not directly opposed to each other and those forces only come about as a result of the lateral load transfer. The rockers are all oriented with their rotational axes longitudinal, and the springs act on the same side of the rocker as the pushrod does, therefore the pushrod and spring forces partially cancel (more or less, depending on the lever ratios for the pushrod and spring) and reduce the stress on the rocker arm pivot.

In the front, the heim joints must be oriented with their rotational axes vertical in order to accommodate steering. This then creates challenges when changing camber because this must be accommodated by the limited misalignment capability of the rod-ends. With the chosen front view swing arm length of approximately half track and roll center height at the center of the bottom chassis tube the pivot points fixed to the chassis do not need to change position or angle in order to retain similar kinematics when varying camber. The clevis angles on the upright do need to change angle, however, and this led at first to a three-piece design for the front upright, with a central section serving as a brake caliper mount and a locator for the wheel bearings, an upper clevis piece where the top two suspension links would mount along with the pushrod, and a lower clevis piece which would mount the bottom two suspension links and the steering link. There would be three bolt holes in the center section for each clevis piece. Two through-bolts would pass through both the clevis piece and center section, occupying two of the holes. One bolt would serve as a pivot point and in order to change camber the second bolt would be removed and inserted into the third hole in the upright and clevis piece. This would change the angle of the clevis and the location of the outer pivot point. The change in location of the pivot point was beneficial to steering geometry (with the initial steering rack placement) and front-view kinematics. Only two angle positions were necessary to cover the desired range of camber when using relatively compact heim joints.

The three-piece design was abandoned when the steering system was finalized. A major goal was to use a single-piece steering column (rather than one or more universal joints) to reduce the backlash and deflection in the steering mechanism as much as possible. To achieve this, the steering rack had to be mounted very far forward do to the short wheelbase (required for

acceptable weight distribution). The initial rack placement behind the front wheel centerline would have required a gearbox or several universal joints. With the front-mounted rack, the steering link's outer pivot point had to be much closer to the tire than the other suspension links' pivots in order to achieve the desired Ackermann effect. The result of this was that when the lower clevis was changed to the low-camber configuration the steering arm would hit the tire. Since the same clevis piece could not be used for both configurations, it was decided to move to a single-piece, sheet-steel, welded upright that would be lighter and stiffer than the three-piece one. Two different uprights would be required per side, however: a high-camber one and a low-camber one.

The multilink system allows much more freedom in steering geometry than dual A-arms do. This is because the steering axis is defined by the instantaneous centers formed from the two pairs of lateral control arms, rather than constrained by two physical pivot points on the A-arms. This allowed the scrub radius to be reduced significantly from the previous suspension despite the wheels and tires being too small and narrow to house any steering or brake components. The previous (A-arm) suspension had more than 2 inches of scrub radius and about 30 degrees of steering included angle which combined for significant steering kick-back and also lifted the front of the car an amount equal to about 50% of the ride height and would shift weight rearward when steered, adding understeer which was a problem in the previous car. The multilink has a scrub radius of approximately zero at -22 degrees camber and about 0.75 inches at zero camber with a steering included angle approximately equal to the camber angle. Front-end lift has been reduced to nearly zero, partially due to the placement of the pushrod on the top of the upright. As the upright turns the pushrod changes its angle and effectively shortens which cancels-out the effect of the rising front upright so that the sprung mass remains at the same height. Self-centering on the new suspension is achieved via mechanical and pneumatic trail rather than the front-end lift used previously and this means steering weight changes with speed and how close to the limit of adhesion the tires are, a feeling that the driver expects and relies on to judge grip levels.

Ackermann of at least 6° is desirable for maximum grip according to research. When turning, the inside tires needs much more slip angle than the outsides due to the adverse camber. To achieve this at the steep steering angles and small turn radii expected in competition, a goal of 100% geometric Ackermann was set. About 80% was achieved because more resulted in too much nonlinearity.

The steering link's outer pivot was positioned on the front of the upright so that the rack could be mounted in its forward location without forcing the steering link to cross over the lower lateral control arms. Crossover is not possible because the outer steering rod end must be mounted low and nearly in line with the lower control arm pivot points in order to both clear the brake rotor and give a reasonable steering ratio with the available rack (which already has an optional, faster-ratio pinion installed). A rack was used because it provides a more linear steering ratio for the outside, dominant wheel than a rocker arm steering system (like a go-kart) and the team's drivers placed a high value on linear steering.

Bump steer with the rack was also less than with the kart-style steering, but only when special drop-down clevises were used. These allow the rack to mount on top of the lower frame

rail while the clevis itself extends down to the correct position. This then creates the possible problem of the clevis hitting the frame when steering, but due to the steering ratio selected there was sufficient clearance simply by extending the bottom control arm tabs by about 0.5 inches (meaning the frame rails are narrower while the lower control arm pivots stay in the same spot). The clevises therefore also act as steering stops to prevent the heim joints from binding and failing. These clevis pieces were milled manually from blocks of 7075-T651 aluminum alloy and use a circlamp design similar to a two-piece shaft collar. Four ¼”-28 bolts clamp the clevis to the 7/8 inch diameter steel rack, and provide a sufficient level of friction to transfer the expected loads with a healthy margin of safety when torques properly. These clevises also circumvent the problem of the steering rack being too wide, which prevented the rack from being mounted at the correct height with clevises on the ends and the frame going around the rack housing. A final benefit is that the rack can be slightly further forward (and higher) than it otherwise would be, which decreases the steering column angle and increases driver comfort. Figure 37 shows the actual steering clevises and they can be seen in the CAD rendering of Figure 35 installed on the rack.

Figure 37: Anti-Bumpsteer Steering Rack Clevises

Ideally, the driver and roll hoop would be moved back, with the motor controller area shortened. This would allow the chassis proper to end just ahead of the front suspension attachment points, permitting the steering rack to be positioned at any height without interfering with the driver’s range of motion. Before setting the width of the suspension pivot points, the rack would be chosen (if a rack was to be used) so that the problem of the rack being too wide would not occur. This would then allow much lighter, simpler clevises to bolt to the end of the rack and not apply any torsional moments about the long axis of the rack. Eliminating these moments reduces the friction in the gear mesh and eradicates the problem of angular backlash in the rack. This angular backlash was not discovered until the steering clevises, with their longer lever arms to amplify the motion, were installed. If the rack had a slot with a linear bearing that would prevent rotation of the rack this would not be an issue. Fortunately, the front axle does not transmit forward thrust and so the rack will take a seat in one orientation and stay there once in motion. The angular backlash does cause toe changes and irritating steering slop at near-zero speed.

The steering ratio of about 2 (two degrees of steering wheel turn per degree of road wheel steering) means that the driver's arms do not cross-over each other, even in the tightest turns and that he or she does not need to reposition his or her hands on the wheel. This is safer, more comfortable, and faster than a slower ratio. The steering weight has been kept under control by setting the mechanical trail appropriately (to a value of about 0.4 inches). This results in an expected steering weight of about 12 pounds per g of lateral acceleration, measured at the rim of the 9.375" diameter steering wheel. The fast steering ratio also means that the steering rod's inner pivot point moves less when steered in a turn than it would with a slower ratio, causing less bump steer when turning. This improves driver confidence through more consistent steering feel, which usually means a faster lap time. The steering weight is similar to that on the MX-1 which William F. Milliken found satisfactory.[55]

The front-view inclination of the steering axis appears (from analysis of kinematic sketches in SolidWorks) to cause the mechanical trail to reverse with large steering angles, but this phenomenon is present in a static camber, A-arm setup as well, or any one with kingpin inclination, even if the static scrub radius is zero. The contact patch "orbits" the tire as it steers. This should result in a reversal of steering self-centering at high lateral acceleration and with nearly complete lateral load transfer, but no such effect was experienced with the A-arm suspension on the previous camber car, nor was any reported by Milliken. Still, to help ensure steering self-centering in high lateral acceleration situations the brake calipers were placed on the front of the upright so that their inertial forces will exert a stabilizing, self-centering steering torque.

With the multilink design the brake rotor does not necessarily need to be positioned on the inner face of the upright, but since the caliper would not fit in the wheel, the spindle would be severely cantilevered out from the bearings and so would need to be stronger and heavier to handle the bending stresses, and the bearings would need to be larger. Therefore, weight is reduced by locating the brakes on the inner face of the upright (as seen in Figure 35), which is where they were on the previous suspension. This also eliminates the complex plunging shafts necessary for the front inboard brakes on the Polynx design, but means the bottom front links are very highly stressed by the outboard brakes. By having the lateral links' outer pivot points as close as possible to their desired instantaneous centers, the steering geometry changes less when the wheel is steered than if the pivot points were spaced far apart (and so far from their instantaneous centers). Consistent steering behavior, in particular the buildup of opposing torque on the steering wheel in response to lateral force, is desirable so this was another factor in making the decision to keep the brake rotors on the inside of the uprights.

The front pushrod mounts to the top of the upright, and this placement was determined initially by the need to clear the brake rotor but more importantly is the need to accommodate large changes in camber while also allowing large steering angles up to 45 degrees. Ordinary heim joints and ball joints did not have the right range of motion and or were too bulky and heavy. The solution was to use a clevis that holds the spherical bearing on the end of the pushrod and which also rotates within the upright. This rotation is accommodated by fiber-reinforced

[55] Milliken, William F.: Equations of Motion, page 515

PTFE flange bushings from igus. The thrust face of the bushing mates with a face lathed into the 303 stainless-steel clevis and there is a 3/8" shaft protruding from that face and going through the bushings. This keeps the clevis aligned properly. In the high camber configuration the pushrod's force is almost directly normal to the thrust face of the bushing but the low camber configuration will put significant side-loads on the clevis and the smooth rotation of the clevis is essential for steering. This clevis was turned on a lathe from a large rod of stainless steel stock and then put into a mill to make the clevis mouth. Because the machining was done accurately, the bushings have met and exceeded all expectations of smooth rotation under combined loading. The bushings are pressed into a machined tube that was welded into the top clevis of the front upright between the top control arm pivot points. This tube adds rigidity to the upright and because of the small size of the bushing it can be a small diameter. This therefore allows the top control arm pivots to be closer together for a more consistent steering axis as the upright is steered. The pushrod and rocker geometry is positioned so as to reduce the front end lift when the front wheels are steered. The clevis is in between the two pivot points in the clevis in order to reduce the torque about the steering axis caused by the force in the pushrod. The igus bushings are an essential component to this design and were sourced from Rebel Racing Products. Figure 38 shows close-ups of the clevis and the bushing area. A circlip and washer keep the clevis from coming out of the bushing when all weight is off of the tire, such as if the car were driven off a jump or if it were on a jack. The circlip only needs to support the weight of the upright and wheel and is unloaded in normal operation.

Figure 38: Front Pushrod Rotating Clevis and Bushing Area

Figure 39 shows the high-camber front uprights and links assembled.

Figure 39: Front Uprights and Links

Figure 40 shows the installed rotating clevis piece for the front pushrod.

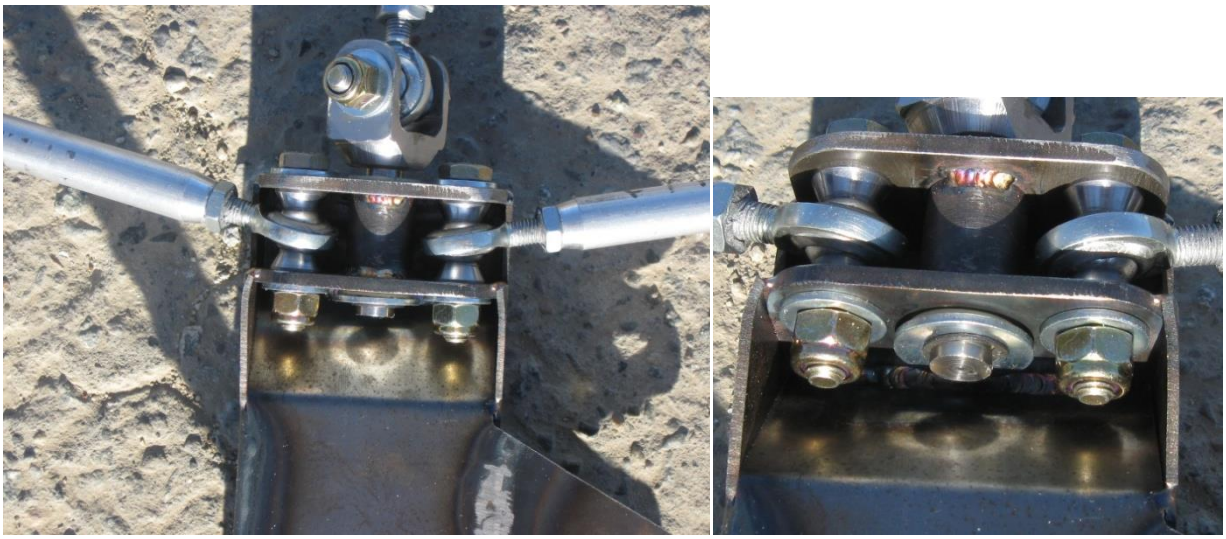

Figure 40: Installed Rotating Clevis

Figure 41 shows the lower control arm pivots and the steering rod attached to the front upright. It also shows the precision, 4340 steel, high-angularity heim joint cone spacers which were outsourced to a machinist with a CNC lathe because nearly 100 of these small but precision components were required and the Formula Electric team did not have the time or skill to manufacture them.

Figure 41: Front (High Camber) Lower Control Arm Pivots, Steering Pivot, and Heim Joint Spacers

Figure 42 shows all of the suspension corners laid-out together with the steering clevises.

Figure 42: Suspension Corners and Steering Clevises

The analysis of the suspension system was completed using free-body diagrams of each upright. The forces at the tire contact patch were known from the car's expected mass properties and the maximum longitudinal and lateral accelerations desired. With 6 two-force members, each corner of the car is statically determinant and, using the known geometry, the forces in each link can be found by solving the sum of forces and sum of moments equations simultaneously. A more advanced analysis would incorporate the use of vector loop equations (and the Newton-Rhapson method due to the nonlinear trigonometric functions involved) to find the exact geometry for any steering angle or camber angle, then solving the load equations for each case and finding the maximum tensile and compressive loads each link will encounter. To ensure the links are not extremely heavy or bulky it must be acknowledged that the car cannot reach maximum lateral acceleration at the same time as maximum longitudinal acceleration because the magnitude of the force vector from the tire can only be so great. Therefore, when the front suspension is steered the braking force must be reduced while the lateral force is increased and in a straight-ahead configuration the opposite is true. The front braking analysis must take into account the outboard brakes, which means the links need to react both the deceleration force at the corner as well as the torque from the caliper-wheel bearing couple. The maximum deceleration assumed was 1.6g and the maximum lateral force was assumed to be 2g with a car weight of 550 pounds (which turned out to be very close to the actual weight) with a 180 pound driver.

It was discovered that the largest load during cornering was in the pushrod, with very little in the lateral links. This is due to the angle of the pushrod in front view. From the braking analysis, however forces through the front, lower control arms determined to be on the order of 2,000 pounds and less than 1,000 in the rear control arms. As a result, larger, ¼" heim joints would be necessary on the front bottom links, although the #10 rod ends would suffice on the top links and in the rear. To simplify the manufacturing, it was decided to use ¼" heim joints and bolts throughout the suspension, even if the #10 hardware originally specified was sufficient and lighter. The marginal weight gain from the larger rod ends was determined to be an acceptable trade-off for simplicity and the extra safety margin.

6061-T6 aluminum alloy was chosen for the suspension links because the largest loads are compressive and the extra yield strength of the more expensive 7075 alloy would not help modulus-controlled buckling, since the elastic modulus of 7075 and 6061 is essentially the same. An Euler buckling model was used, with an effective length of 14 inches, which is longer than the longest link is from center to center of the rod-ends. A pin-pin connection was assumed since the links have spherical bearings at each end. Thread pullout strength for 6061 was also determined to have a factor of safety of about 2, and to be stronger than the heim joints in theory. A test showed a tensile force of 3,000 pounds was required to pull the rod-end out of the 6061 threads. The rod ends used in this test were ones found in a spare parts box and were not of the same type being used on the multilink suspension. Failure occurred in the aluminum and stripped the threads cleanly out of the link. A subsequent test using 7075 and heim joints of the type to be used showed failure in the heim joint's threaded portion at the load expected. The 7075 internal threads showed no distortion and were still usable. The extra strength of the 7075 alloy is therefore primarily beneficial for maintaining thread quality over more fatigue cycles. 7075 was not in the original budget but some additional funds were procured in order to make the more highly stressed links from the stronger alloy. The link rods' outside diameters were chosen to be

½” for most of the links and 5/8” for the front suspension’s lower rear control arm which sees large enough compressive forces under braking that ½” diameter rods would buckle.

1/16” sheet steel was chosen for the outer walls of the uprights because it is easier to weld to the 1/8” metal used for the clevises and the thick bearing race tube than thinner metal (which would still have met strength requirements). It also has better dent resistance to keep the uprights safe from unexpected impacts during construction and from cones or rocks on the race track. The clevis pieces are thicker because they see out-of-plane loads. The front, top clevis must react the pushrod force and this is done in the form of shear in the welds between the bushing tube and the clevis pieces. The flat clevis pieces are therefore loaded in bending, although the support span is short, being boxed in on three sides and with the tube itself adding rigidity and linking the top and bottom flat clevis piece. The front, bottom clevis uses the thicker metal because it is not boxed in as much because the lower links would hit any additional webs of metal and restrict steering angle. The steering arm is two cantilevered pieces, but the majority of the loads on them are in-plane where the section modulus is much greater. For the out-of plane loads, the cantilever distance is short and the heim joint spacers add rigidity when the bolt clamps them in. The thicker material adds minimal weight (since the clevis tabs are small) but increases the rigidity of the steering system and makes the upright more durable. 4130 normalized chrome-molybdenum steel was chosen for a higher safety factor and because the chassis is made from 4130 tubes so the team will be accustomed to welding it. The rear upright was originally designed as a CNC-machined aluminum part but the large material waste as well as the unreliability of the availability of CNC machines in the required timeframe caused the decision to move to a boxed, sheet steel weldment similar in construction to the front.

The uprights both were constructed using jigs (shown in Figure 43 and Figure 45) consisting of steel plates with through-holes. Aluminum blocks bolted to the plate and then upright pieces were bolted to the aluminum blocks and held in place for welding. The base of the uprights were bearing race tubes made on a lathe and which had a lip on the inside diameter for locating the wheel bearing races when they were pressed into the tube until hitting the lip. A lip on the outside diameter mated with a sheet of steel which formed one side of the main box of the upright. All the sheet metal for the uprights was cut precisely on a water-jet machine and bent using a press-break. The SolidWorks sheet metal tool was crucial for constructing the upright in CAD and then converting the pieces to flat patterns with bend lines. Protrusions from the edges of the sheets mated with slots in other pieces to locate the sheets relative to each other and to help hold them together for welding. The uprights were self-jigging in this regard. This and the bearing cup lip are shown in Figures 43 and 44, depicting the high-camber front left upright.

The front, high-camber jig could be used for both left and right uprights without modification while the rear jig could also be used for both left and right uprights but this required relocating the clevis tab spacer blocks on the bottom. The blocks were taken off the jig plate and used to make the top and bottom clevis sub-assemblies. These were made from a piece of square 4130 tube cut diagonally to make a right angle. This was used to box the clevises and make it easier to weld up the rest of the main upright box. Care was needed to ensure the bottom clevises were mirrored, as they are asymmetrical. The welding process involved putting one block with two tabs on, welding both of those tabs, then inserting another block and tab and welding that until a series of three clevises were welded on one end of the angle piece. Those were then bolted

to the jig plate along with the fourth clevis block and tabs. The outer tab for the fourth clevis was welded and then the clevis blocks were removed from the jig plate so the inner tab of the fourth clevis could be welded. Finally, the blocks were put back on the jig plate along with the simpler top clevis piece and the rest of the sheet metal so that the whole upright could be welded. The first piece to weld is around the bearing tube on the inside of the inner face sheet. Then the rest can be done in any order. Revisions to the jig that would be made with the knowledge gleaned from actually making an upright would include windows in the jig plate to allow some welding of blind joints without taking the clevis pieces off the jig so much.

The front upright also began with making the top and bottom clevis pieces, then bolting them to the jig along with the bearing tube and inner face sheet, welding the inner face sheet to the bearing tube, and then welding the rest of the sides of the upright on.

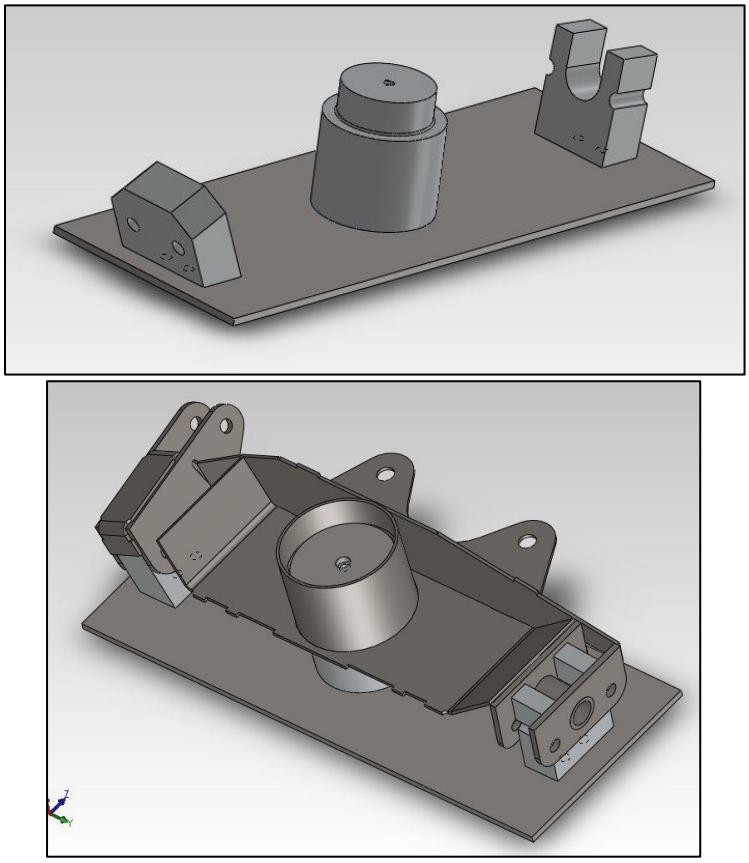

Figure 43: Front Upright Jig and Partially-Constructed Left Front Upright

The low-camber front uprights require different hole spacing in the jig plate as well as different top and bottom clevis blocks. The same jig plate could have both hole patterns cut in it so only one would be required. The center aluminum round piece which locates the bearing tube can also be reused.

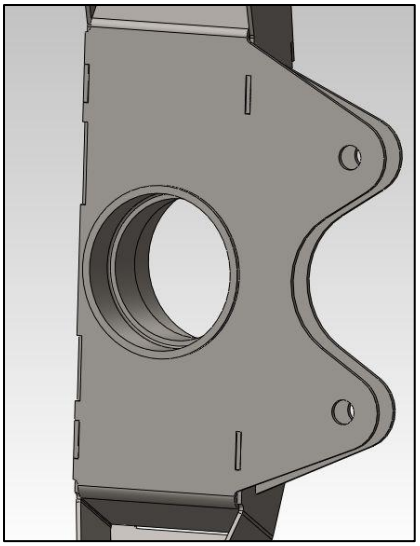

Figure 44: Tongue-and-Groove Joints for Self-Jigging

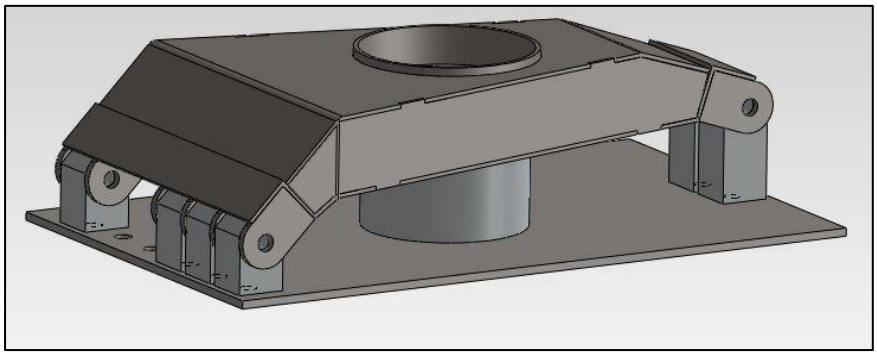

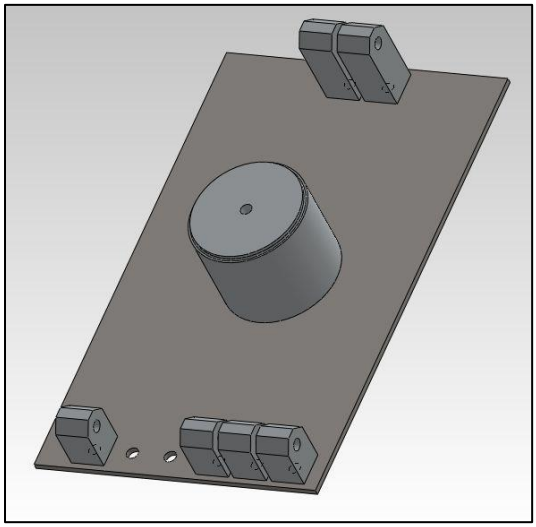

Figure 45: Rear Upright Jig

The suspension rockers are simple weldments consisting primarily of two triangular sheets of 1/16" 4130 steel sheetmetal and a tube connecting the two. The pivot points on the chassis will have two ½" inside diameter by 3/8" long igus L280 flange bushings pressed into a 0.95" wall thickness, ¾" outside diameter 4130 steel tube. These bushings are lighter, cheaper, and smaller than ball bearings and do well when dirt gets in them. A 303 stainless-steel sleeve

will go around a ¼" bolt and have the ½" diameter bearing surface. The stainless steel sleeve will be clamped by the bolt between two 4130 steel tabs welded to the chassis. Stainless steel is one of the best (lowest friction and wear) materials for use with igus L280.

Heim joint rod ends are EM4 (right hand thread) and EML4 (left hand thread) from Rod End Supply, sourced through Rebel Racing Products because they offered to sponsor the team by providing these rod ends at a much reduced price. Wheel bearing are tapered roller bearings from SKF and FAG, who offer discounts for FSAE.

The most challenging part of fabrication involved accommodating an inaccurate chassis and a change in the chassis necessitated by an incomplete SolidWorks model of the drivetrain. Jigs were fabricated to place the suspension tabs in the correct relative positions (particularly important in the front for the steering geometry) and these helped very much when welding. The simple 1/8" 4130 steel tabs had to be re-made and notched in back to accommodate a complete re-do of the rear half of the chassis, since a tube was interfering with the inner constant velocity joint. This meant the suspension tabs had to rotate and become longer to compensate. The rockers and springs also had to move but these are more flexible. In the front, one side is nearly perfect because of the jig being used before the upper chassis tube was welded in, but the other side has the top suspension point too high. Nothing could be done other than to move the suspension point up as well because the angle of the clevis was important. Figure 46 is a rendering of the front tab jig. It is made out of 6061-T6 aluminum alloy and can be used for both right and left sides of the car by switching which holes the center piece connects to. The bottom tabs clamp onto the square frame rail that makes up the floor of the chassis. The tops go over the round tube that runs from the front roll hoop to the front bulkhead.

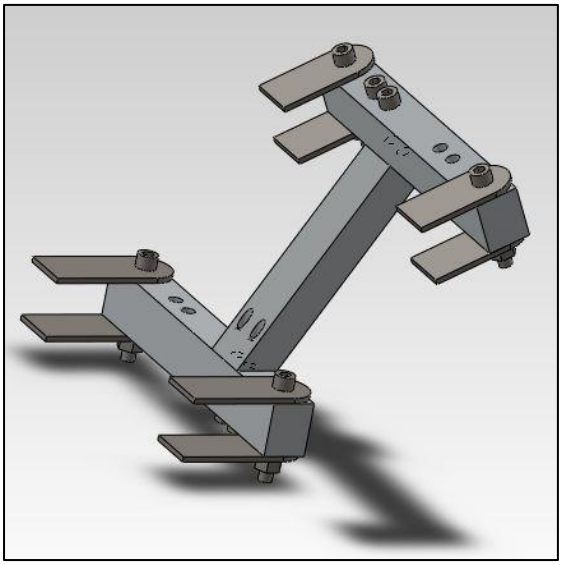

Figure 46: Front Suspension Tab Jig

Recommended Revisions

- Increase the magnitude of the scrub radius (either negative or positive) in order to reduce the steering weight at very slow speeds.

- Do not use drop clevises because these stress the gear mesh too much. Either get a rack that is narrow enough or change the kinematics to suit the rack being used (which was not possible this year due to late design changes, insufficient time to make a new rack or modify the old one, and insufficient funds to buy a new one).
- Make the chassis go around the rack and accept the weight penalty if the same stiffness is necessary. Otherwise, end the chassis at driver's feet (if driver can be moved back) and mount the rack at the proper height. Bump steer should be kept to a minimum so do not merely move the inner steering arm pivot point because this will reduce maximum steering angle (due to heim joint binding), increase bump steer, and adversely affect Ackermann.
- Use bearings instead of bushings for the rocker arms. The bushings require too much precision on the running surface of the inner race. Bearings come with the precision machining already done.
- Put more extensive jigging in the budget so that the chassis can be made to fit the suspension points and not the other way around. Link the left and right jigs of the front suspension and rear suspension together so that each is kept in the same plane. Include rocker arm pivot points and spring pivot points in the jigging, along with steering rack mounts in the front. Linking the front and rear suspension jigs together is not a high priority because the wheelbase can vary within the current manufacturing tolerances without significant changes in the front-to-rear weight distribution.
- Use 7075 aluminum alloy and alloy steel rod ends for all links, if the budget allows, in order to increase fatigue life and safety margins.

Design Verification

Structural Testing

Tests were carried out on the link assemblies using the model 1331 Instron Servo Hydraulic Load Frame in the Cal Poly Composites Lab. Initial tests were done for thread pullout, and more extensive tests done following a very unexpected failure of the right front suspension on the maiden drive, following a relatively low-speed turn and without impacting any obstacles. The driver was completely unhurt and the rest of the car was fine.

Link loads are known to a high degree of confidence because the 6 link system is statically-determinant and the heim joints closely approximate a joint which does not support a moment. Therefore, overloading was not believed to be the cause. During a post-accident investigation, it appeared that one heim joint sheared cleanly, with no bending, necking, or bulging. This failure occurred near the spherical bearing housing at the end of the threaded shank portion. There also appeared to be a small nick in the minor diameter of the thread which may have been a manufacturing flaw which weakened the rod end and caused it to fatigue quickly (the car had been towed to the senior project exposition without incident). Another probable cause is the improper handling of the links during the construction of the car. To the concern of the suspension team, links were allowed to fall, sometimes with the weight of the upright on them, and be caught by the misalignment cones. This produces a large bending moment in the links, and particularly the rod end threads, which they were not designed to take. Additionally, the threaded sections sometimes supported the weight of the car on the edge of the table. In the

future, much more care should be taken during assembly and the suspension should be either assembled completely (on a corner-by corner basis) or taken off entirely.

Due to the simple-to-manufacture design, a new link was made the day after the failure (only one was damaged) and all heim joints were replaced on that corner, with the car running briefly that night with the suspension functioning properly. The test drive was halted due to a ground fault detected in the electrical system. Some of the rod ends from the failed corner which did not appear to be damaged (many were bent after the first one failed) were tested the next day, along with several brand new joints.

Link buckling strength did not agree with Euler buckling calculations for a solid aluminum rod with pinned ends and a length equal to the center-to-center distance between the heim joint balls. The longer rod in Figure 47 showed a buckling strength of about 2250 pounds, which is about what the Euler calculation is for an aluminum rod with pinned ends and a length equal to only the aluminum part of the link, not the actual support span. The calculation for the actual center-to-center distance gives a result of about 1750 pounds, close to where the short link went nonlinear. The longer link assembly failed when the aluminum rod buckled in the first mode shape.

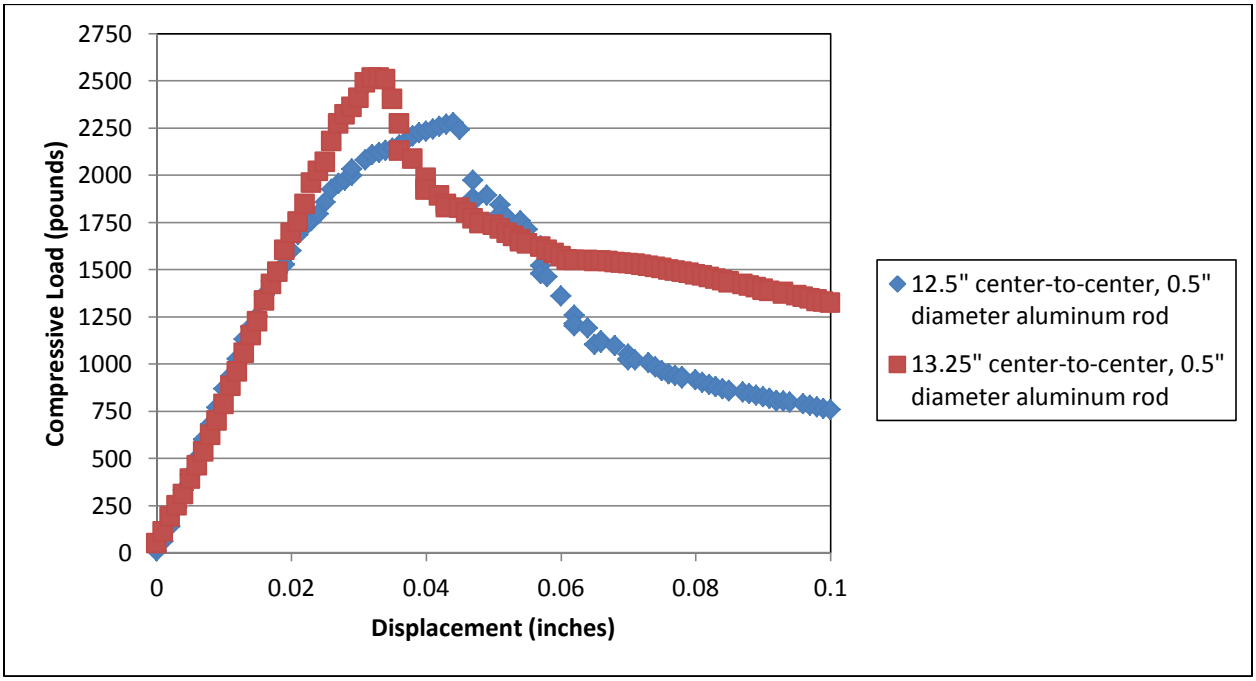

Figure 47: Link Buckling Test Results

The shorter link departed from a linear load-displacement curve at about 250 pounds below the Euler buckling strength for the center-to-center distance. The failure mode was bending of one of the heim joints at the threaded shank, just above the face of the aluminum rod which it was screwed into. The exposed thread length was greater than that of the longer link, but the heim joints were new. The rod ends on the long link were ones that appeared unbent but which were from the failed right front corner. This suggests that there is a critical length for exposed heim joint threads below which the aluminum rod fails and above which the heim joint

fails. In both cases the 6061-T6 aluminum threads were still usable after the test, supporting the tensile testing in Figure 48 which shows that the pullout strength of these 0.5 inch diameter rods was about 3000 pounds. 7075 threads were also tested using a piece of 0.75 inch diameter scrap but with the same ¼-28 threads. The 7075 thread pullout strength could not be measured because the heim joints would break first. The link was so strong that it was used for at least half a dozen tensile and compression tests, even up to 4000 pounds, without damaging the interior threads.

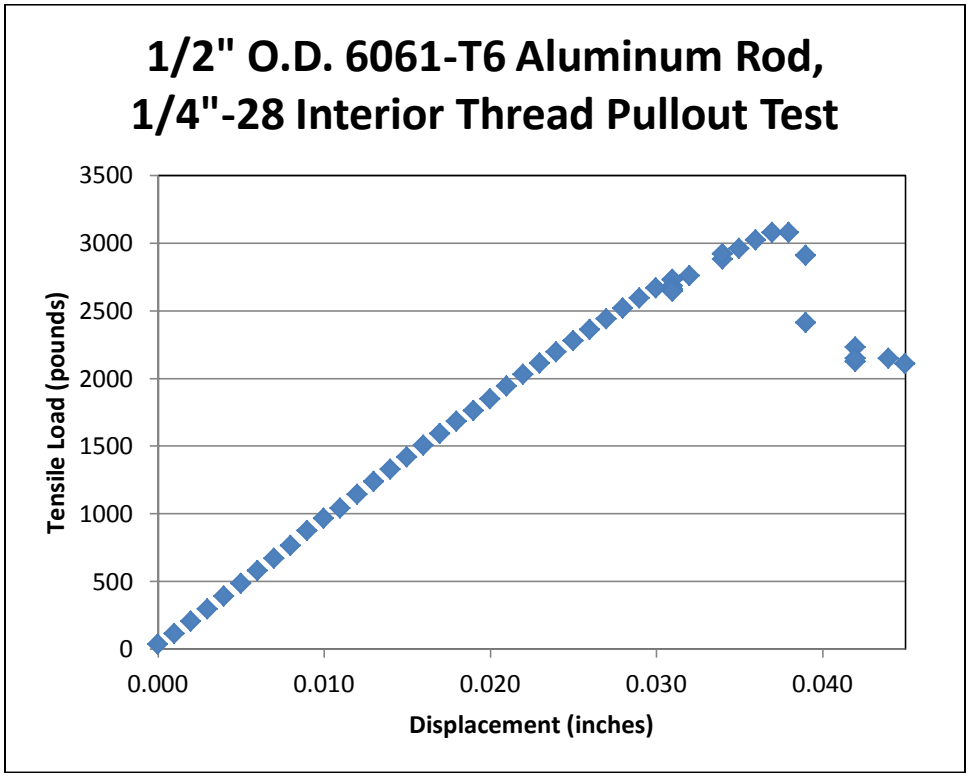

Figure 48: 6061-T6 Aluminum Alloy Thread Pullout Test Data

The buckling of the rod ends themselves was then tested, with results shown in Figure 49. It can be seen that exposing twice as much total shank length results in a lower effective modulus for the link, because the series where both heim joints were extended shows a shallower slope to the load-displacement curve. Also apparent is that the new heim joint took about 1500 pounds, or about 66%, more load than the "old" heim joint which came from the failed front right corner but which appeared undamaged. All of the rod ends in this test had performed either a tensile or link buckling test beforehand but emerged seemingly undamaged. Any undetectable necking from tension or bending from compression could cause early buckling. The softer release of load from the old heim joints means they were probably slightly bent. The reason why the 0.649 inch thread exposure was chosen is that this was as far into the 0.75 inch diameter 7075-T651 link that one of the rod ends would go, even though the others would go further. This was one of the joints in the double exposure test. A slight bend could cause the joint to not go all the way into the rod. The new heim joint failed nearer to its theoretical compressive strength limit (3400 pounds) than its Euler buckling strength (24000 pounds), though the end condition for the length of the shank was more complicated than pin-pin, having the spherical bearing housing at one end and a rigidly fixed to a very stout aluminum link (about 6 inches long) at its other end with another pin connection at the end of that. This buckling failure was very rapid and energetic,

releasing more load in a split second that the other joints held at their peaks. The nonlinearity of the loading curve could be plastic deformation due to straight compressive loading rather than bending. Figure 48 and Figure 49 show that predicting the buckling strength of a link is difficult.

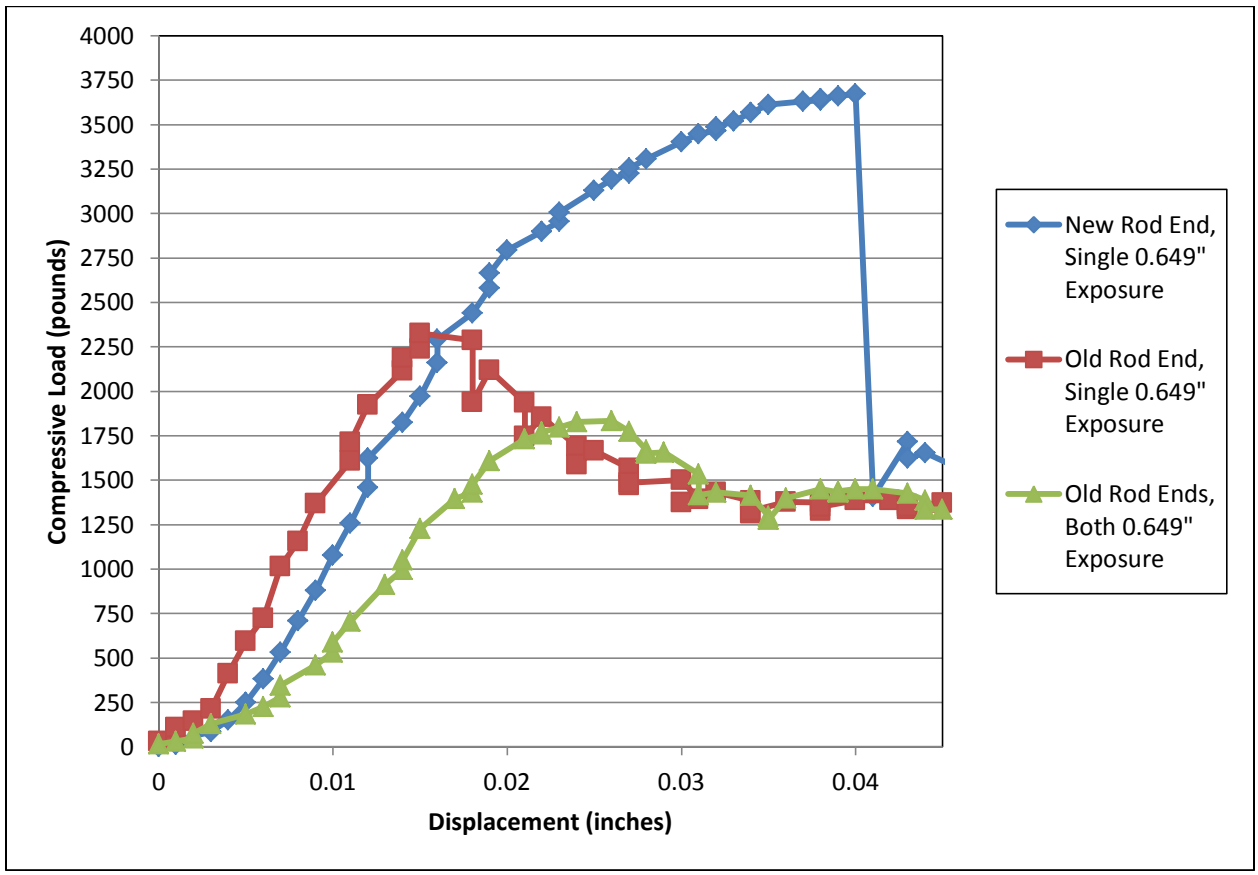

Figure 49: Rod End Shank Buckling Test

The tensile strength of the heim joints was twice what it was expected to be after preliminary tests using similar looking rod ends found in a box of spare hardware from previous Formula Electric cars. These broke at only 2300 pounds, or 700 pounds short of the 6061-T6 aluminum thread pullout strength. Fortunately, the heim joints obtained through Rebel Racing Products met and exceeded their claimed ultimate strength of 3820 pounds. This can be seen in Figure 50. The new heim joint was subjected to multiple pulls because the spherical bearings began to slip out of the hydraulic grips on the first two runs. Clamp pressure was set low on the first run in order to minimize the distortion out-of-round of the spherical bearing, which would cause more friction in the rod end and change the stress state in the housing, possibly even binding enough to change the end conditions on the links. For run 2 the clamp pressure was raised but the grips still slipped. Run 3 had the spherical bearing inserted further into the clamps, where the knurling was deeper, and this resulted in a good enough grip to break the joint on the third run at a peak load of 3940 pounds. The joint behaved remarkably linearly (elastically) up to 3800 pounds, almost exactly its rated load. This means the joint has a lot of usable strength when new, despite its low price and high angularity capability. The rod end from the failed suspension corner went to a higher ultimate load of 4070 pounds, but departed from the linear region at only 2500 pounds, perhaps due to damage in the accident or due to slippage in the clamps since it

occurs near where the trend of the second run becomes nonlinear. The spherical bearing may have been located in a slightly different location in the clamps which did not have as much grip. Strain hardening due to accident damage would have resulted in a longer linear region and a lower ultimate strength, which is likely what occurred for the new heim joint after three loading cycles. The first three plots have been shifted so that they all begin at zero displacement, so any hysteresis due to strain hardening cannot be seen. The rod end was not visibly deformed so the plastic deformation was small and apparently the joint does not lose much ultimate strength from the process. Therefore, peak loads greater than those due to the maneuvering forces of the vehicle could produce some strain hardening, but the joint should still function normally and have a greater elastic limit afterwards. There is about a 1000 pound margin before the onset of strain hardening in the link with the highest load, which occurs in the front links during braking.

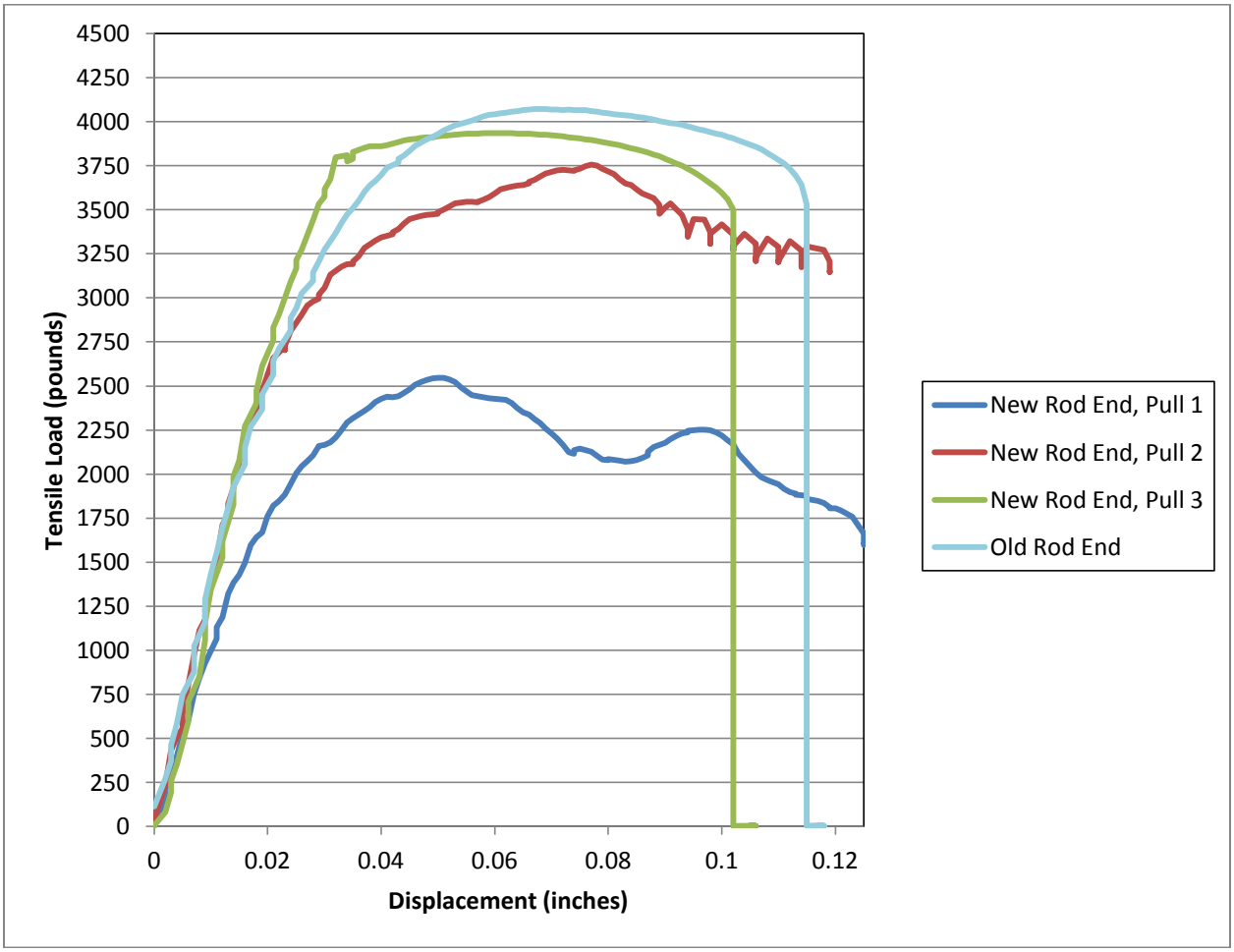

Figure 50: Tensile Strength of Heim Joints Sourced from Rebel Racing Products

Testing Procedure

Research suggests that -40 degrees of camber is best for lateral acceleration but 0 degrees is best for longitudinal acceleration. The intermediate goals of testing are to determine the correlation between camber and lateral grip and the relationship between camber and longitudinal grip. This data will then be used towards the final goals of developing a formula to

determine optimum camber angle for a particular track and determining if Polynx would have produced more lateral acceleration.

Our testing procedure will be to first perform left and right skidpad tests with the high camber setup of -22 degrees. We will measure maximum lateral acceleration using an accelerometer attached to the floor of the car. Each test will be performed multiple times. Next we will measure maximum longitudinal acceleration through straight line acceleration tests. Once we are satisfied with the amount of data for the high camber setup, we will replace the right suspension with a low camber setup of approximately 0 degrees. This will simulate the Polynx design of dynamic camber. A right skidpad test will then be performed with the maximum lateral acceleration being recorded after every run. Next we will replace the left suspension with a low camber setup and preform the same skidpad and longitudinal acceleration tests as for the high camber configuration. The right suspension will then be changed back to a high camber setup and left skidpad tests will be performed. The ideal camber angle will be determined by whatever set-up produces the greatest lateral acceleration. Following the tests, the car will be returned to a full high camber configuration.

Further skidpad testing would include comparing cambered round-section tires to square-shouldered racing car tires, shifting ballast to change the front-to-rear weight distribution, and shifting ballast to change the mass center height. Additional tests would include a steering wheel position sensor in combination with the accelerometer so that transient response can be measured along with the oversteer/understeer balance.

References

Milliken, William F. *Equations of Motion.* Cambridge MA, U.S.A.: Bentley Publishers, 2006. Print.

Milliken, William F., & Douglas L. Milliken. *Race Car Vehicle Dynamics*. Warrendale, PA, U.S.A.: SAE International, 1995. Print.

Pacejka, Hans B. *Tire and Vehicle Dynamics.* 3rd ed. Oxford, UK: Elsevier Ltd., 2012. Print.

Cossalter, Vittore. *Motorcycle Dynamics.* 2nd English edition. Lexington, KY, U.S.A.: Lulu, 2006. Print.

Fonda, Albert G. *Tyre Tests and Interpretation of Data*. Sage Publications on behalf of the Institution for Mechanical Engineers, 1956. PDF.

Formula Electric SAE Advisor: Professor Fabijanic, jfabijan@calpoly.edu, 805-756-5547

Appendix A: Simulink Modeling

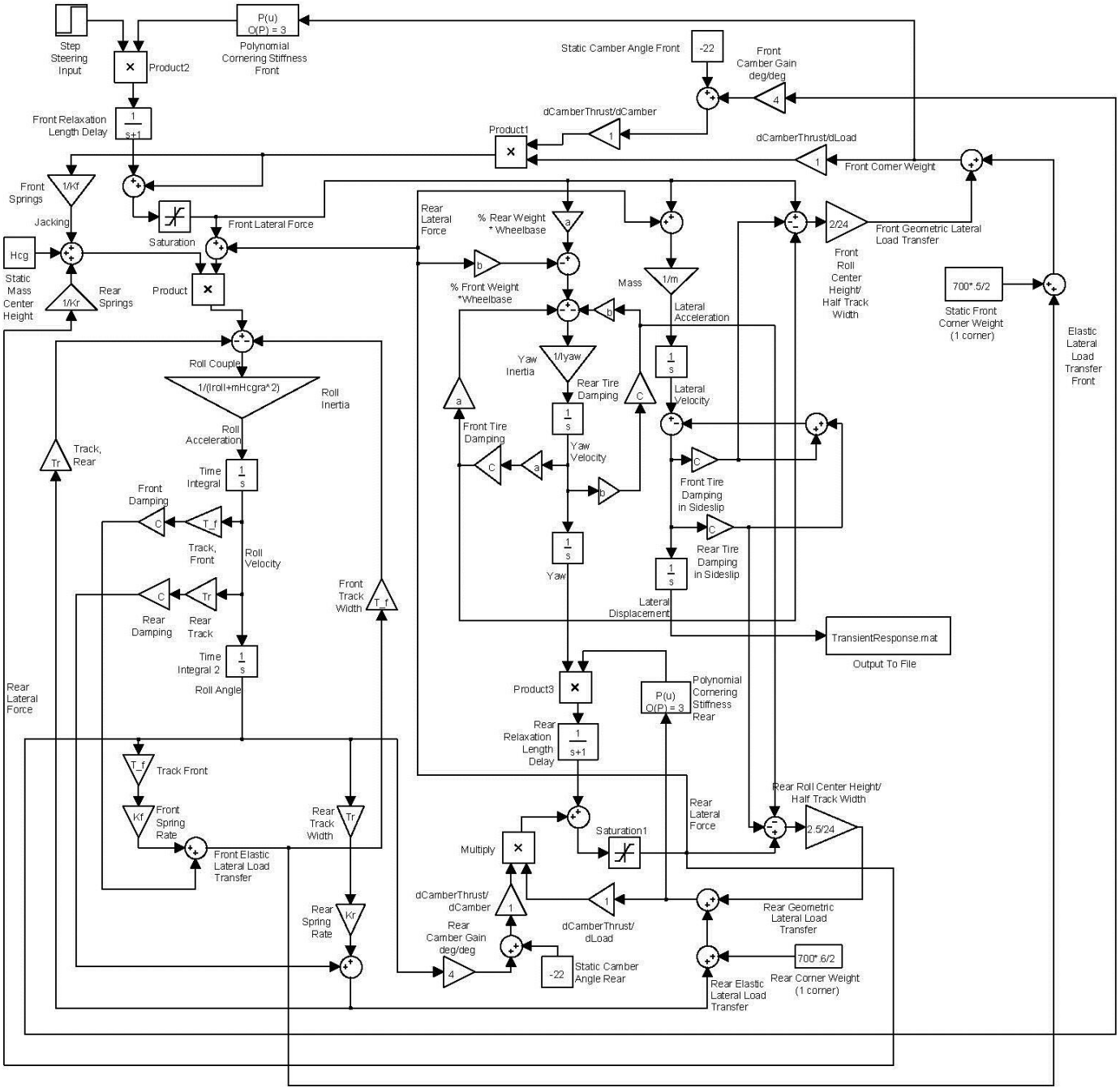

Appendix B: Vendors

Aircraft Spruce
http://www.aircraftspruce.com/

Speedy Metals
http://www.speedymetals.com/

McMaster Carr
http://www.mcmaster.com/#

Online Metals
http://www.onlinemetals.com/

Rebel Racing Products
http://rebelracingproducts.com/

Rod End Supply
http://www.rodendsupply.com/index.php

Grainger
http://www.grainger.com/Grainger/wwg/start.shtml

Mid-South Minimoto
http://www.midsouthminimoto.com/

SKF Bearings
http://www.skf.com/group/products/bearings-units-housings/index.html

FAG Bearings
http://www.fag.com/content.fag.de/en/index.jsp

igus
http://www.igus.com/default.asp?c=us&L=en

Appendix C: Supporting Analysis

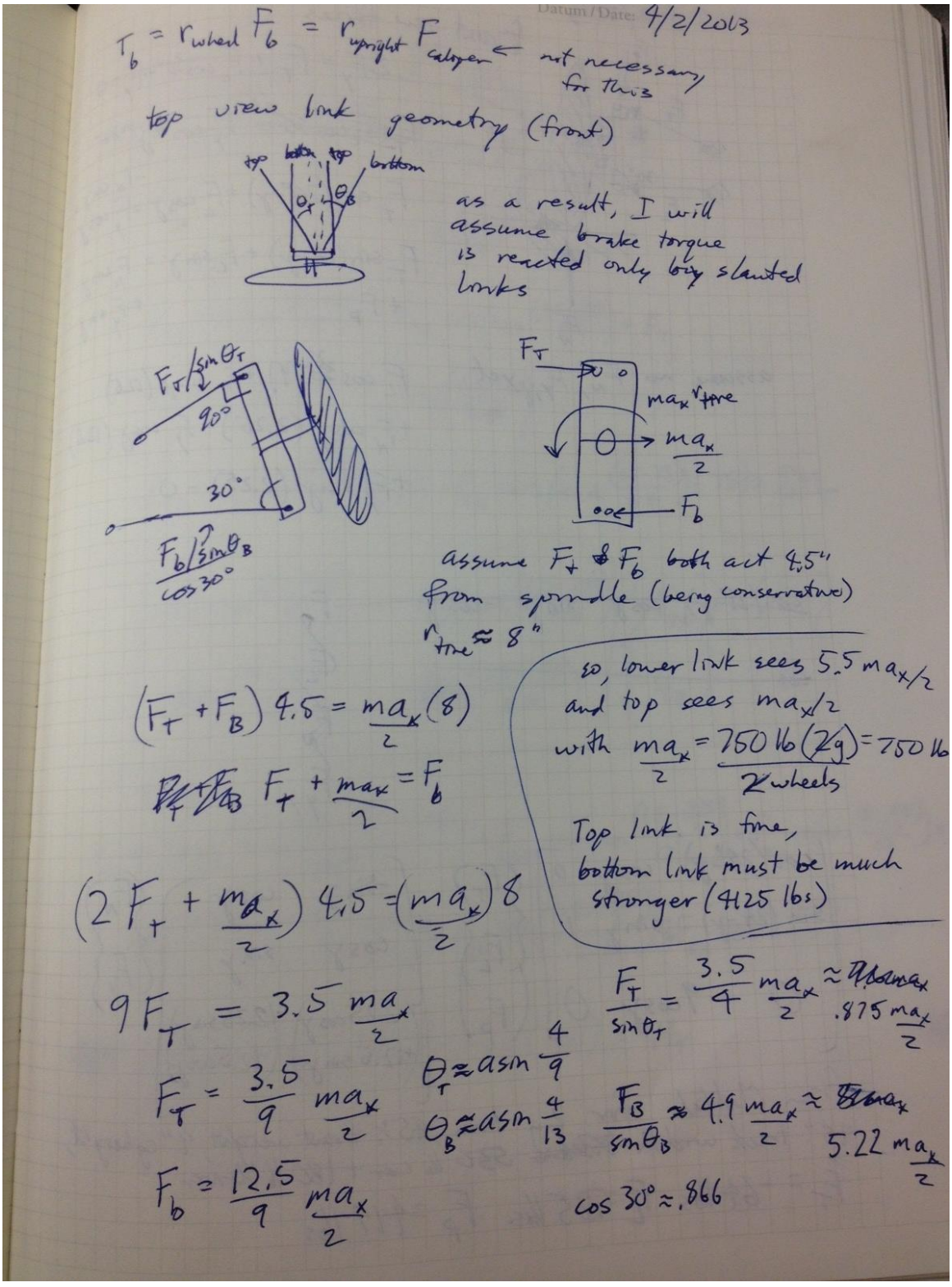

Datum / Date: 6/2/2013

front view forces

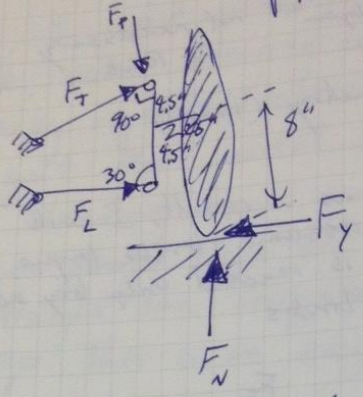

assume no F_N, F_Y, γ yet

~~$\Sigma F_y = F_T + F_L \cos 30° - F_Y = 0$~~

~~$F_T + F_L \cos 30° = F_Y \cos \gamma$~~ $\gamma \approx 22°$

$F_T \cos(24° - \gamma) + F_L \cos\gamma = F_N \sin\gamma + F_Y \cos\gamma$

$F_T \sin(24° - \gamma) + F_L \sin\gamma = F_N \cos\gamma + F_Y \sin\gamma + F_P$

$F_L \cos 30° (9) + F_N \sin\gamma (12.5) + F_N \cos\gamma (2.25) - F_Y \cos\gamma (12.5) + F_Y \sin\gamma (2.25) = 0$

~~$\cos(24° - \gamma)$~~ ~~$\cos\gamma$~~ $\sin\gamma$ $-\cos\gamma$ F_P

~~cos~~ F_L

F_N

F_{Y1}

$$\begin{bmatrix} \cos(24°-\gamma) & \cos\gamma & 0 \\ \sin(24°-\gamma) & \sin\gamma & 1 \\ 0 & 9\cos\gamma & 0 \end{bmatrix} \begin{Bmatrix} F_T \\ F_L \\ F_P \end{Bmatrix} = \begin{bmatrix} -\sin\gamma & \cos\gamma \\ \cos\gamma & \sin\gamma \\ -(2.25\cos\gamma + 12.5\sin\gamma) & -(2.25\sin\gamma - 12.5\cos\gamma) \end{bmatrix} \begin{Bmatrix} F_N \\ F_Y \end{Bmatrix}$$

from Matlab for 2g turn, 45% front weight, 9" cg height, 48" track width ~~550~~ 550 lb car + 180 lb driver

$F_T = -64$ lbs $F_L = 725$ lbs $F_P = 419$ lbs

Datum / Date: 6/2/2023

Top view

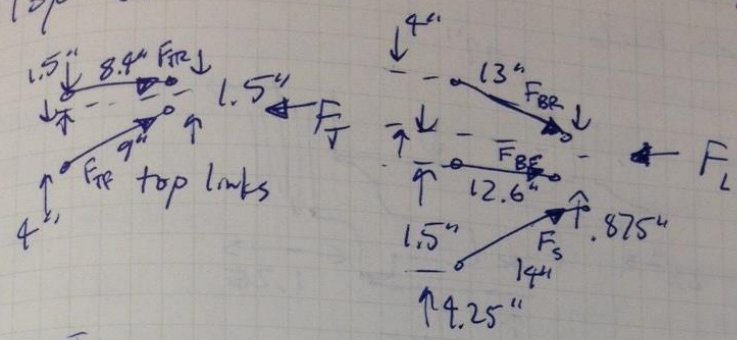

Top

$$F_{TF}\cos\left(\text{asin}\frac{(4-.75)}{9}\right)+F_{TR}\cos\left(\text{asin}\frac{(1.5-.75)}{8.4}\right)=F_T$$

$$F_{TF}\sin\left(\frac{4-.75}{9}\right)=F_{TR}\sin\left(\frac{1.5-.75}{8.4}\right)$$

$$F_{TF}\cos\left(\text{asin}\frac{(4-.75)}{9}\right)(.75)-F_{TR}\cos\left(\text{asin}\frac{(1.5-.75)}{8.4}\right)(.75)=\sum M_T$$

$$\begin{bmatrix}\cos\left(\text{asin}\frac{(4-.75)}{9}\right) & \cos\left(\text{asin}\frac{(1.5-.75)}{8.4}\right)\\ \sin\left(\frac{4-.75}{9}\right) & -\sin\left(\frac{1.5-.75}{8.4}\right)\end{bmatrix}\begin{Bmatrix}F_{TF}\\ F_{TR}\end{Bmatrix}=\begin{Bmatrix}F_T\\ 0\end{Bmatrix}$$

Bottom

$$F_s\cos\left(\text{asin}\frac{(1.5+4.25-\frac{.875}{2}-1.18)}{14}\right)+F_{BF}\cos\left(\text{asin}\frac{(1.5-\frac{.875}{2})}{12.6}\right)+F_{BR}\cos\left(\text{asin}\frac{(4-\frac{.875}{2}}{13}\right.$$

$$F_s\sin\left(\frac{(1.5+4.25-\frac{.875}{2}-1.18)}{14}\right)+F_{BF}\sin\left(\frac{(1.5-\frac{.875}{2})}{12.6}\right)-F_{BR}\sin\left(\frac{4-\frac{.875}{2}}{13}\right)=0$$

$$F_s(1.8)+F_{BF}(.436)-F_{BR}(.421)=-M_T$$

```
% Maximilian Sluiter
% maximiliansluiter@gmail.com
%
clear
clc
% Link Load Program
%
% Car Parameters
TotalWeight = 550+180; % pounds
WeightDistF = 0.45;
Hcg = 9; % inches Above Ground
T = 48; % Track Width, inches
camber = 22; % Negative Camber, degrees
latG = 2; % lateral acceleration (g)
%
WfStatic = TotalWeight*WeightDistF/2;
weight = WfStatic+TotalWeight*WeightDistF*Hcg/(T/2)*latG; %
pounds
lateral =
TotalWeight*WeightDistF*latG*weight/(TotalWeight*WeightDistF); %
pounds
%
% Applied Loads
A = [-sind(camber) cosd(camber);
           -cosd(camber)  -sind(camber);
           -(2.7*cosd(camber)+12.75*sind(camber)) ...
            -(2.7*sind(camber)-12.75*cosd(camber))]*...
       [weight;lateral];
%
% Link Load Coefficient Matrix
C = [cosd(24-camber) cosd(-camber)   0;
        sind(24-camber) sind(-camber)   1;
              0 (4.75+4.62)*cosd(camber) 0];
%
% Front View Link Reactions
Lfv = C\A;
%
% Pushrod Load (+ = compression), pounds
Fp = Lfv(3,1);
%
% Accounting for Top View Geometry
% Top Links
T = [cosd(asind((4-.75)/9)) cos(asind((1.5-.75)/8.4));
        (4-.75)/9        -(1.5-.75)/8.4];
Ft = [Lfv(1,1) ; 0];
Lt = T\Ft;
%
```

```
% Force in Front, Top, Front Link (+ = compression), pounds
Ftf = Lt(1,1);
% Force in Front, Top, Rear Link (+ = compression), pounds
Ftr = Lt(2,1);
%
% Moment due to unbalanced forces, inch-pounds
Mt = Ftf*cosd(asind((4-.75)/9))*.75-Ftr*cosd(asind((1.5-
.75)/8.4))*.75;
%
% Bottom Links
B = [cosd(asind((1.5+4.25-1.125/2-1.356)/14)) cosd(asind((1.5-
1.125/2)/12.6)) cosd(asind((4-1.125/2)/13));
        (1.5+4.25-1.125/2-1.356)/14 (1.5-1.125/2)/12.6 -(4-
1.125/2)/13;
        (1.356+1.125/2)*cosd(asind((1.5+4.25-1.125/2-
1.356)/14))+.906*(1.5+4.25-1.125/2-1.356)/14 ...
          (1.125/2)*cosd(asind((1.5-1.125/2)/12.6)) -
(1.125/2)*cosd(asind((4-1.125/2)/13))];
Fb = [Lfv(2,1) ; 0 ; -Mt];
Lb = B\Fb;
%
% Force in Steering Link (+ = compression), pounds
Fs = Lb(1,1);
% Force in Front, Bottom, Front Link (+ = compression), pounds
Fbf = Lb(2,1);
% Force in Front, Bottom, Rear Link (+ = compression), pounds
Fbr = Lb(3,1);
%
%
fprintf('Link Loads Due to Lateral Weight Transfer and %1 .1f g
Lateral Acceleration \n',latG)
fprintf('Front Top Front Link Load = %4 .0f pounds \n',Ftf)
fprintf('Front Top Rear Link Load = %4 .0f pounds \n',Ftr)
fprintf('Steering Link Load = %4 .0f pounds \n',Fs)
fprintf('Front Bottom Front Link Load = %4 .0f pounds \n',Fbf)
fprintf('Front Bottom Rear Link Load = %4 .0f pounds \n',Fbr)
fprintf('Pushrod Load = %4 .0f pounds \n \n',Fp)
%
%
% Braking
ax = 1.6; % g
PercentFront = (WfStatic+Hcg*ax/62/2)/(TotalWeight/2); % percent
of braking work the fronts are doing
% looking normal to upright
UprightTorque = [4.75 4.62;
                     -1   1];
BrakeLoad = TotalWeight*ax/2*PercentFront*[8 ; 1];
```

```
%
% Side View Link Reactions
Fsv = UprightTorque\BrakeLoad;
%
% Accounting for Top View Geometry
% Top Links
T = [cosd(asind((4-.75)/9)) cos(asind((1.5-.75)/8.4));
        (4-.75)/9        -(1.5-.75)/8.4];
Ft = [0 ; Fsv(1,1)];
Lt = T\Ft;
%
% Force in Front, Top, Front Link (+ = compression), pounds
Ftf = Lt(1,1);
% Force in Front, Top, Rear Link (+ = compression), pounds
Ftr = Lt(2,1);
%
% Moment due to unbalanced forces, inch-pounds
Mt = Ftf*cosd(asind((4-.75)/9))*.75-Ftr*cosd(asind((1.5-
.75)/8.4))*.75;
%
% Bottom Links
B = [cosd(asind((1.5+4.25-1.125/2-1.356)/14)) cosd(asind((1.5-
1.125/2)/12.6)) cosd(asind((4-1.125/2)/13));
        (1.5+4.25-1.125/2-1.356)/14 (1.5-1.125/2)/12.6 -(4-
1.125/2)/13;
        (1.356+1.125/2)*cosd(asind((1.5+4.25-1.125/2-
1.356)/14))+.906*(1.5+4.25-.875/2-1.356)/14 ...
          (1.125/2)*cosd(asind((1.5-1.125/2)/12.6)) -
(1.125/2)*cosd(asind((4-1.125/2)/13))];
Fb = [0 ; -Fsv(2,1) ; -Mt];
Lb = B\Fb;
%
% Force in Steering Link (+ = compression), pounds
Fs = Lb(1,1);
% Force in Front, Bottom, Front Link (+ = compression), pounds
Fbf = Lb(2,1);
% Force in Front, Bottom, Rear Link (+ = compression), pounds
Fbr = Lb(3,1);
%

%
fprintf('Link Loads Due to Longitudinal Weight Transfer and %1
.1f g Deceleration \n',ax)
fprintf('Front Top Front Link Load = %4 .0f pounds \n',Ftf)
fprintf('Front Top Rear Link Load = %4 .0f pounds \n',Ftr)
fprintf('Steering Link Load = %4 .0f pounds \n',Fs)
fprintf('Front Bottom Front Link Load = %4 .0f pounds \n',Fbf)
```

```
fprintf('Front Bottom Rear Link Load = %4 .0f pounds \n \n',Fbr)
%
```

Appendix D: Gantt Chart

	Task Mode	Task Name	Duration	Start	Finish
1		Final Design	13 days	Tue 11/13/12	Thu 11/29/12
2		CDR	0 days	Fri 11/30/12	Fri 11/30/12
3		Minor Changes	10 days	Tue 12/4/12	Sat 12/15/12
4		Fabrication	80 days	Mon 1/7/13	Fri 4/26/13
5	✓	Assembly	22 days	Sun 2/24/13	Sat 3/23/13
6		Testing	2 days	Mon 6/3/13	Tue 6/4/13
7		Go/NoGo	0 days	Mon 4/8/13	Mon 4/8/13
8		Go/NoGo Polynx	0 days	Thu 11/15/12	Thu 11/15/12
9		Competion	0 days	Wed 6/19/13	Wed 6/19/13
10		Yellow Tag Completion	0 days	Tue 1/15/13	Tue 1/15/13
11		Senior Exit Exam	0 days	Thu 4/25/13	Thu 4/25/13
12		Senior Project Expo	0 days	Thu 5/30/13	Thu 5/30/13
13		Report Due	0 days	Fri 6/7/13	Fri 6/7/13
14		Extension for Go/NoGo	14 days	Mon 4/8/13	Thu 4/25/13
15		Redesign	14 days	Mon 12/17/12	Thu 1/3/13

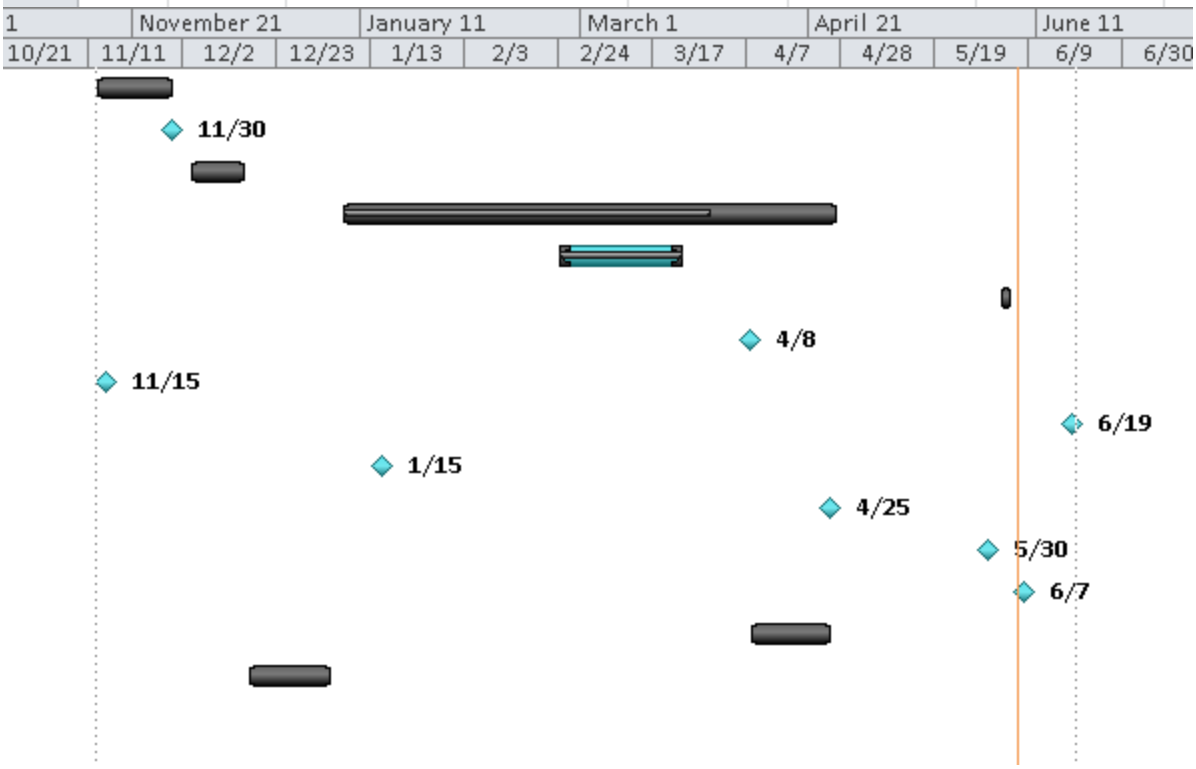

Appendix E: Part Drawings

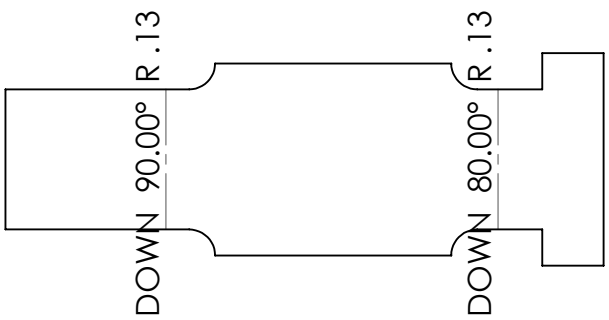

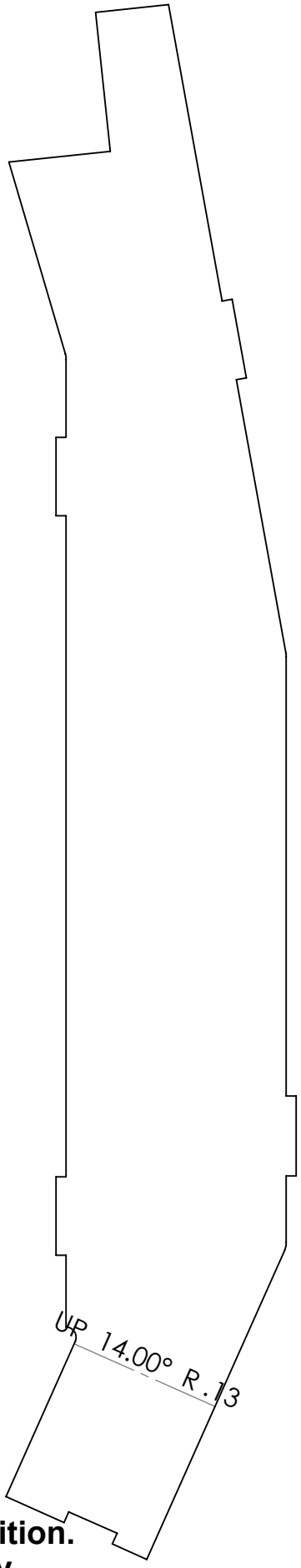

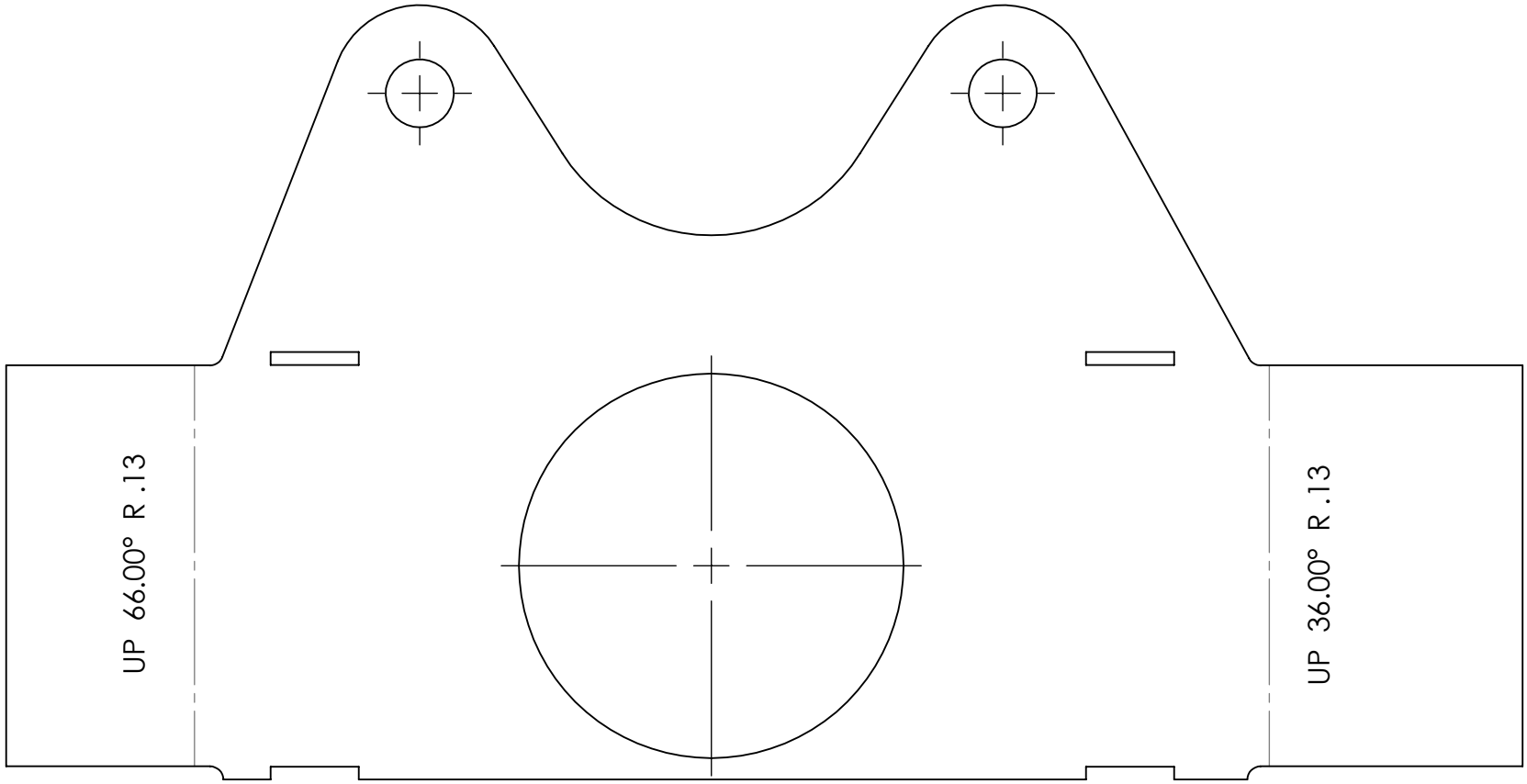

FrontUpright,HighCamber,InnerSheet
Scale 1:1

Bend one part up at specified angle for left side upright,
the other down for right side upright.

Drawn by: Maximilian Sluiter
maximiliansluiter@gmail.com

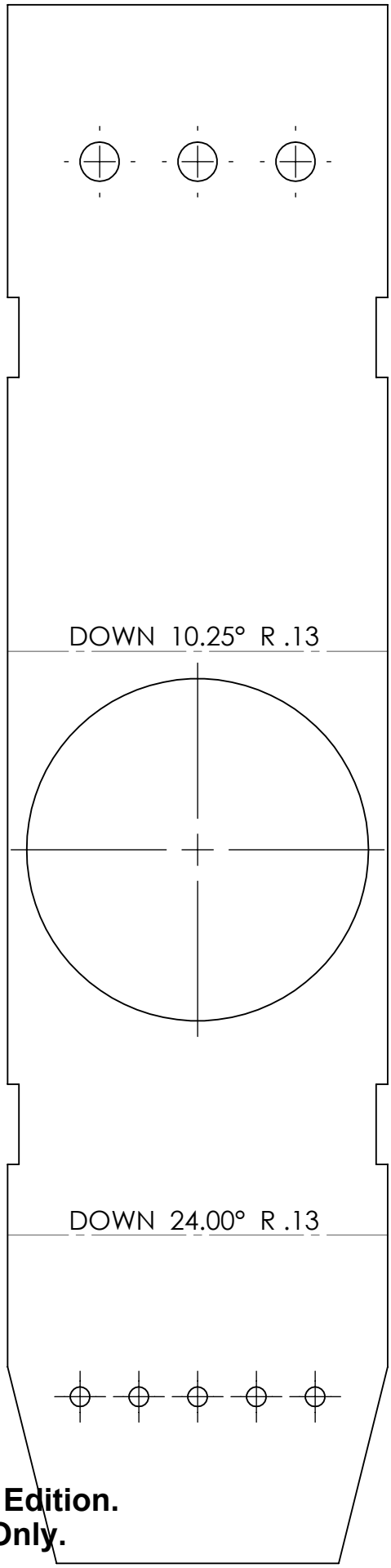

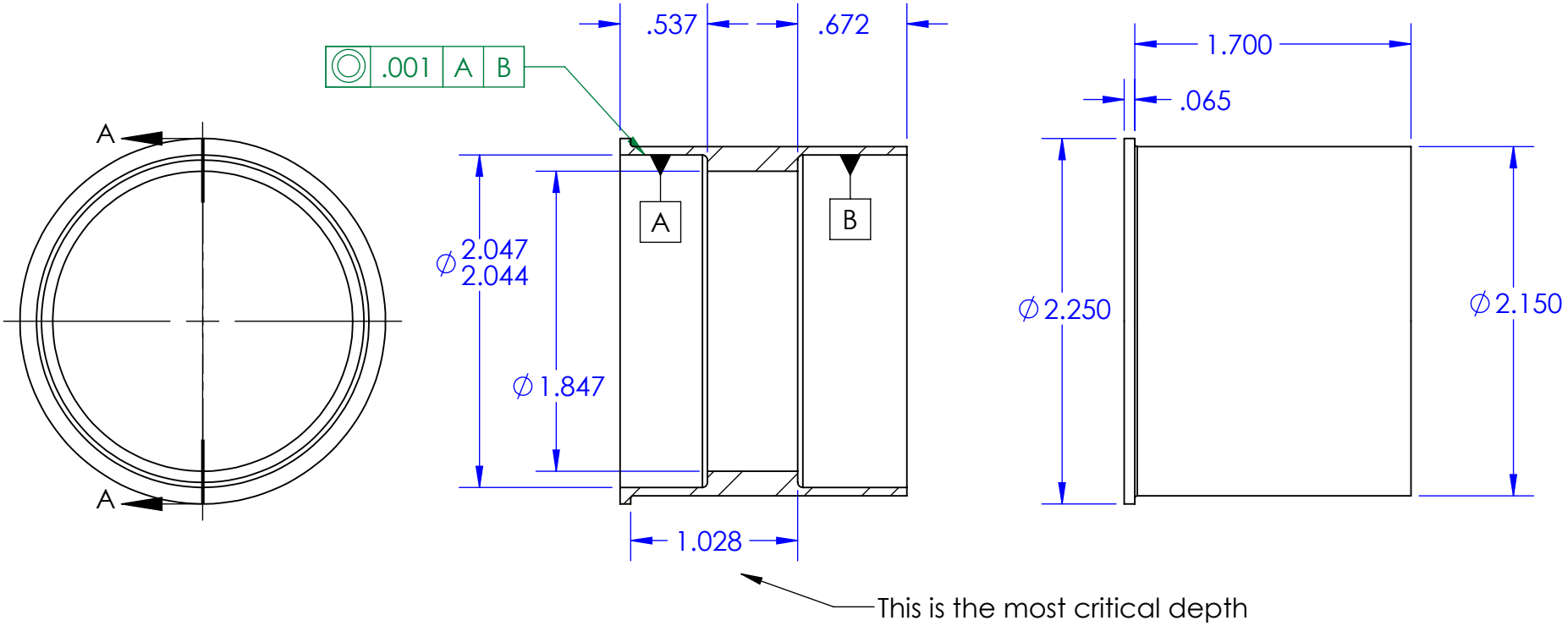

Front Upright Bearing Cup
Material: 4130 Cr-Mo Alloy Steel
Scale 1:1
Dimensions: Inches
Tolerance: +/- 0.005 unless otherwise noted

Quantity Required: 4

Drawn by: Maximilian Sluiter
maximiliansluiter@gmail.com

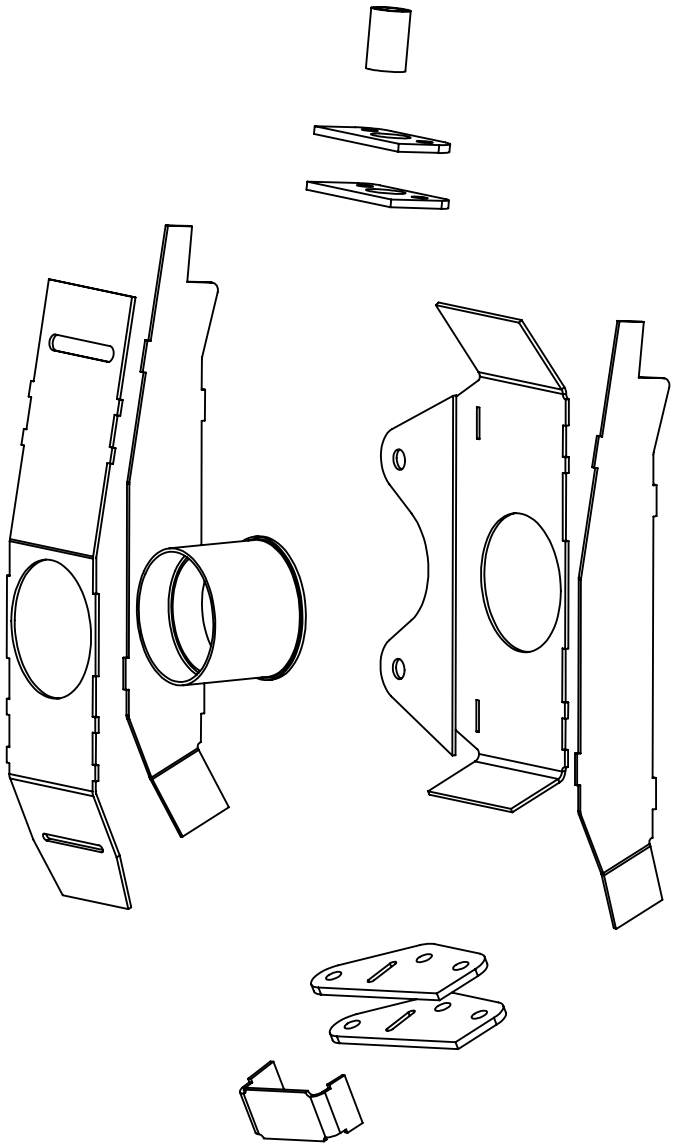

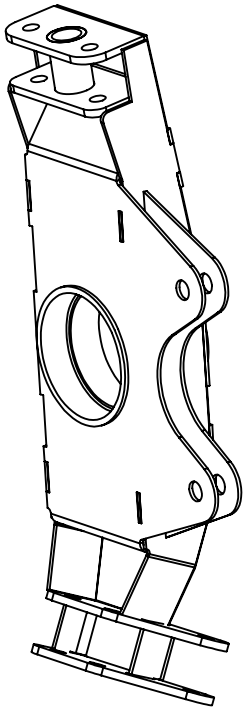

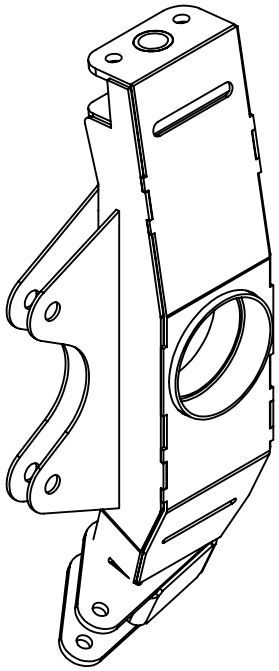

High Camber Front Upright
Material: 4130 Steel
Scale 3:1

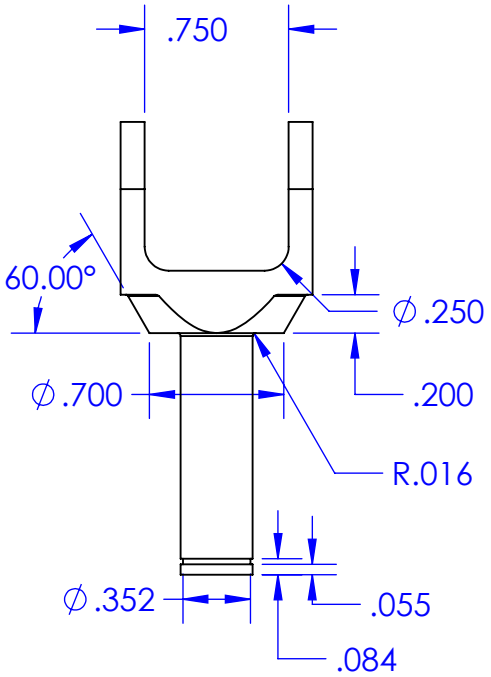

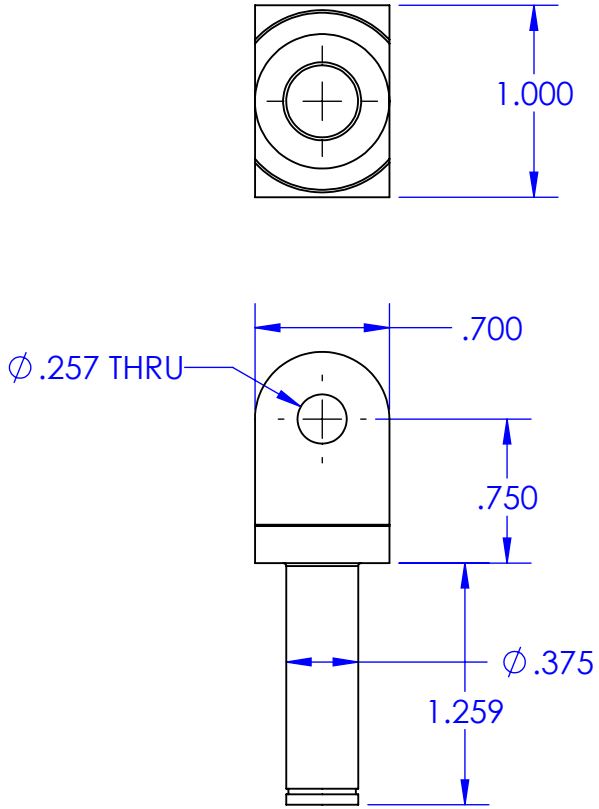

Front Upright Rotating Clevis for Pushrod
Material: 303 Stainless Steel
Scale 1:1
Dimensions: Inches
Tolerance: +/- 0.005

Make 2 of these

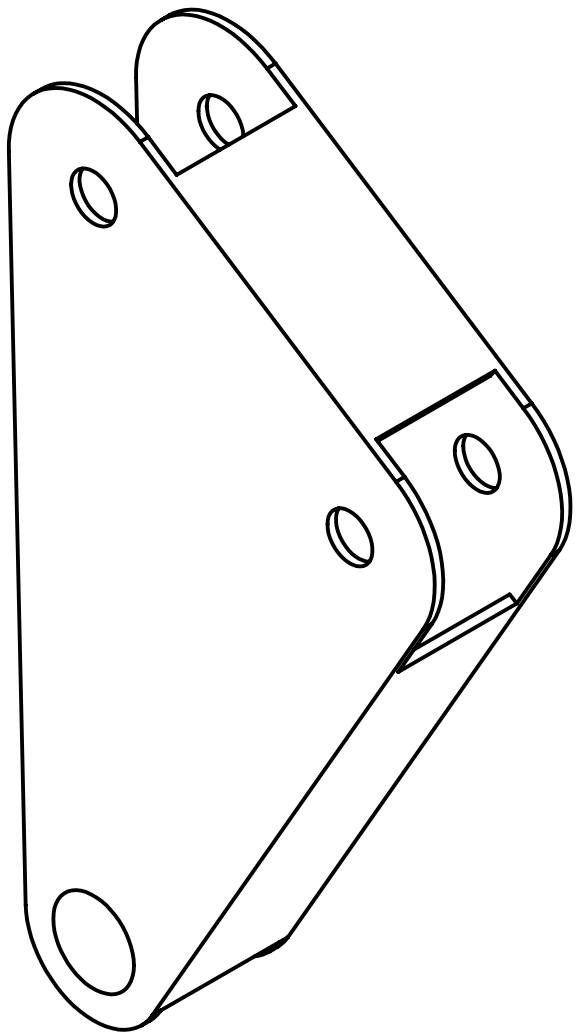

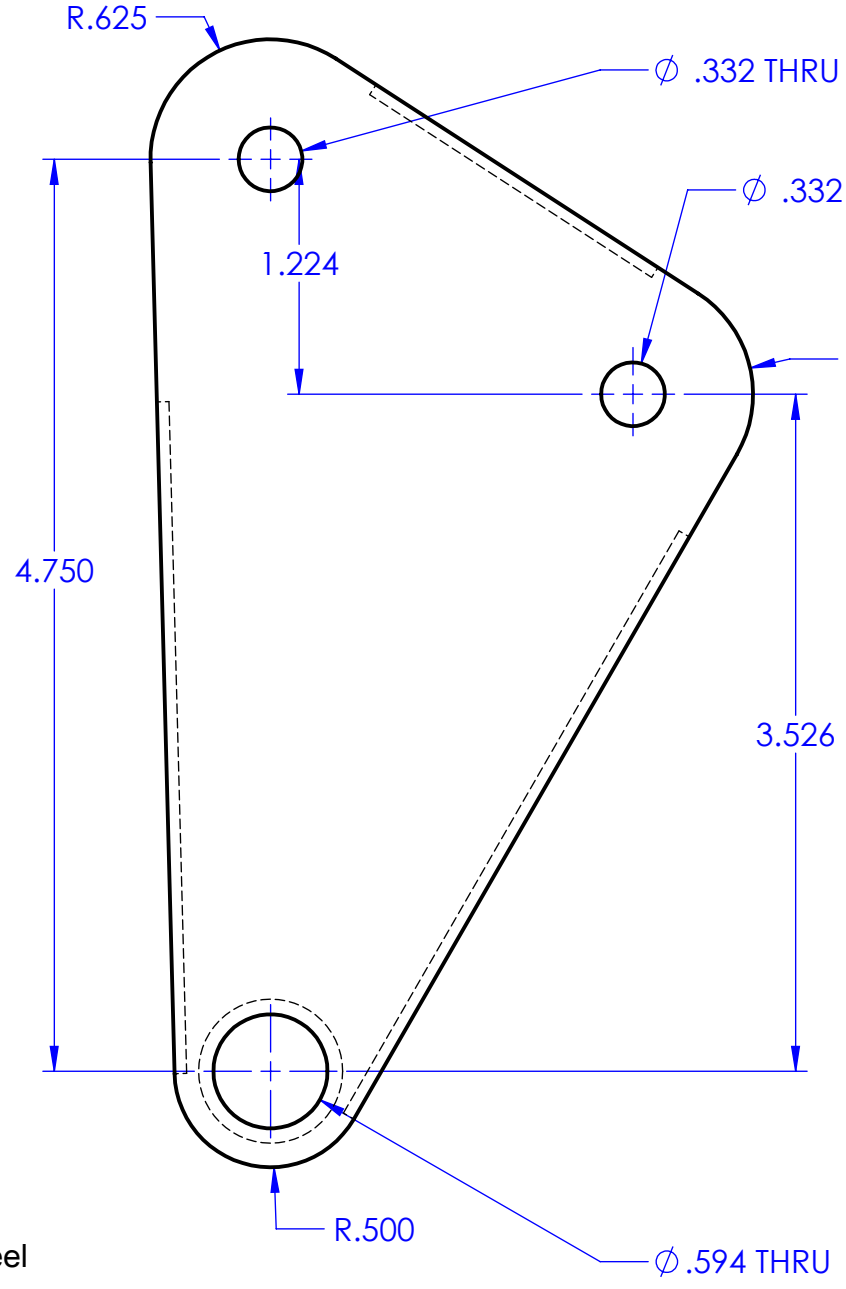

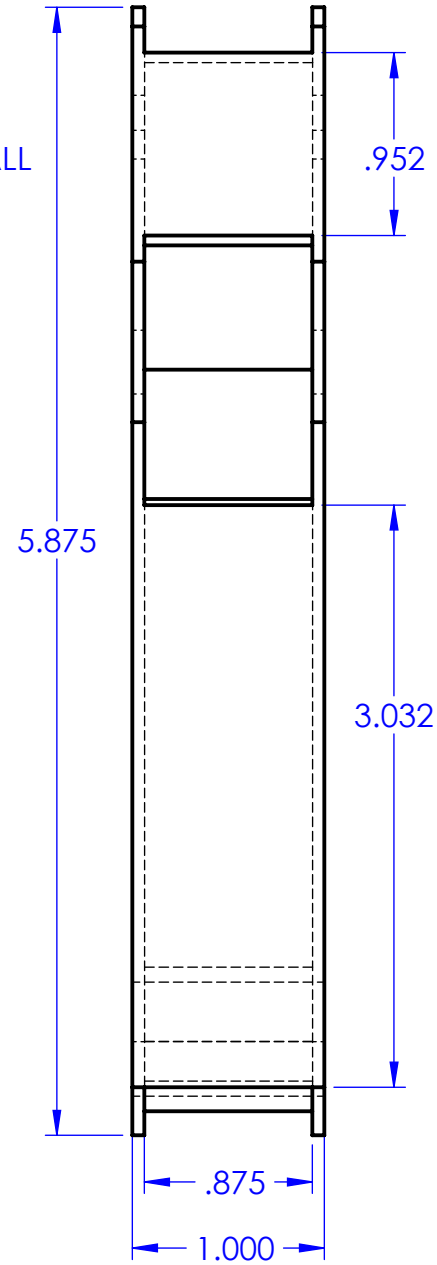

Front Rocker
Material: 4130 Steel
Scale 1:1
Dimensions: Inches

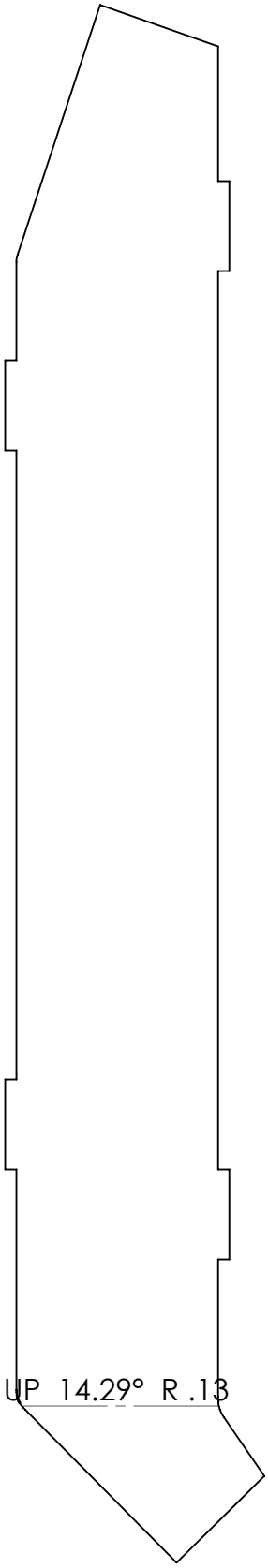

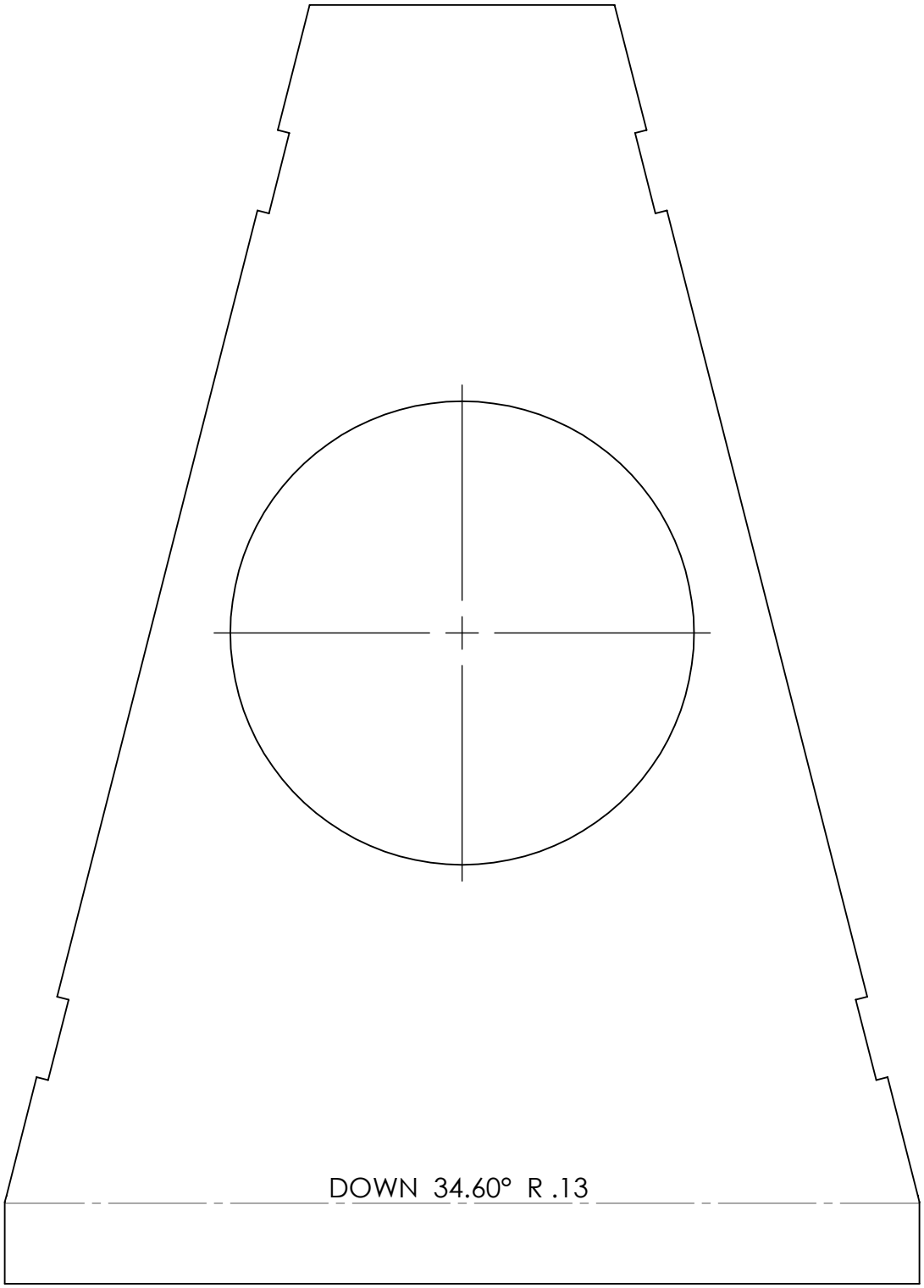

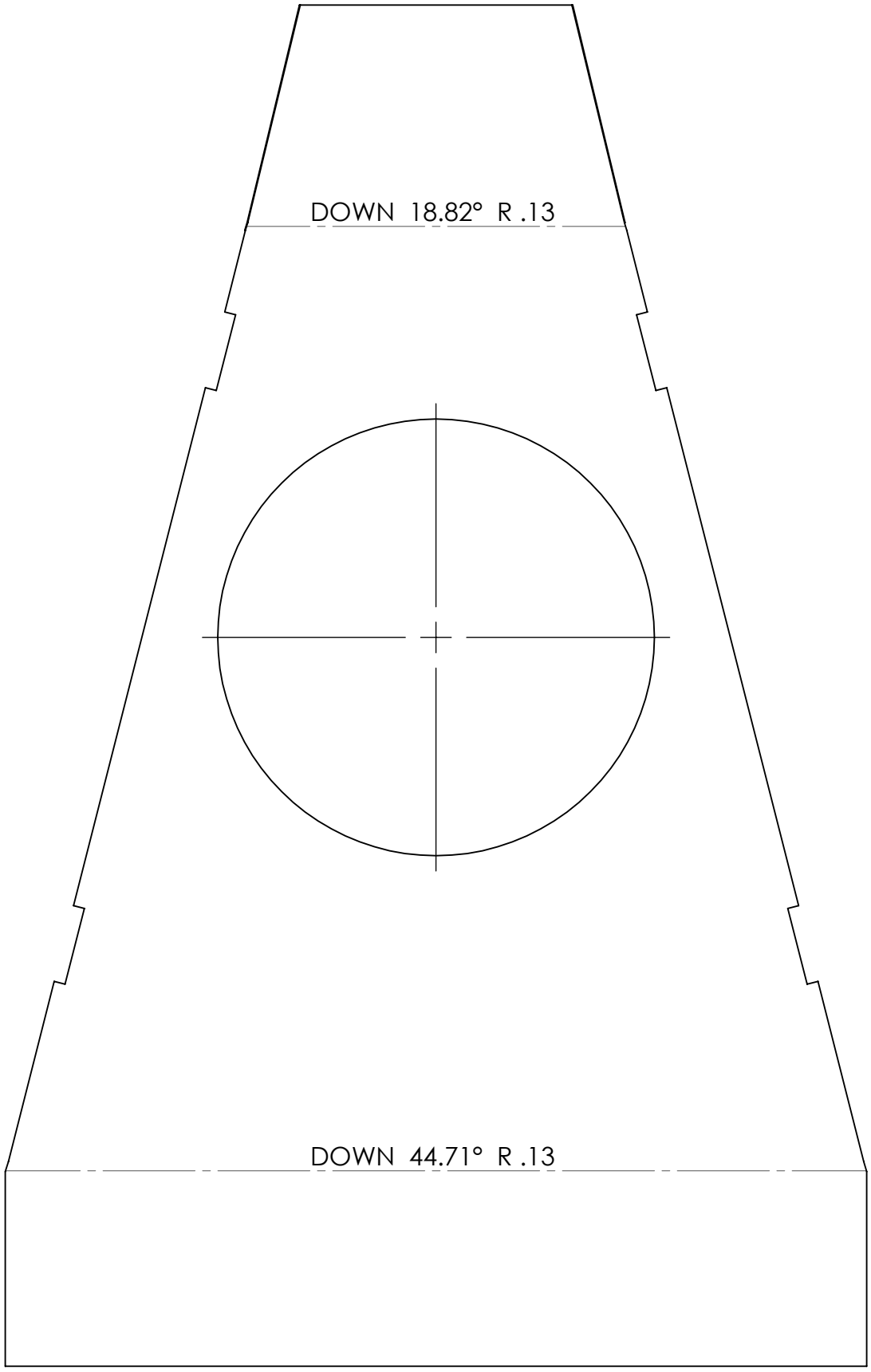

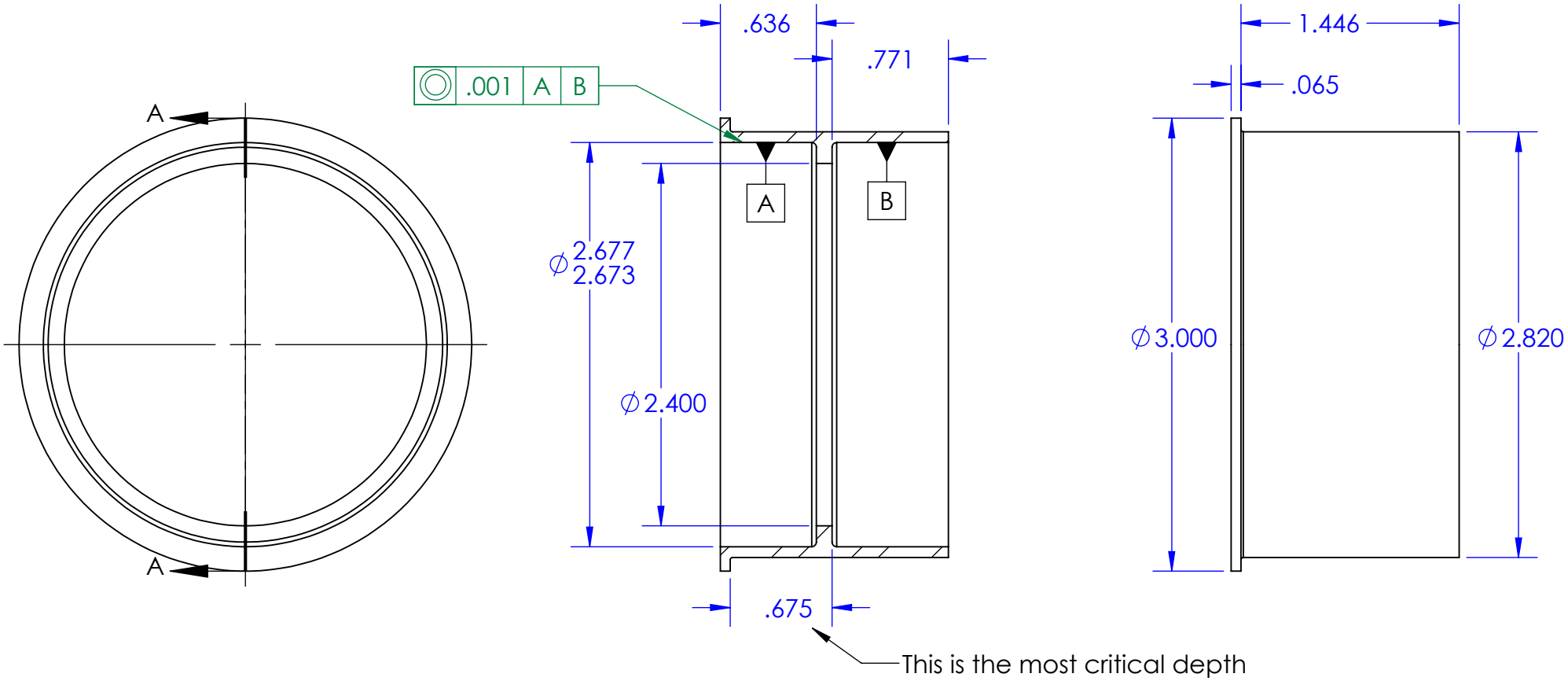

Rear Upright Jig, Bearing Cup
Material: 4130 Cr-MoAlloy Steel
Scale 1:1
Dimensions: Inches
Tolerance: +/- 0.005 unless otherwise noted

Quantity Required: 2

Drawn by: Maximilian Sluiter
maximiliansluiter@gmail.com

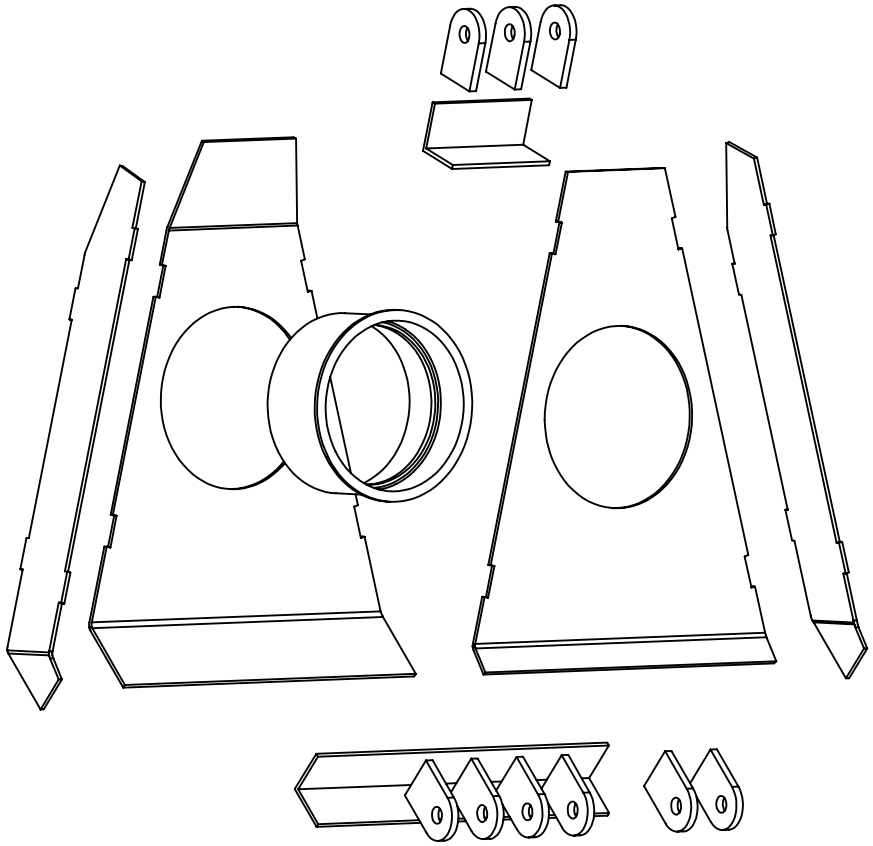

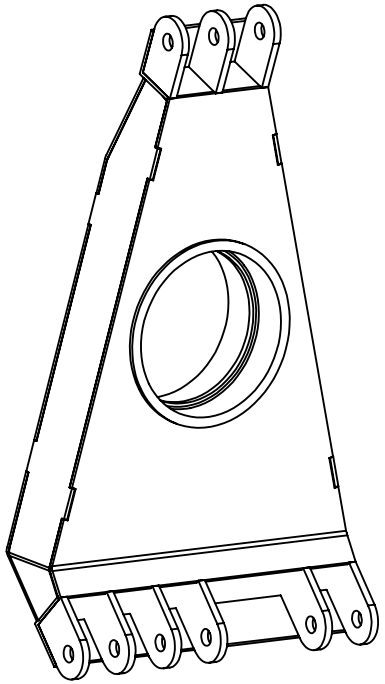

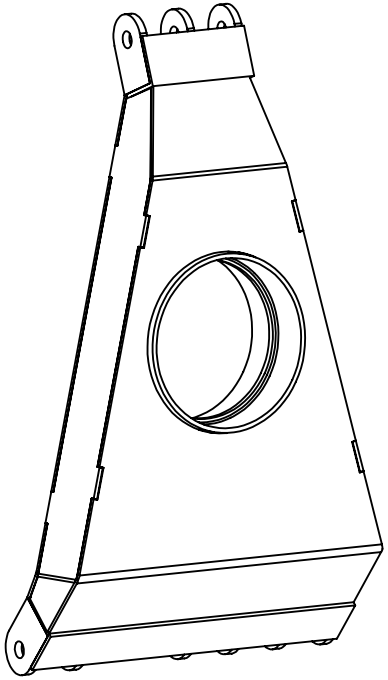

Rear Upright
Material: 4130 Steel
Scale 3:1

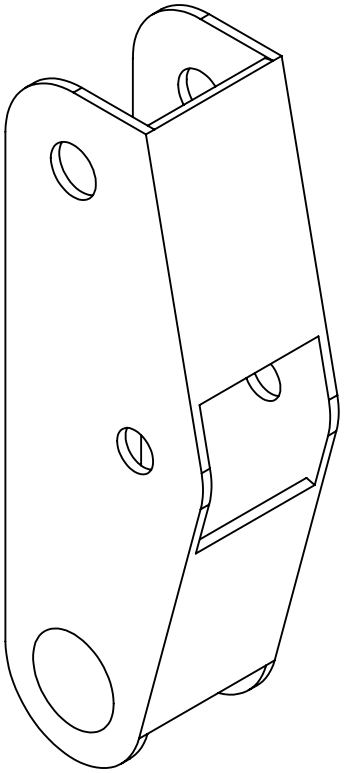

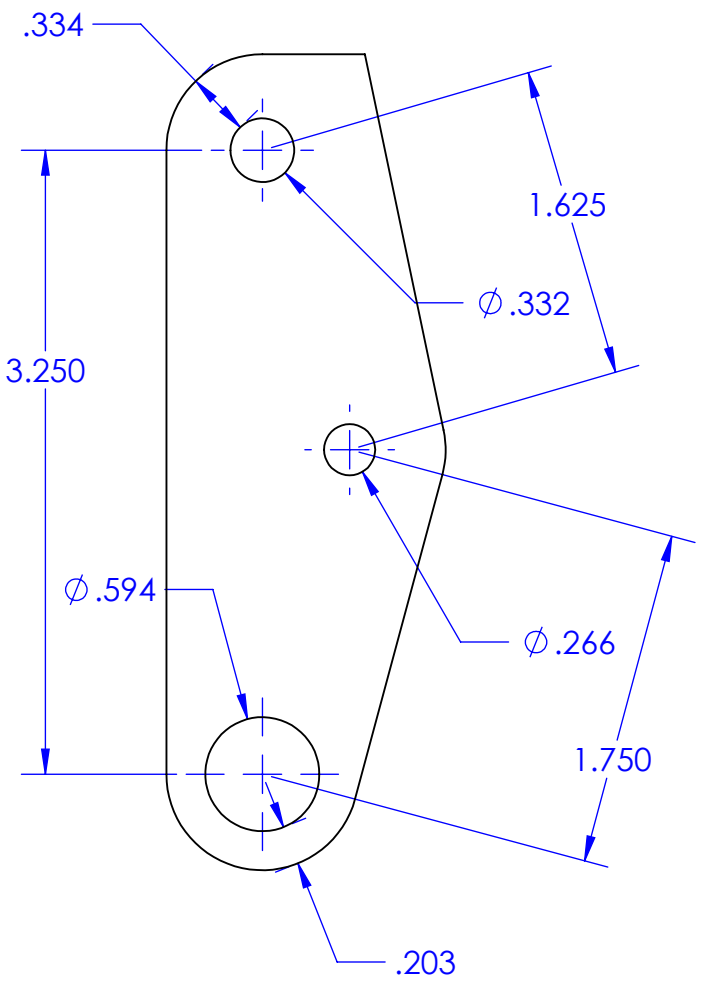

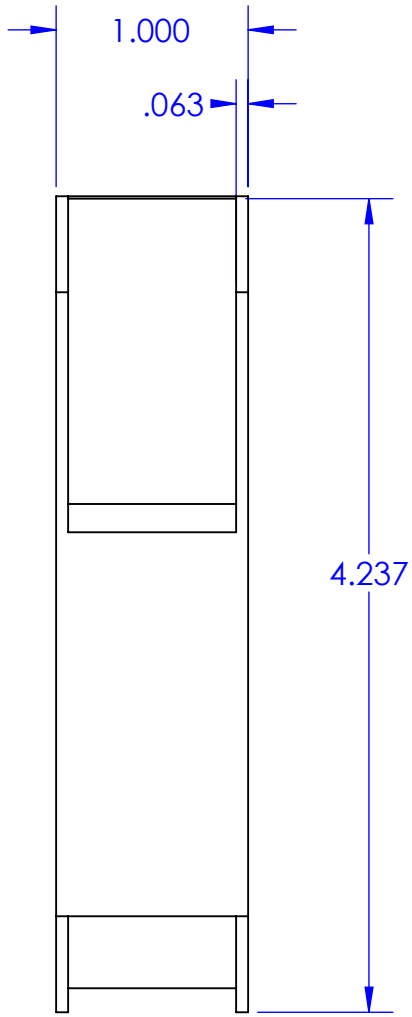

Rear Spring Rocker
Material: 4130 Steel
Scale 1:1
Units: Inches

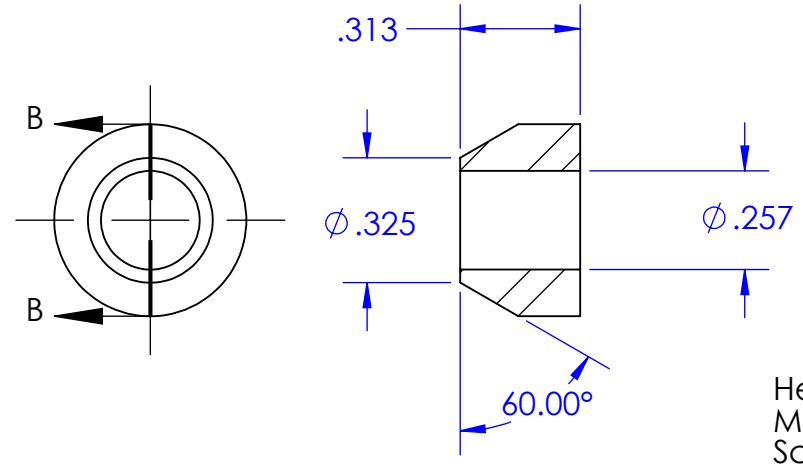

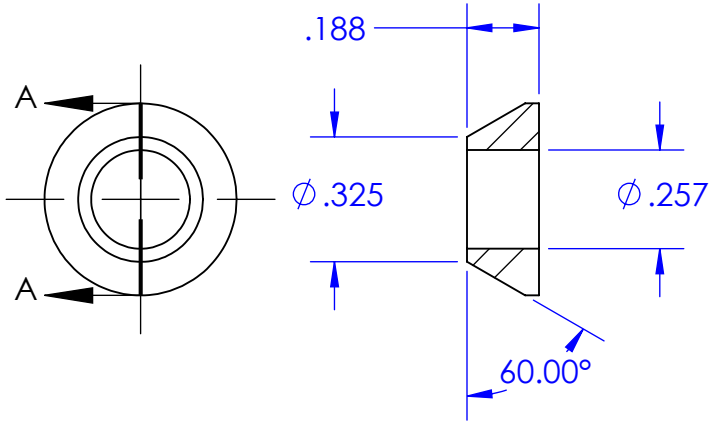

Heim Joint Misalignment Spacer
Material: 4340 Steel
Scale 2:1
Dimensions: Inches
Tolerance: +/- 0.005

Make 52 of 0.188" length,
Make 16 of 0.3125" length

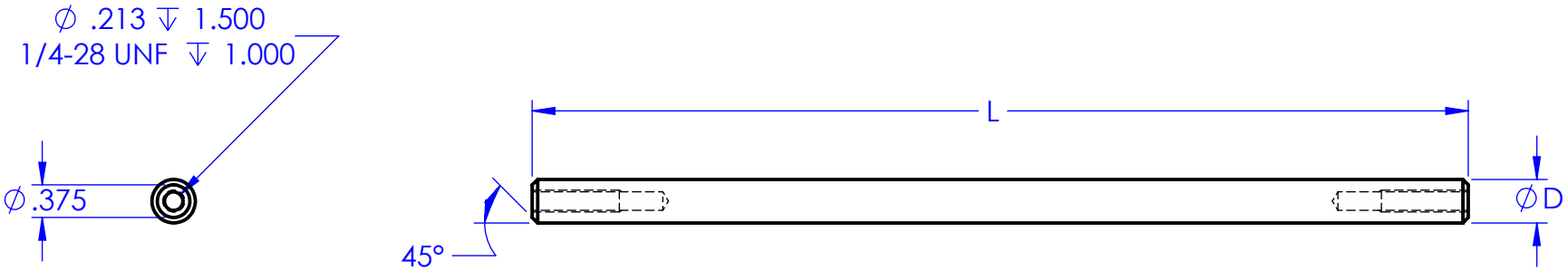

	Link	Diameter - D (inches)	Qty	Faced Length-L (inches)	Center to Center Length (inches)
1	Rear Bottom	0.5	4	10.9971	12.8331
2	Rear Top	0.5	4	10.7378	12.5738
3	Rear Toe	0.5	2	10.7413	12.5773
4	Rear Pushrod	0.5	2	9.8985	11.7345
5	Front Bottom Rear	0.625	2	11.5321	13.3681
6	Front Bottom Front	0.5	2	11.1045	12.9405
7	Front Top Rear	0.5	2	10.5968	12.4328
8	Front Top Front	0.5	2	10.9926	12.8286
9	Steering	0.5	2	12.4504	14.2864
10	Front Pushrod	0.5	2	8.2996	10.1356

Suspension Links
Material: 6061 T6 Aluminum
Scale 1:2
Dimensions: Inches

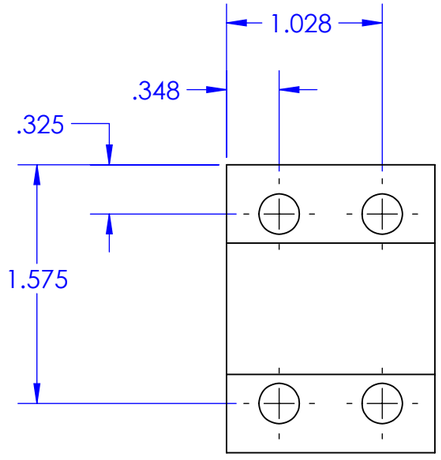

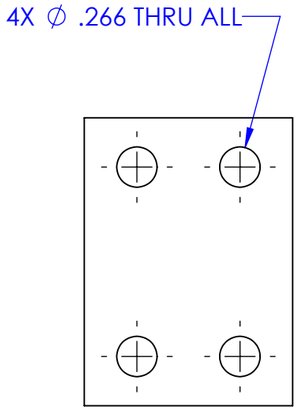

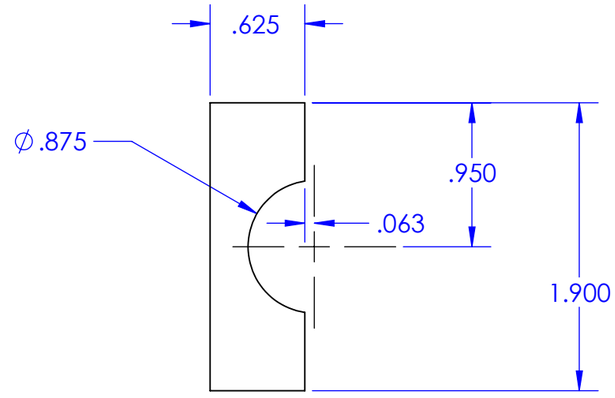

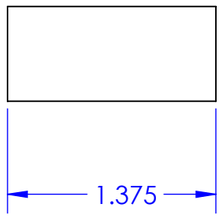

Steering Rack Clevis Clamp Piece
Material: 7075-T6/651 Aluminum Alloy
both sides are the same so make 2 of these
Scale 1:1
Dimensions in Inches
Tolerances: +/- 0.005

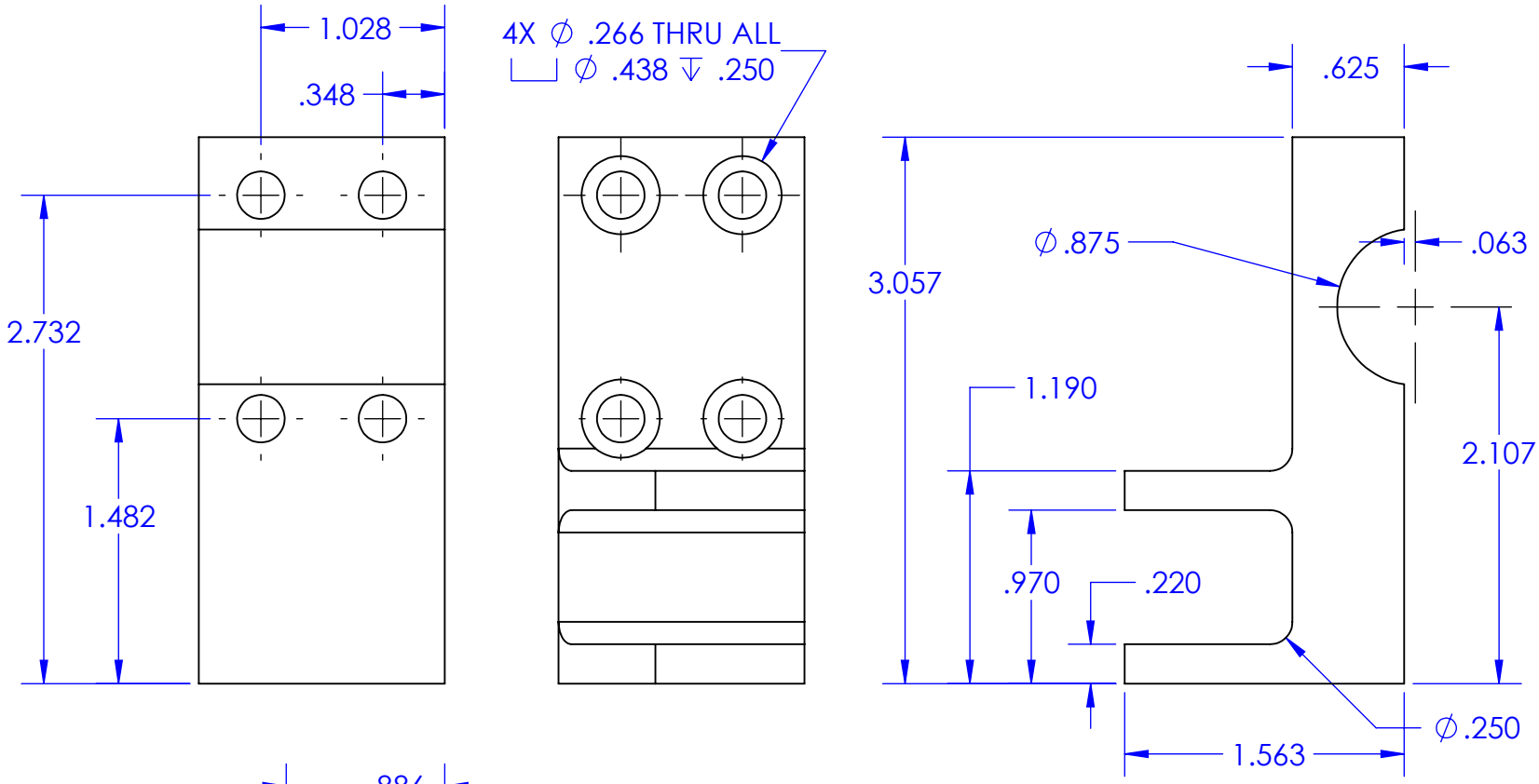

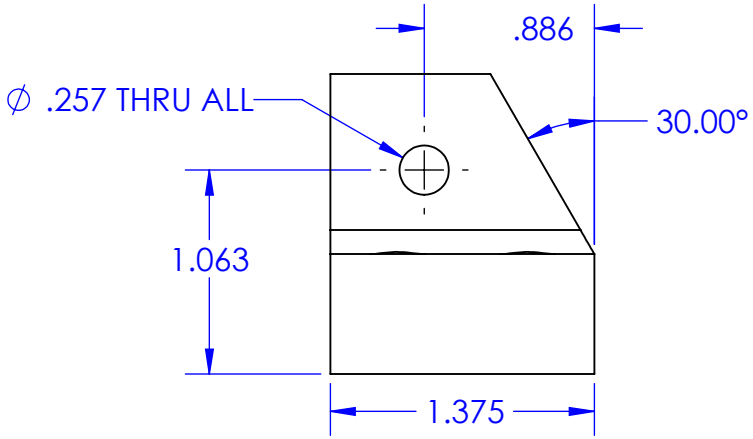

Steering Clevis, Clevis Half, Left
Material: 7075-T6/651 Aluminum Alloy
Scale 1:1
Dimensions in Inches
Tolerance: +/- 0.005

Quantity Required: 1
Everything is the same as the right side piece except the top view. The heim joint bolt hole position and 30 degree angle are on the opposite side (mirrored).

Drawn by: Maximilian Sluiter
maximiliansluiter@gmail.com

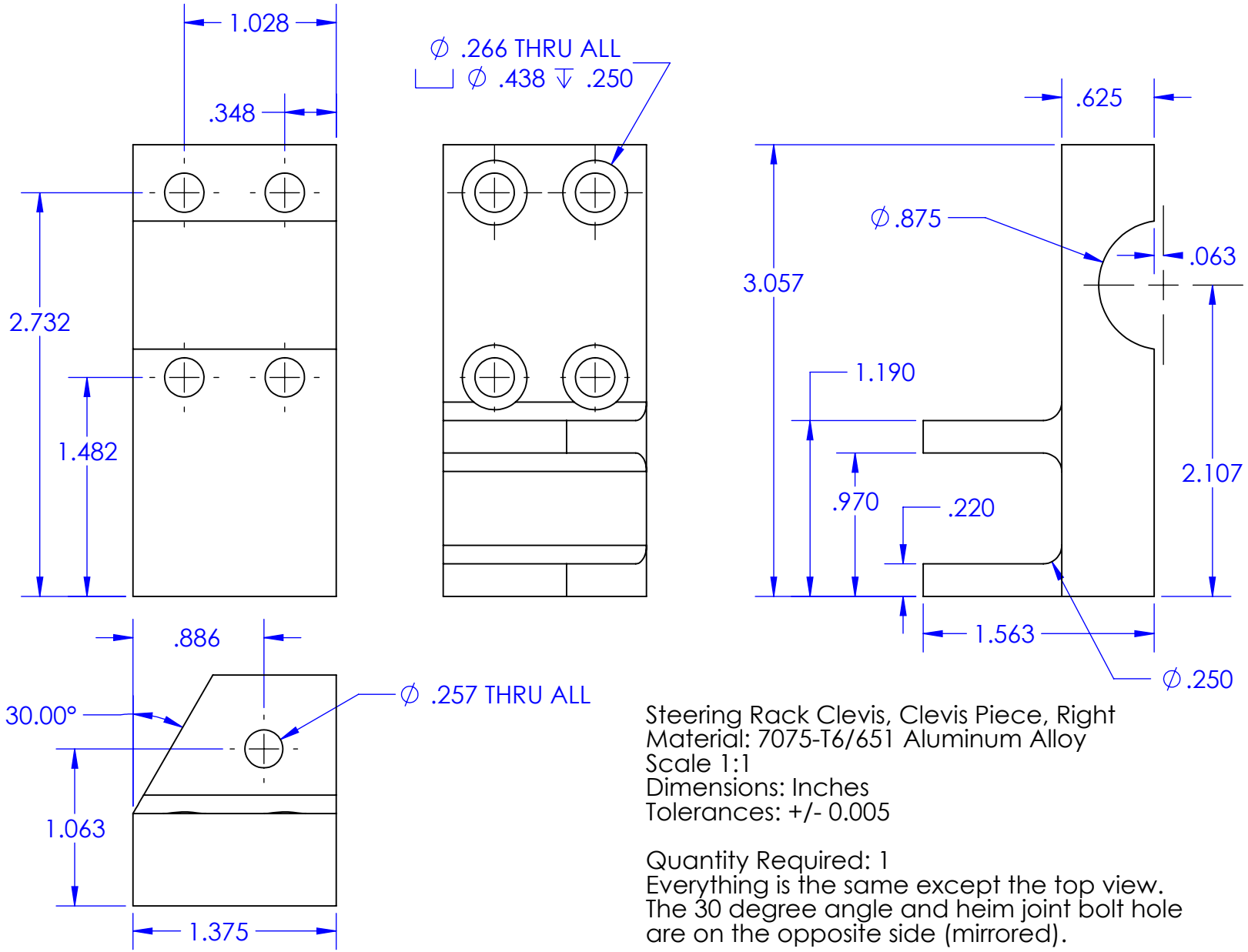

Steering Rack Clevis, Clevis Piece, Right
Material: 7075-T6/651 Aluminum Alloy
Scale 1:1
Dimensions: Inches
Tolerances: +/- 0.005

Quantity Required: 1
Everything is the same except the top view.
The 30 degree angle and heim joint bolt hole are on the opposite side (mirrored).

Drawn by: Maximilian Sluiter
maximiliansluiter@gmail.com